Nanocatalysts for sustainable industrial processes

Dissertation submitted to the University of Madeira in order to obtain the degree of Master in Nanochemistry and Nanomaterials

By Jiawei Wang

Work developed under the supervision of
Prof. Lúsa Margarida D.R.S. Martins and co-supervised by
Prof. João Manuel Cunha Rodrigues

Faculdade de Ciências Exatas e de Engenharia,
Centro de Química da Madeira,
Campus Universitário da Penteada, 9000-390 Funchal, Portugal

Novembro de 2015

Declaration

I hereby declare that this thesis is the result of my own work, is original and was written by me. I also declare that its reproduction and publication by Madeira University will not break any third party rights and that I have not previously (in its entirety or in part) submitted it elsewhere for obtaining any qualification or degree. Furthermore, I certify that all the sources of information used in the thesis were properly cited.

Lisbon, November 2015

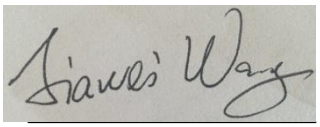

Conference contributions

Nov. 2014 Poster Presentation in *XX Encontro Luso-Galego de Química - XXLGQ*

S.A.C. Carabineiro, J. Wang, M. Sutradhar, L.M.D.R.S. Martins, M.F.C. Guedes da Silva, J.G. Buijnsters, A.J.L. Pombeiro, J.L. Figueiredo, Oxido-vanadium complexes heterogenised on carbon materials as catalysts for the oxidation of alcohols, Encontro Luso-Galego de Química, Porto, 2014, QI/CAT25, pág. 61.

May. 2015 Poster Presentation in *FÓRUM de Engenharia Química e Biológica do ISEL*

J. Wang, A.P.C. Ribeiro, L.M.D.R.S. Martins, J. Rodrigues, A.J.L. Pombeiro, *Fast and efficient degradation of organic dyes with Cu nanocomposites*, Fórum de Engenharia Química e Biológica'15, Instituto Superior de Engenharia de Lisboa, Portugal, 2015, pág. 23.

Oct. 2015 Poster Presentation in *2nd EuCheMS Congress on Green and Sustainable Chemistry*

A.P.C. Ribeiro, J. Wang, L.M.D.R.S. Martins, J. Rodrigues, A.J.L. Pombeiro, *Efficient Cu - MWCNT nanocomposite for the reduction of 4-Nitrophenol*, 2nd EuCheMS Congress on Green and Sustainable Chemistry, Universidade Nova de Lisboa, Portugal, 2015, M1 P11, pág. 135.

Acknowledgements

First of all I owe my greatest debt of gratitude to my supervisors, Professor Luísa Margarida Martins and Professor João Rodrigues, who have given me the opportunity to work in the field of nanoscience and helped me enrich my knowledge and broaden my view.

I would like to express my sincere thanks to my tutor, Dr. Ana Paula Ribeiro, for her most valuable advice and insightful comments and suggestions.

My heartfelt gratitude goes to Group I of CQE-Centro de Química Estrutural that has provided me materials and devices for my research. All the group members, especially my colleagues in lab, Robbe Vervecken, Marta Mendes, Elisa Spada, Goncalo Tiago, Anbu Sellamuthu and Anup Paul, are to be thanked for making my learning process interesting and enjoyable.

I would like to acknowledge the Portuguese Foundation for Science and Technology (FCT) for funding through the projects UID/QUI/00100/2013 and the NMR Portuguese Network PTNMR2014/2015.

Last but not least, I would like to thank my family for their selfless support. And special thanks would be given to my girlfriend, Silvia Wang, for her valuable encouragement and spiritual support during my study.

Abstract

In Chapter 1, rhodium nanoparticles were supported on multiwalled carbon nanotubes (MWCNTs) and bound to the magnetic core-shell system Fe_3O_4@TiO_2. The composite Fe_3O_4@TiO_2-Rh-MWCNT and the intermediates were characterized by SEM, EDS and TEM. Their catalytic activity was studied using i) the hydrogenation transfer of nitroarenes and cyclohexene in the presence of hydrazine hydrate; ii) the reduction of 2-nitrophenol with $NaBH_4$; and iii) the decoloration of pigments in the presence of hydrogen peroxide. The results were monitored by gas chromatography (i) and UV Visible (ii and iii).

In the second chapter, the catalytic activity of six oxidovanadium(V) aroylhydrazone complexes, *viz*. $[VOL^1(OEt)][VOL^1(OEt)(EtOH)]$ (**1**), $[VOL^2(OEt)]$ (**2**), $[Et_3NH][VO_2L^1]$ (**3**), $[VO_2(H_2L^2)]\cdot 2EtOH$ (**4**), $[VOL^1(\mu\text{-}O)VOL^1]$ (**5**) and $[VOL^2(\mu\text{-}O)VOL^2]$ (**6**) (H_2L^1 = 3,5-di-*tert*-butyl-2-hydroxybenzylidene)-2-hydroxybenzohydrazide and H_2L^2 = 3,5-di-*tert*-butyl-2-hydroxybenzylidene)-2-aminobenzohydrazide), anchored on nanodiamonds with different treatments, was studied towards the microwave-assisted partial oxidation of 1-phenylethanol to acetophenone in the presence of *tert*-butyl hydroperoxide (TBHP) as oxidant. A high selectivity for acetophenone was achieved for the optimized conditions. The possibility of recycling and reuse the heterogeneous catalysts was also investigated.

In chapter 3, the catalytic activity of gold nanoparticles supported at different metal oxides, such as Fe_2O_3, Al_2O_3 ZnO or TiO_2, was studied for the above reaction. The effect of the support, quantity of the catalyst and temperature was investigated. The recyclability of the gold catalysts was also studied.

In the last chapter, a new copper nanocomposite with functionalized mutiwalled carbon nanotubes (Cu-MWCNT) was synthesized using a microwave assisted polyol method. The characterization was performed using XRD and SEM. The catalytic activity of Cu-MWCNT was studied through the degradation of pigments, such as amaranth, brilliant blue, indigo, tartrazine and methylene blue.

Keywords: nanoparticle, magnetic catalyst, gold, vanadium, rhodium, copper, heterogenization, oxidation, hydrogenation.

Resumo

No capítulo 1, nanopartículas de ródio foram suportadas em nanotubos de carbono de paredes múltiplas (MWCNT) e ligadas ao sistema magnético constituído por magnetite envolvida em dióxido de titânio (Fe_3O_4@TiO_2). O compósito formado por Fe_3O_4@TiO_2-Rh-MWCNT e respectivos intermediários foram caracterizados por SEM, EDS e TEM. A actividade catalítica foi estudada nos seguintes sistemas: i) hidrogenação por transferência de nitroarenos e ciclohexeno na presença de hidrazina como agente redutor; ii) redução de 2-nitrofenol com $NaBH_4$ como agente redutor; e iii) descoloração de pigmentos utilizando peróxido de hidrogénio como agente oxidante. Todos os resultados experimentais foram monitorizados por cromatografia gasosa no caso de i) e por espectroscopia de UV-Vis no caso de ii) e iii).

No capítulo 2 é reportada a atividade catalítica de seis compostos de aroilhidrazona-oxi-vanádio(V), $[VOL^1(OEt)][VOL^1(OEt)(EtOH)]$ (1), $[VOL^2(OEt)]$ (2), $[Et_3NH][VO2L1]$ (3), $[VO_2(H_2L^2)]\cdot 2EtOH$ (4), $[VOL^1(\mu\text{-}O)VOL^1]$ (5) and $[VOL^2(\mu\text{-}O)VOL^2]$ (6) (H_2L^1 = 3,5-di-terc-butil-2-hidroxibenzilideno)-2-hidroxibenzohidrazida e H_2L^2 = 3,5-di-terc-butil-2-hidroxibenzilideno)-2-aminobenzohidrazida), suportados em nanodiamantes, produzidos recorrendo a diferentes metodologias. Estes compostos foram estudados como catalisadores na oxidação parcial, sob radiação de micro-ondas, de 1-feniletanol a acetofenona utilizando hidroperóxido de terc-butilo (TBHP) como oxidante. Nas condições optimizadas observou-se uma elevada seletividade em relação à formação de acetofenona. Foram efetuados estudos de reciclagem e reutilização dos catalisadores heterogéneos.

No terceiro capítulo, é descrita a atividade catalítica de nanopartículas de ouro suportadas em vários óxidos metálicos (Fe_2O_3, Al_2O_3 ZnO ou TiO_2). Foi estudado o efeito de vários parâmetros reacionais tais como suporte utilizado, quantidade de catalisador e temperatura. Foram também efetuados estudos de reciclagem dos catalisadores de ouro.

No último capítulo é estudada a atividade catalítica de um nanocompósito, formado

por cobre e MWCNT, na degradação de pigmentos, nomeadamente amarant, azul brilhante, indigo, tartazine e azul de metileno. A caracterização do nanocompósito foi feita por SEM, XRD e espectroscopia de IV.

Palavras chave: nanopartículas, catalisador magnético, ouro, vanádio, ródio, cobre, heterogenização, oxidação, hidogenação

Index

List of Figures

List of Schemes

List of Tables

List of acronyms, abbreviations and symbols

CNT	Carbon Nanotube
MWCNT	Multiwalled Carbon Nanotube
TEM	Transmission Electron Microscopy
SEM	Scanning Electron Microscope
EDS	Energy-dispersive X-ray Spectroscopy
MNP	Metal Nanoparticle
TBHP	tert-Butyl Hydroperoxide
XRD	X-ray Diffraction
IR	Infrared Spectrometry
GC	Gas Chromatography
MW	Microwave
GC-MS	Gas Chromatography–Mass Spectrometry
TLC	Thin Layer Chromatography
UV-Vis	Ultraviolet–Visible Spectroscopy
EG	Ethylene Glycol

Chapter 1 Synthesis and catalytic study of rhodium based magnetic nanoparticles

1. Introduction

In 1803, Wollaston[1], a British chemist and physicist, isolated two new elements, rhodium and palladium, from coarse platinum. Rhodium is one of the rarest and the most costly metals. This noble metal has found many catalytic applications, particularly in hydrogenation reactions owing to its specific catalytic properties[1]. This interest for rhodium catalysts concerns also the modern "nanocatalysis" area, situated at the frontier between heterogeneous and homogeneous ones, nanoparticles soluble in a liquid phase being considered as "pseudo homogeneous" systems.

Metal nanoparticles, generally defined as particles between 1 and 10 nm, have received during the last fifteen years an increasing attention from the researchers all over the world. This is mainly due to their particular matter state (very small size and quantum size effects; unusual electronic state) that provides novel physical and chemical properties and further, multiple potential applications in various areas[2, 3]. In the context of the development of nanosciences, nanocatalysis has emerged as a promising domain to answer the demanding conditions for catalyst improvement[4-9]. Thus, metallic nanospecies are expected to display the benefits of both homogenous and heterogeneous catalysts, namely high efficiency and selectivity, as well as recyclability.

Nanomaterial-based catalysts are usually heterogeneous catalysts broken up into metal nanoparticles in order to speed up the catalytic process. Metal nanoparticles have a higher surface area than bulk particles so there is increased catalytic activity because more catalytic interactions with the substrate can occur at the same time. Nanoparticle catalysts can also be easily separated and recycled with more retention of catalytic activity than their bulk counterparts[10]. These composites can play two different roles in catalytic processes: they can be the site of catalysis or they can act as a support for

catalytic processes[11]. They are typically used under mild conditions to prevent decomposition of the nanoparticles[12].

1.1 Catalytic importance in hydrogenation

Hydrogenation reactions are one of the most important methods in organic synthesis. They have extensive uses in modern industry, especially in pharmaceutical synthesis. Using a proper catalyst can not only shorten the reaction time, increase the yield, but also reduce the costs. In this field, one of the most famous rhodium catalysts is Wilkinson's catalyst[13] (**Figure 1- 1**). In the field of nanocatalysis, hydrogenation reactions are the most often cited reactions for which rhodium nanoparticles are developed[13].

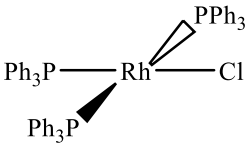

Figure 1- 1 Structure of Wilkinson's catalyst.

In order to make a rhodium catalyst more active, stable and separable from the reaction mixture, its anchorage on a solid support is usually one of the most efficient strategies. Carbon nanotubes (CNTs) due to their large length-to-diameter ratio, physical and chemical stabilities, nontoxic nature, low cost, thermal conductivity and electronic properties are widely applied as additive or support to various materials [14]. Some recent papers reported that the CNT supported catalysts had a significant high catalytic activity and selectivity compared with the non-supported ones [15].

Pan and coworkers[16] described a simple and capping agent free method to synthesize a CNT-supported rhodium catalyst for the hydrogenation of arenes at room temperature. The synthetic method, TEM image of CNT-supported rhodium nanoparticles and the hydrogenation of arenes are shown in **Figure 1- 2**. The rhodium nanocatalyst has advantages of high activity, selectivity and recyclability. They[16] also described a one-step sonochemical method to synthesize the multiwalled carbon

nanotubes (MWCNTs) supported rhodium nanoparticles. The size of the material was controlled by adding boron containing reducing agents to reduce Rh^{3+} ions. The average size of the particles is in nanoscale (2-8 nm) [17]. The size-tunable rhodium nanoparticles supported at MWCNTs have a high catalytic activity and stereoselectivity for the hydrogenation of xylene. Therefore the MWCNT supported catalysts have broad prospects for industrial applications[14].

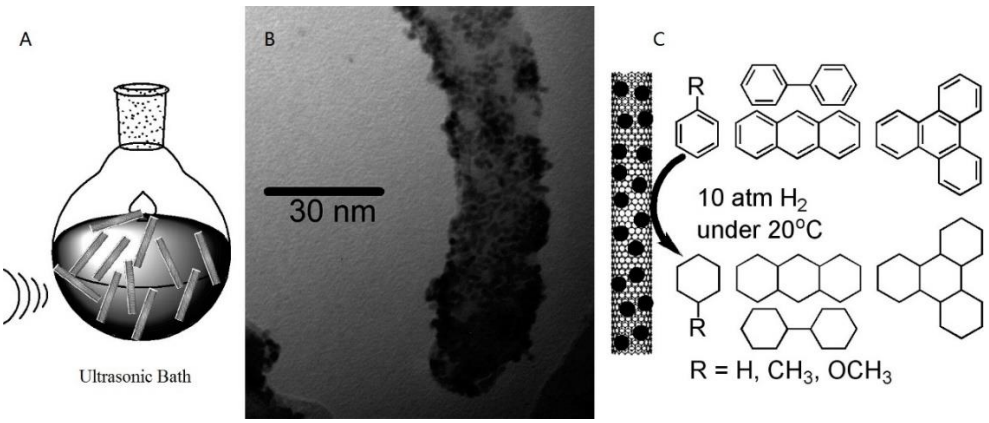

Figure 1- 2 A) Synthesis of MWCNT supported rhodium nanoparticles in ultrasonic bath. B) TEM images of MWCNT supported rhodium nanoparticles. C) Hydrogenation of arenes catalyzed by MWCNT supported rhodium nanoparticles [16].

Because of the unique properties of CNTs, they not only serve as supports for the nanoparticles, but also provide straight pathways, which are conductive, for the electrons to transfer through. Therefore MWCNTs with multiple layers have more potential than single wall CNTs. A recent paper reported by Casella and coworkers [18] described a method to synthesize the MWCNT-Rh catalyst used for electrochemical reduction of nitrate and nitrite species. They[18] acid-treated the MWCNTs to contain carboxyl acid groups on the surface. Then the acid-treated MWCNTs were treated with polished glassy carbon substrate and cycled in $RhCl_3$ containing H_2SO_4 to form glassy carbon/MWCNT-Rh catalyst. Finally the electrodes based on rhodium particles were demonstrated to have a high catalytic activity on electrochemical reduction of nitrate and nitrite species.

Another common solid support for rhodium is TiO_2 nanoparticles. TiO_2 is used as a support, because some of the chemicals, such as methanol, can be well adsorbed on its

surface. Moreover, TiO_2 can release energy, free $\cdot OH$ and $\cdot O_2^-$ to promote the process of reactions [19]. Hubert and coworkers [20] reported a simple one-pot method to prepare rhodium(0) colloid catalyst on TiO_2 in the presence of N,N-dimethyl-N-cetyl-N-(2-hydroxyethyl) ammonium chloride (HEA16Cl) and $NaBH_4$ at room temperature (**Figure 1- 3**). The colloidal catalyst is highly active and recyclable for the hydrogenation of aromatics with TOF (turnover frequency) values up to 33000 h^{-1}. The same authors compared the prepared $Rh@TiO_2$ with $Rh@SiO_2$, concluding that a higher catalytic selectivity and activity were obatained with $Rh@TiO_2$ catalysts.

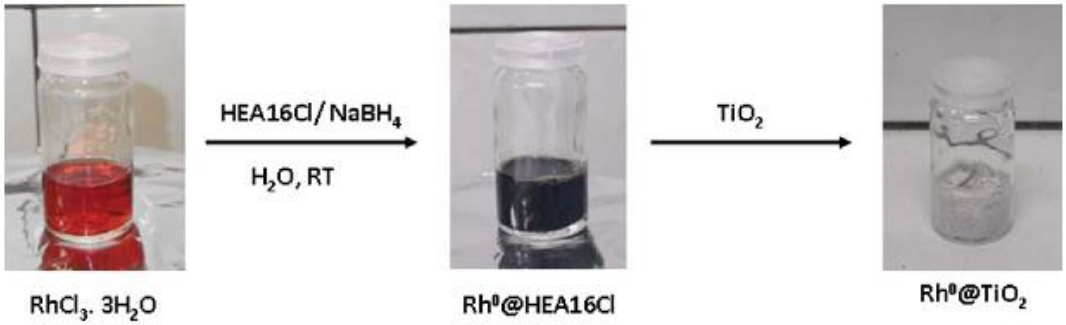

Figure 1- 3 One pot preparation of TiO_2 supported Rh(0) nanoparticles[20].

1.2 Magnetic Supports

The development of new strategies for recovery and recycling of catalysts to enhance their lifetime and minimize the consumption of auxiliary substances and devices used in achieving separations can result in significant economic and environmental benefits[21]. Ongoing research activities in this area include the use of metal nanoparticles (MNPs) [21-23]. It is widely accepted that MNPs are very active catalysts because of their large surface area and great ratio of atoms remaining at the surface, and so available to the chemical transformation of substrates. However, MNPs must be stabilized by protective agents to prevent agglomeration to the thermodynamically favoured bulk metal. In addition, the separation of the catalysts from the reaction products is also very important[24]. Attempts to improve separation include the use of biphasic aqueous/organic systems [25-27], ionic-liquid biphasic conditions [28-31] and MNPs supported on large surface area solids [21, 32-34]. From a

practical point of view, catalysts that are not soluble in the same phase as organic reactants have the inherent advantage of easy separation. However, supported catalysts may also exhibit severe problems (*e.g.* TiO_2 supported Cu causes reduction in specific surface area) with respect to catalyst recovery in liquid-phase batch reactions. In this scenario, immobilization of catalysts on magnetically separable solid supports appears as an attractive way to give better handling properties to homogeneous[35-40] and MNP catalysts[41, 42]. Solid supports containing magnetic nanoparticles can be easily separated from the product of interest due to the magnetic interaction between the magnetic nanoparticles and an external applied magnetic field. Furthermore, magnetic separation constitutes an alternative approach to traditional time- and solvent-consuming steps during the purification process since it is fast, it can be easily scaled-up, and it does not make use of other chemical reagents and solvents that present considerable environmental hazards[41].

Magnetic nanoparticles, including Co, Fe, Ni, Fe_3O_4 and their alloys, have been developed to have various industrial applications. Among all the magnetic nanoparticles, Fe_3O_4 has been applied most widely. Considering the synthesis of Fe_3O_4 nanoparticles, coprecipitation is the most facile and convenient way to synthesize iron oxide by aqueous solution. Saira-Riaz and coworkers[43] reported a simple coprecipitation method to synthesize Fe_3O_4 from dissolving $FeCl_3.6H_2O$ and $FeCl_2.4H_2O$ in deionized water with the molar ratio of 2:1. The solution was stirred and protected by argon atmosphere at 80 ℃. Then, an NaOH solution was added dropwise to adjust the pH value. Finally the Fe_3O_4 nanoparticles were obtained with size between 25 and 100 nm. With the increase in pH values, an increase in nanoparticles' diameter was observed.

In order to maintain a stable material for a longer time, to improve the stability of magnetic nanoparticles during the synthesis is important. Since the magnetic nanoparticles are sensitive to air, an efficient strategy to improve the stability[44] is applying a coating layer to protect the magnetic nanoparticles from corrosion. As reported by Ma and coworkers[45], magnetic core-shell nanoparticles of $Fe_3O_4@SiO_2@TiO_2$ were successfully prepared (**Figure 1- 4**). They synthesized

superparamagnetic Fe_3O_4 spheres using a modified one-step solvothermal method. Then the magnetic Fe_3O_4 nanoparticles were coated by SiO_2 through a sol–gel process with minor modifications[46]. Finally TiO_2 nanoparticles were coated on the surface of Fe_3O_4@SiO_2 in an ultrasonic bath (**Figure 1- 4**).

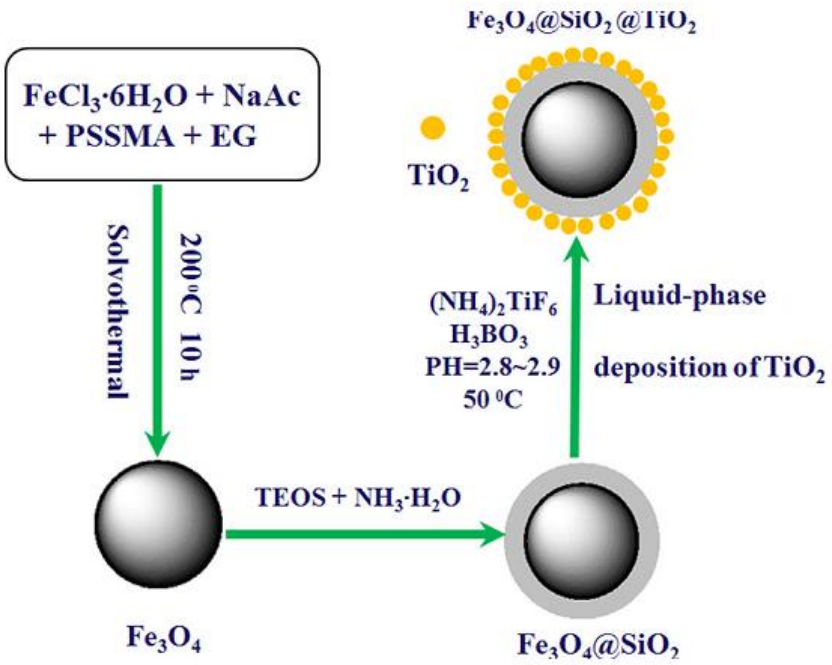

Figure 1- 4 Synthesis of Fe_3O_4@SiO_2@TiO_2 composite spheres[45].

Based on the MWCNT and TiO_2 support, in our study, we combined both of the above methods to achieve a rhodium composite that has the advantages of both CNT and TiO_2 supports. In addition, we treated the TiO_2 to form a core-shell system, which was Fe_3O_4 coated by TiO_2. To study the catalytic properties of the synthesized nanoparticles, we used our nanoparticles as catalysts for hydrogenation reactions (**Table 1- 1**) and oxidation of pigments (**Table 1- 2**). Thanks to the supermagnetic property of Fe_3O_4 nanoparticles, the rhodium based nanoparticles can inherit the magnetic property. As a result, the catalysts are easier to separate and be reused for several cycles. To the best of our knowledge, there is no report in the literature using this method to support rhodium and analysed using hydrogenation of nitroarenes and cyclohexene. We also report the possibility of the decoloration of several pigments using our nanoparticles as catalysts.

2. Experimental

2.1 Materials

Ethyl acetate (99.9%), acetone (C_3H_6O; purity of 99.8%), diethyl ether (99.97%) acetonitrile (ACN, 99.99%) were from Fisher Scientific. Nitric acid (HNO_3, purity of 65%) and hydrochloric acid (HCl; purity of 37%) were purchased from Panreac. 2-nitrophenol, 2-aminophenol, 4-nitrophenol, 4-aminophenol, nitrobenzene, aniline, cyclohexene (C_6H_{12}; purity >99%), hydrogen peroxide (H_2O_2; purity of 30% v/v), cyclohexane, $(NH_4)_2Fe(SO_4)_2$•$6H_2O$, $FeCl_3$•$6H_2O$, solid TiO_2 nanopowder (< 25 nm), titanium(IV) isopropoxide (98%) $Ti\{OCH(CH_3)_2\}_4$ solution, absolute ethanol (EtOH; purity of 99.9%), isopropanol, $NaBH_4$, hydrazine hydrate, $RhCl_3$, NaOH, $MgSO_4$ were all from Sigma-Aldrich. MWCNTs were supplied by Bayer Materials. The pigments of methylene blue, brilliant blue, tartrazine and amaranth were from Merck. All chemicals used were analytical grade without further purification. TLC plates (Silica Gel 60) were from WVR.

2.2 Instruments

2.2.1 Characterization

The synthesized nanoparticles were characterized by scanning electron microscope (SEM), transmission electron microscopy (TEM) and energy-dispersive X-ray spectroscopy (EDS) techniques. SEM images of the synthesized nanoparticles were performed on a scanning electron microscope JEOL 7001F with Oxford light elements EDS detector and EBSD detector. TEM measurements were carried out on a Transmission Electron Microscope Hitachi 8100 with ThermoNoran light elements EDS detector and digital image acquisition. X-Ray Photoelectron Spectrometer (XPS) measurements were performed with ESCALAB 250 XPS spectrometer,

2.2.2 Catalysis

For catalytic purposes it was used a heating plate with a set temperature and

agitation function, to keep the reaction at a constant temperature, making convection possible and thus preventing diffusion to become a restrictive factor. Microwave reactor (MW) Anton Paar Monowave 300 was used for the MW-assisted hydrogenation of cyclohexene and nitroarenes. The gas chromatograph MFC 8000 from Fisons instruments, was utilized for the analysis of the product containing water phase. It is a GC with flame ionization detector and capillary column (DB-WAX, column length: 30 m; internal diameter: 0.32 mm) and the Jasco-Borwin v.1.50 software. 0.045 μL of the sample got injected and subsequently analyzed. A temperature program with an initial temperature of 100 ℃ (1 min) and a ramp of 10 ℃/min with a final temperature of 180 ℃ (1 min).

GC-MS (PerkinElmer Clarus 600C Mass spectrometer, Clarus 600 Gas Chromatography) was used to identify compounds. UV-visible spectroscopic measurements were carried out on a PerkinElmer Lambda 750 UV-Visible spectrophotometer.

2.3 Synthesis

2.3.1 Synthesis of Fe_3O_4@TiO_2 core-shell system

The preparation of Fe_3O_4@TiO_2 core-shell particles was separated into two parts. The first step was the synthesis of magnetic Fe_3O_4 nanoparticles using the co-precipitation method. 1 mmol of $(NH_4)_2Fe(SO_4)_2$•$6H_2O$ and 2 mmol of $FeCl_3$•$6H_2O$ were added to 80 mL of H_2O in a round bottom flask. The mixture was stirred at 600 RPM in a 50 ℃ oil bath. Then a 1 mol/L NaOH solution was dropped into the mixed solution until the pH value reached 10. After that, instead of brown solid particles, black precipitates appeared rapidly in the flask, which was Fe_3O_4 nanoparticles (**Scheme 1-1**). The reaction was stopped and cooled down to room temperature. The Fe_3O_4 precipitate was filtered and washed with distilled water and ethanol several times. Then the Fe_3O_4 nanoparticles were dried in oven and collected for next synthesis. TEM and SEM images, and EDS are shown in **Figures 1- 8**, **1- 9** and **1- 10** respectively.

$$(NH_4)_2Fe(SO_4)_2{\bullet}6H_2O + FeCl_3{\bullet}6H_2O \xrightarrow{NaOH,\ 50°C,\ 600RPM} Fe_3O_4$$

Scheme 1- 1 Synthesis of Fe_3O_4 magnetic nanoparticles.

The second step is the coating of Fe_3O_4 by TiO_2 [47]. The core-shell system of Fe_3O_4 was prepared by 0.43 mmol (100 mg) of Fe_3O_4 nanoparticles and 3.38 mmol (1 mL) of titanium(IV) isopropoxide (98%) $Ti\{OCH(CH_3)_2\}_4$ solution in 250 mL of dry ethanol stirred under 1500 RPM. Then 7 mL of dry ethanol and 1 mL of distilled H_2O were added into the mixture. The mixed solution was heated at reflux (75 ℃) under magnetic stirring for 3 hours (**Figure 1- 5**). At the end, the samples were cooled down till room temperature and separated magnetically. The particles were washed with ethanol and distilled water, dried in oven at 80 ℃ and stored for future applications. TEM and SEM images, and EDS are shown in **Figure 1- 11**, **1- 12** and **1- 13** respectively.

Figure 1- 5 Synthesis of Fe_3O_4@TiO_2.

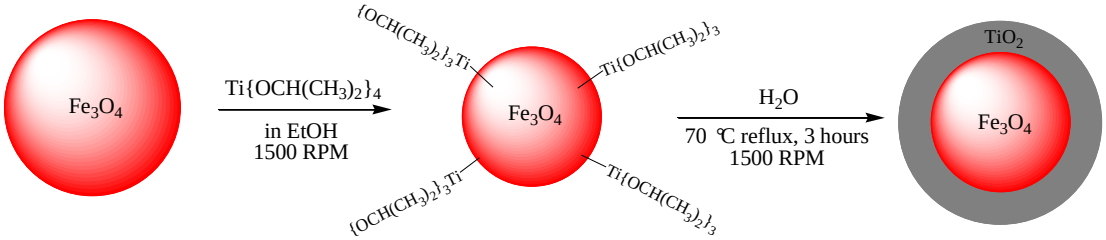

Scheme 1- 2 Representation of the synthesis of Fe_3O_4@TiO_2 core-shell nanoparticles.

2.3.2 Functionalization of MWCNT

According to literature, the functionalization of these nanomaterials can be performed with various methods, such as ball milling, plasma treatment and acid treatment[48]. In the present study, a non-destructive acid treatment was carried out. For this purpose, 1 g of MWCNT was added to 200 mL of concentrated HCl (37%) in a round bottom flask (500 mL). After that, the mixture was stirred for 2 hours. Subsequently, a vacuum filtration was developed with several washing steps (deionized water) until a pH= 7 was obtained. Finally, the resulting material was dried in a convection oven at 40 ℃ overnight.

2.3.3 Synthesis of size-tunable rhodium nanoparticles supported on carbon nanotubes

For this procedure, 80 mg of carboxyl group functionalized multiwalled carbon nanotubes (MWCNTs) were charged in a 250 mL flask containing 80 mL of ethanol. The solution was sonicated for 1 h to disperse the carbon nanotubes. After, 0.16 mmol (33.44 mg) of $RhCl_3$ and 1.60 mmol (60.53 mg) of $NaBH_4$ were added. The mixture was sonicated for another 30 min. The formation and deposition of Rh nanoparticles on the MWCNTs surface was complete after this procedure. Finally, the MWCNT-supported rhodium nanoparticles were filtered, washed with ethanol several times, and dried at 80 ℃ for 12 h in the oven. TEM and SEM images, and EDS are shown in **Figures 1- 19**, **1- 20** and **1-21** respectively.

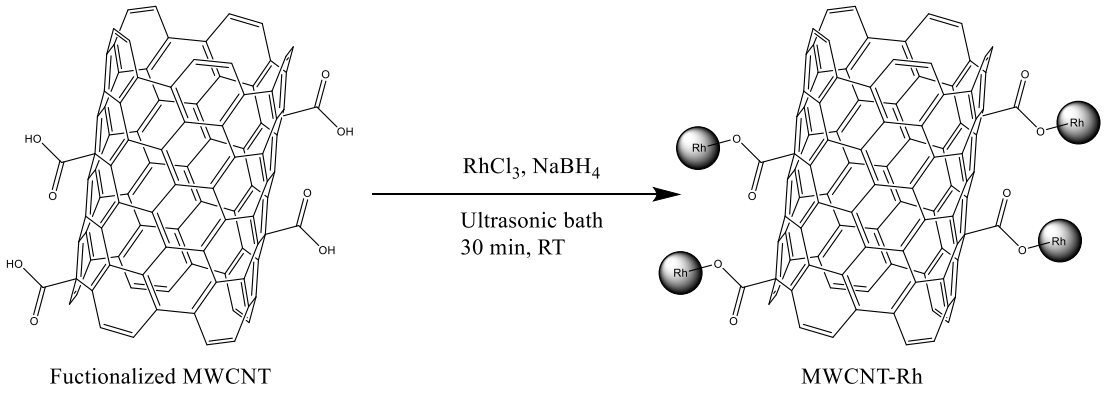

Scheme 1- 3 Proposed representation of the synthesis of MWCNT-Rh.

2.3.4 Synthesis of Rh supported on Fe_3O_4@TiO_2

In this procedure, rhodium(0) was supported at Fe_3O_4@TiO_2. Firstly, 50 mg of Fe_3O_4@TiO_2 nanoparticles and 0.1 mmol (20.9 mg) of $RhCl_3$ were added in 50 mL of isopropanol solution in a 250 ml round bottom flask. The mixture was stirred under 1500 RPM at room temperature. Then 2.9 mmol (110.0 mg) of $NaBH_4$ were added into the solution (**Figure 1- 6**). After 3 h, the precipitate was filtrated, washed and dried in oven at 80 ℃ over night. TEM and SEM images, and EDS are shown in **Figures 1- 22**, **1- 23** and **1- 24** respectively.

Figure 1- 6 Synthesis of Rh- Fe_3O_4@TiO_2.

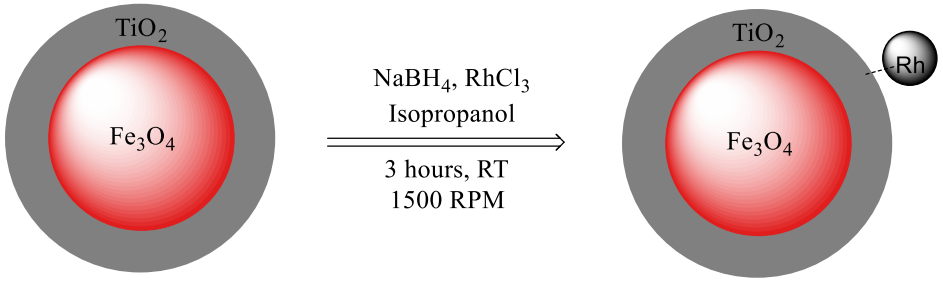

Scheme 1- 4 Representation of the synthesis of Fe_3O_4@TiO_2-Rh.

2.3.5 Synthesis of MWCNT-Rh supported on Fe_3O_4@TiO_2

This procedure is the same as the synthesis of Fe_3O_4@TiO_2-Rh system. 50 mg of Fe_3O_4@TiO_2 nanoparticles and 20 mg of MWCNT-Rh were added in 50 mL of isopropanol solution. The mixture was stirred under 1500 RPM at room temperature. Then 2.9 mmol (110 mg) of $NaBH_4$ were added into the mixture. After 12 h of reaction the products were filtrated and dried in oven at 80 ℃ over night. TEM and SEM images,

and EDS are shown in **Figures 1- 25**, **1- 26** and **1- 27** respectively.

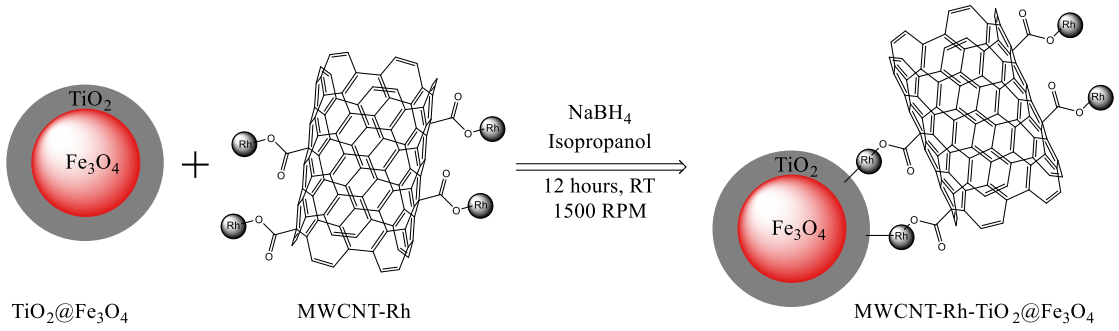

Scheme 1- 5 Proposed **r**epresentation of the synthesis of Fe_3O_4@TiO_2-Rh-MWCNT.

2.4 Catalytic studies

2.4.1 MW-assisted catalytic hydrogenation transfer of cyclohexene and nitroarenes

First of all, it is worth mentioning that, as reported[49, 50], Rh has a high catalytic activity in hydrogenation reactions. Therefore we used hydrogenation transfer of cyclohexene and nitroarenes as a model to study the catalytic activity of our Rh nanoparticles. Instead of traditional thermal heat source, microwave radiation was used in the hydrogenation of cyclohexene and nitroarenes. With the assistance of microwave reactor mixtures can absorb microwave energy and heat up from the interior of the system towards the boundaries, which works conversely to conductive-convective heat transfer[51]. In this case, the reaction is more selective and products are precipitated selective [52].

In this procedure, 1 mmol of substrate, 3 mmol (140 μL) of hydrazine hydrate and 10 mg of catalyst were taken into an oven dried G30 reaction tube equipped with a screw cap. 2 mL of ethylene glycol was added into the reaction mixture. The reaction was then irradiated in the microwave reactor for 10 minutes at 80 ℃. After the reaction, the mixture was cooled down to room temperature, the catalyst was easily separated magnetically, and the product could be removed by extraction with ethyl acetate (3*2 mL) and distilled water (1 mL). The combined organic layers were dried over anhydrous $MgSO_4$ and the solvent was removed. During some of the reactions, thin layer chromatography (TLC) was used to track the products of the reactions.

After extraction, the samples were tested by GC or GC-MS. Based on the boiling points of the substrate, internal standard and product, the program of GC was maintained at 120 ℃ for 1 min, heating from 120 ℃ to 200 ℃ at a rate of 10 ℃/min, holding at 200 ℃ for 1 min and then cooling to 120 ℃. The program of GC-MS for both FID and MS channels was holding at 50 ℃ for 1 min, heating from 50 ℃ to 250 ℃ at a rate of 13.33 ℃/min, then heating from 250 ℃ to 330 ℃ at a rate of 26.67 ℃/min, at last cooling down to 50 ℃.

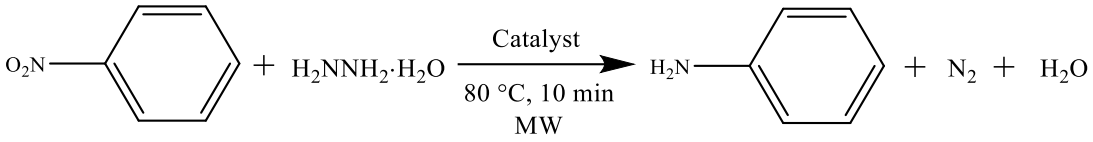

Scheme 1- 6 Hydrogenation transfer of nitrobenzene catalyzed by different nanoparticles.

Table 1- 1 MW-assisted catalytic hydrogenation transfer of different substrates.

Entry	Catalyst	Substrate
1	-	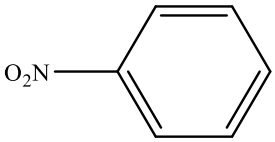 nitrobenzene
2	Fe_3O_4@TiO_2	
3	MWCNT	
4	MWCNT-Rh	
5	$RhCl_3$	
6	Fe_3O_4@TiO_2-Rh	
7	Fe_3O_4@TiO_2-Rh-MWCNT	
8	-	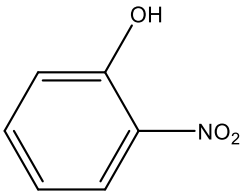 2-nitrophenol
9	Fe_3O_4@TiO_2	
10	MWCNT	
11	MWCNT-Rh	
12	$RhCl_3$	
13	Fe_3O_4@TiO_2-Rh	
14	Fe_3O_4@TiO_2-Rh-MWCNT	
15	-	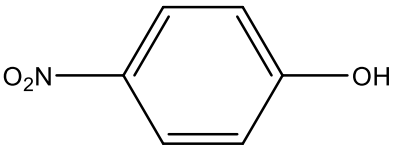 4-nitrophenol
16	Fe_3O_4@TiO_2	
17	MWCNT	
18	MWCNT-Rh	
19	$RhCl_3$	
20	Fe_3O_4@TiO_2-Rh	
21	Fe_3O_4@TiO_2-Rh-MWCNT	

22	-	
23	$Fe_3O_4@TiO_2$	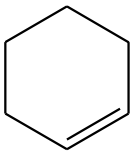
24	MWCNT	
25	MWCNT-Rh	
26	$RhCl_3$	
27	$Fe_3O_4@TiO_2$-Rh	cyclohexene
28	$Fe_3O_4@TiO_2$-Rh-MWCNT	

Nitrobenzene was chosen as a model to test the catalytic recycling properties of $Fe_3O_4@TiO_2$-Rh-MWCNT, because it's the highest active catalyst for the hydrogenation reactions. Four consecutive cycles of reactions were carried out (**Table 1- 2**). For each cycle, the catalyst was separated by using a magnet to attract the solid phase and dropping off the liquid phase. Then the solid was dried by compressed air and resued for a new set of nitrobenzene hydrogenation experiment.

Table 1- 2 Recycling experiments of the MW-assisted hydrogenation (10 min) of nitrobenzene with hydrazine at 80 ℃ catalyzed by $Fe_3O_4@TiO_2$-Rh-MWCNT.

Entry	**Catalyst**	**m(mg)**[a]	**Substrate**
7	$Fe_3O_4@TiO_2$-Rh-MWCNT 1st cycle	5.2	
29	$Fe_3O_4@TiO_2$-Rh-MWCNT 2nd cycle	5.2	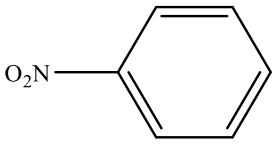
30	$Fe_3O_4@TiO_2$-Rh-MWCNT 3rd cycle	5.2	
31	$Fe_3O_4@TiO_2$-Rh-MWCNT 4th cycle	5.2	nitrobenzene

[a] There was some loss in mass during separation in each cycle.

2.4.2 Catalytic reduction of 2-nitrophenol with $NaBH_4$.

Firstly 0.03 mmol (4 mg) of 2-nitrophenol were dissolved in a flask by 7.5 mL of acetonitrile. Then 5 mg of catalyst (MWCNT-Rh or $Fe_3O_4@TiO_2$-Rh-MWCNT) was added into the solution. The mixture was magnetically stirred at room temperature. 0.3 mmol (12 mg) of $NaBH_4$ was dissolved in 2 mL of acetonitrile. Once the reducing agent was dropped into the mixture, the mixed solution was carried out 30 μL to 2970 μL of acetonitrile into a 10 mm quartz cell every 5 minutes. The diluted solution was tested by UV-Vis (PerkinElmer Lambda 750 UV-Visible spectrophotometer).

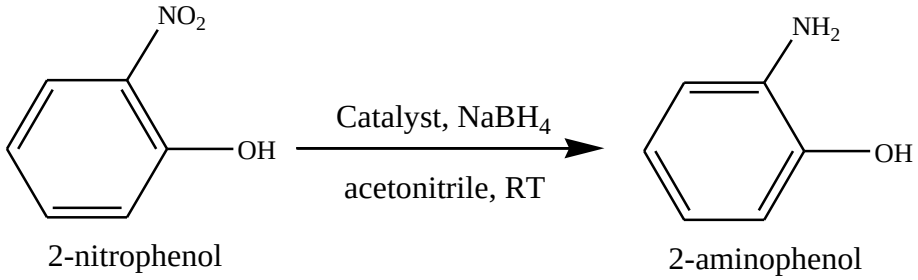

2-nitrophenol 2-aminophenol

Scheme 1- 7 Reduction of 2-nitrophenol catalyzed by MWCNT-Rh or Fe_3O_4@TiO_2-Rh-MWCNT.

2.4.3 Catalytic decoloration of organic pigments

In this procedure, three pigments (brilliant blue, amaranth and tartrazine) (**Table 1-3**) were chosen as models to study the catalytic activity of Fe_3O_4@TiO_2-Rh-MWCNT nanoparticles. UV-Vis was used to monitor the decoloration. The pH value and the initial concentration of pigment were also investigated.

Firstly, the pigment solution was prepared in a concentration of 1 g/L. After, this solution was introduced into a 10 mm quartz cell and diluted by adding solvent. Then 5 mg of catalyst was added. After, 100 μL of 30% H_2O_2 solution was dropped into the cell. A UV test was carried out every two minutes.

Table 1- 3 Structure of the pigments used in the catalytic study.

Structure	Name
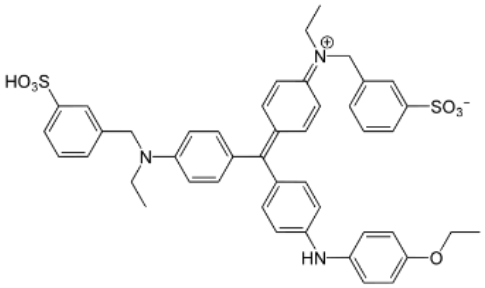	brilliant blue[a]
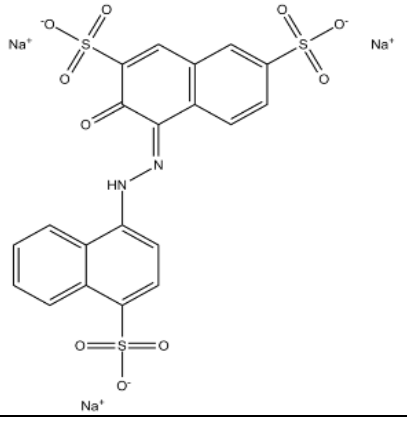	amaranth[b]
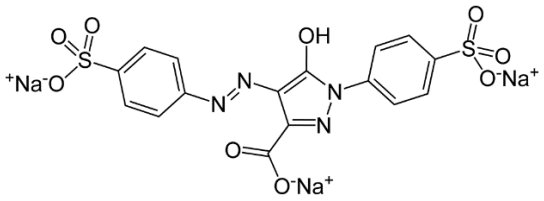	tartrazine[c]

IUPAC name of each pigment, [a] ethyl-[4-{[4-[ethyl-[(3-sulfophenyl)methyl]amino]phenyl]-(2-sulfophenyl)methylidene]-1-cyclohexa-2, 5-dienylidene]-[(3-sulfophenyl)methyl]azanium; [b] Trisodium(4E)-3-oxo-4-[(4-sulfonato-1-naphthyl)hydrazono]naphthalene-2,7-disulfonate; [c] Trisodium(4E)-5-oxo-1-(4-sulfonatophenyl)-4-[(4-sulfonatophenyl)hydrazono]-3-pyrazolecarboxylate

3. Results and discussion

3.1 Synthesis of metallic nanoparticles

One of the aims of the work developed was to apply an easy method, with simple conditions, to achieve the production of the chosen nanomaterials.

Preparation of Fe_3O_4 nanoparticles

The preparation of Fe_3O_4 nanoparticles was made by the co-precipitation method[53]. In this procedure the most important step to control is the speed of adding base to the solution, that has an influence on the product formed. When the base solution (NaOH) was added dropwise, the color of the product was brown and the magnetic strength was weak. Therefore, the addition was made immediately, which afforded strong magnetic nanoparticles (**Figure 1- 7(A)**). Moreover, the temperature also influenced the results. Since we did not use nitrogen to protect our reaction medium, a higher temperature (80 ℃) made Fe_3O_4 nanoparticles easily to be oxidized to Fe_2O_3 in the presence of air. When the reactions were made at 80 ℃, the product was a mixture of Fe_2O_3 and Fe_3O_4, with low magnetism (**Figure 1- 7(B)**). The color of the nanoparticles mixture is brown instead of the black color from Fe_3O_4 nanoparticles.

(A) (B)

Figure 1- 7 Fe_3O_4 nanoparticles produced at (A) 50 ℃ and (B) 80 ℃.

Using the optimized method regarding the addition of base and control of

temperature (fast addition and 50 ℃) the yield obtained was 72%. Because the separation was made just by adding a magnet to the surface of the round bottom flask, the used procedure is an easy way to synthesize the Fe_3O_4 magnetic nanoparticles.

The synthesized Fe_3O_4 nanoparticles were characterized by TEM, SEM and EDS. TEM images (**Figure 1- 8**) show that the average size of the particles is smaller than 50 nm. The surface of Fe_3O_4 nanoparticles are observed in SEM images (**Figure 1- 9**). Some of the nanoparticles were aggregated to form bigger particles. In EDS (**Figure 1-10**), as we expect, Fe presents the highest percentage in the nanoparticles. There is still some Na, S and Cl elements in the particles, indicating that more times of washing by distilled water are necessary to remove them.

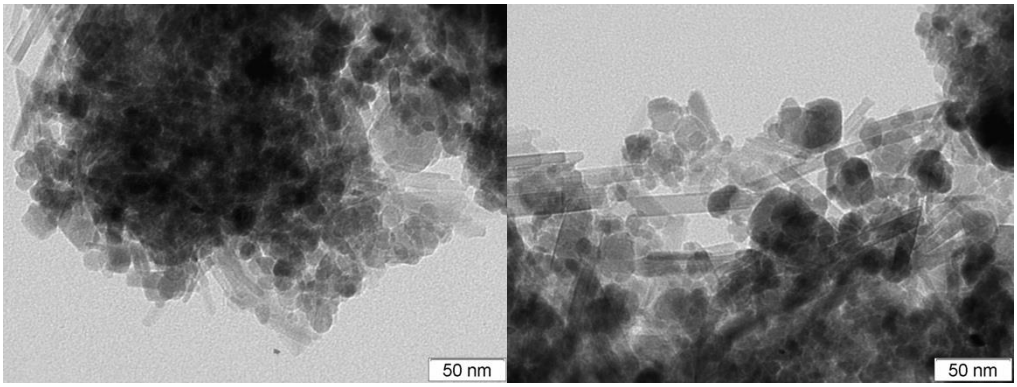

Figure 1- 8 TEM images of Fe_3O_4 nanoparticles.

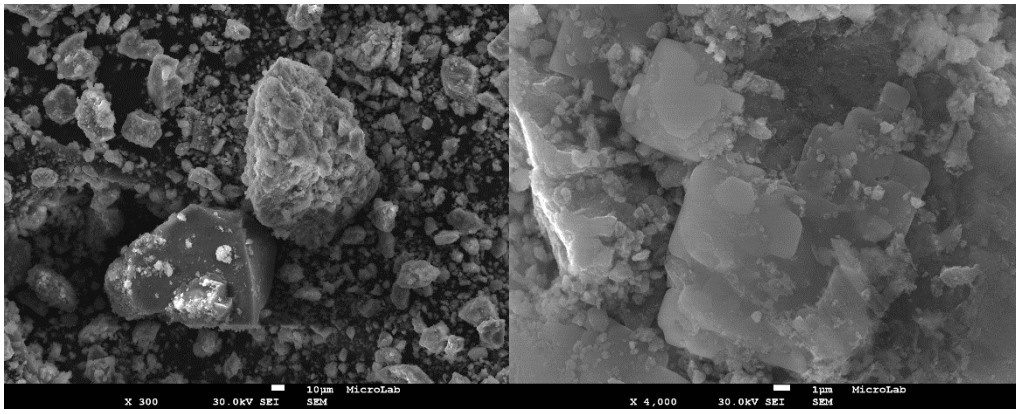

Figure 1- 9 SEM images of Fe_3O_4 nanoparticles.

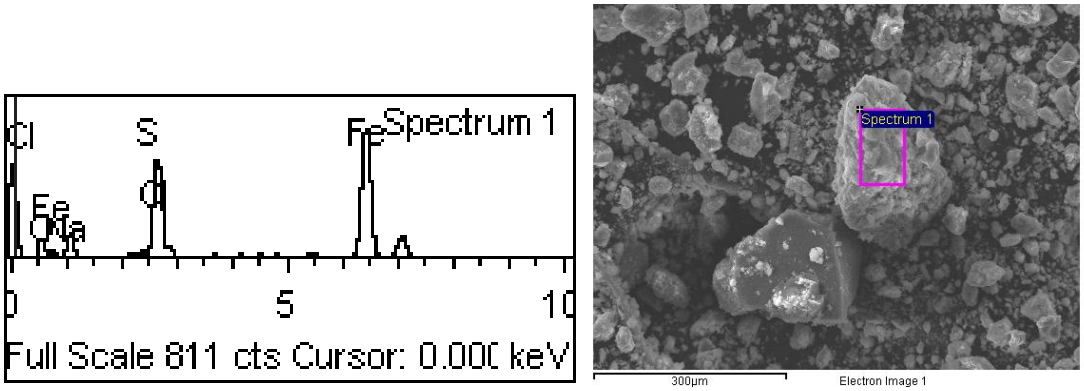

Figure 1- 10 EDS spectrum of Fe_3O_4 nanoparticles.

Preparation of Fe_3O_4@TiO_2 nanoparticles

In the preparation of Fe_3O_4@TiO_2 core shell nanoparticles, titanium and iron were linked by Ti-O-Fe bond. Due to the presence of TiO_2, the degree of whiteness became higher.

It is important to mention that the solvent also makes a difference in preparation of Fe_3O_4@TiO_2 core-shell nanoparticles. Because the source of TiO_2 was titanium(IV) isopropoxide (98%) $Ti\{OCH(CH_3)_2\}_4$ solution, it was soluble in isopropanol. So when we used isopropanol as the solvent, TiO_2 could not coat on Fe_3O_4, because isopropanol did not promote the formation of TiO_2. When absolute ethanol was used as solvent together with water (sol-gel synthesis), TiO_2 was generated *in situ* and dispersed. For that reason we chose ethanol as the solvent of the reaction. Moreover, the order of adding the chemicals also influenced the coating. From the tests performed, the best order involves adding titanium(IV) isopropoxide (98%) solution first and dispersed it for one or two minutes. The remaining reagents order did not influence the outcome of the reaction.

After the reaction, we can easily separate the particles magnetically. All the liquid was decanted having a magnet at the bottom of the flask and the magnetic nanoparticles attached to the magnet surface through the glass. Herein some particles without magnetic property or with a low magnetic property were also dropped together with the solvent. The particles that showed strong magnetic property stayed attached the bottom due to the presence of the magnet. After being washed with water, filtrated and dried in oven over night, the particles were whiter than Fe_3O_4 and darker than TiO_2. The core-

shell system Fe_3O_4@TiO_2 was successfully synthesized, and their magnetism did not changed, even after several weeks. The nanoparticles were composed of Fe_3O_4 magnetic particles coated with TiO_2. The characterization by TEM (**Figure 1- 11**) shows that the average diameter of the core shell particles is between 100 nm to 200 nm, and SEM (**Figure 1- 12**) shows a the typical surface for a ceramic (metal oxide) coating. EDS shows the presence of titanium, iron and oxygen **(Figure 1- 13)** and there was only a small amount (5.77%) of carbon, therefore indicating that the purification step (washing) was efficient.

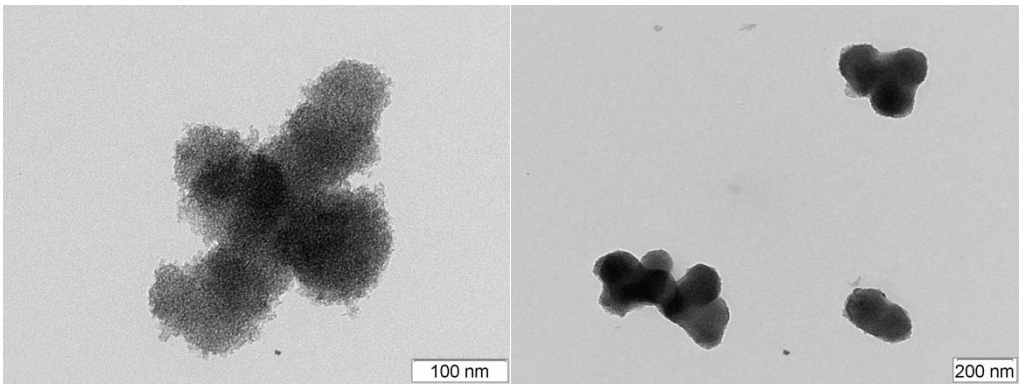

Figure 1- 11 TEM images of Fe_3O_4@TiO_2 nanoparticles.

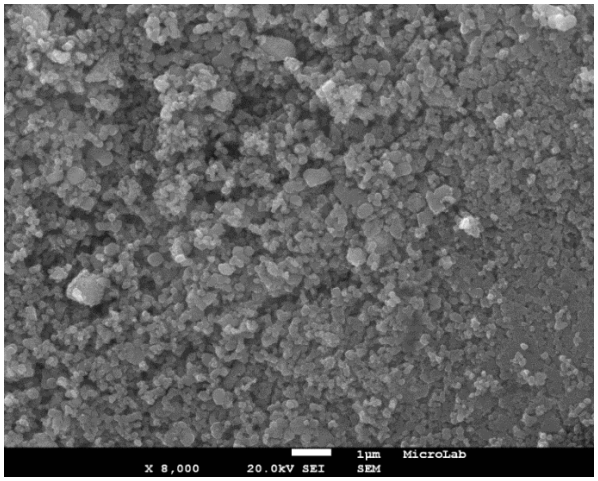

Figure 1- 12 SEM image of Fe_3O_4@TiO_2 nanoparticles.

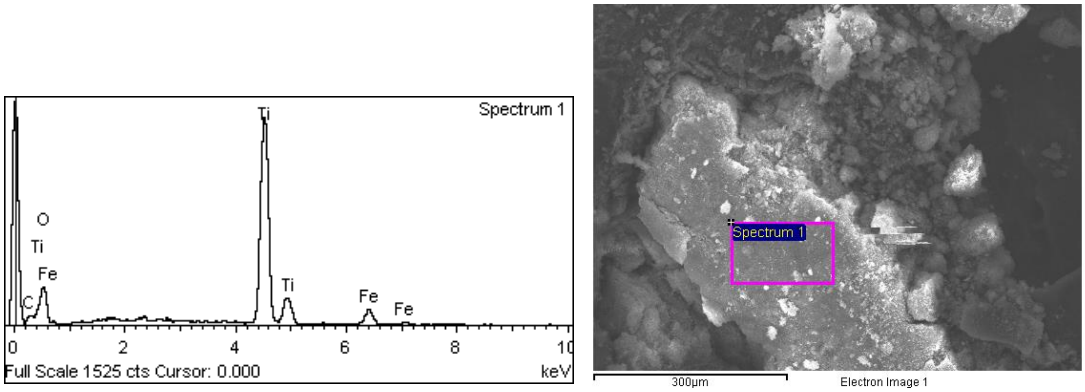

Figure 1- 13 EDS spectrum of Fe_3O_4@TiO_2 nanoparticles.

Functionalization of WMCNT

The characterization of the starting material (MWCNT) was performed to confirm purity. Due to the intrinsic nature of MWCNT, the main structural features are closely related to graphite. For this reason, diffraction techniques are used to determine the purity of the starting material.

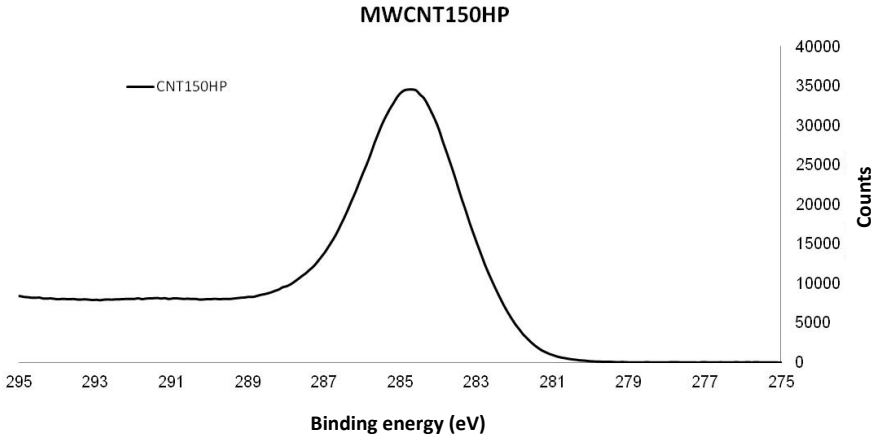

Figure 1- 14 XPS spectra of Baytubes 150HP.

From the spectra, it's possible to observe a peak in the region of 285 eV, confirmed by literature[54], attributed to the presence of oxygen, probably in the extremities of the tubes, that are easy to functionalize.

The X-ray pattern of the MWCNT, in the figure below, displays the presence of two peaks at 25.80 ° (3.47 Å) and 42.75 ° (2.12 Å) assigned to (002) and (100) diffractions corresponding to the interlayer spacing (0.34 nm) of the nanotube and

reflection of the carbon atoms, respectively, in good agreement with that of the previous literature[55].

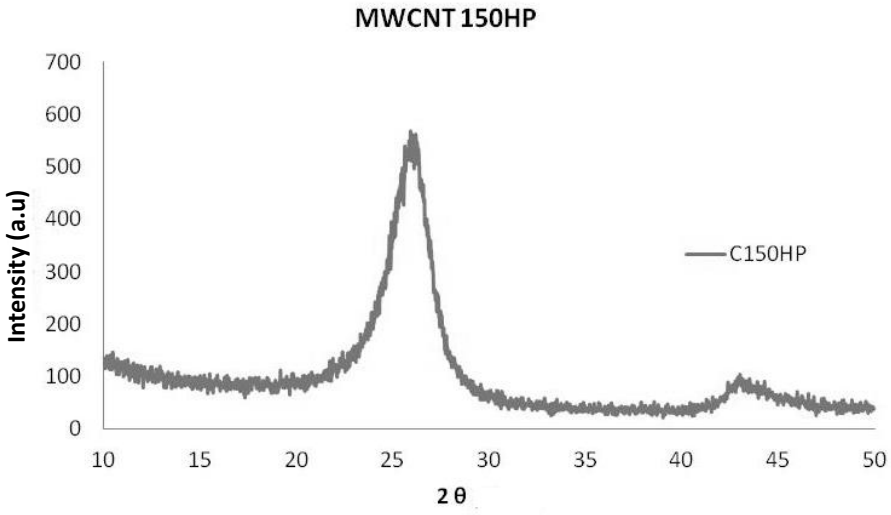

Figure 1- 15 XRD analysis of Baytubes 150HP.

TEM analysis (**Figure 1- 16**) of untreated MWCNT shows a large number of MWCNT bundles, with several concentrically and well defined layers. We cannot detect the presence of other morphological forms of carbon, namely Buckminsterfulerene (C_{60}), Fulerene (C_{540} or C_{70}) or amorphous carbon, which confirms the high purity of the initial sample.

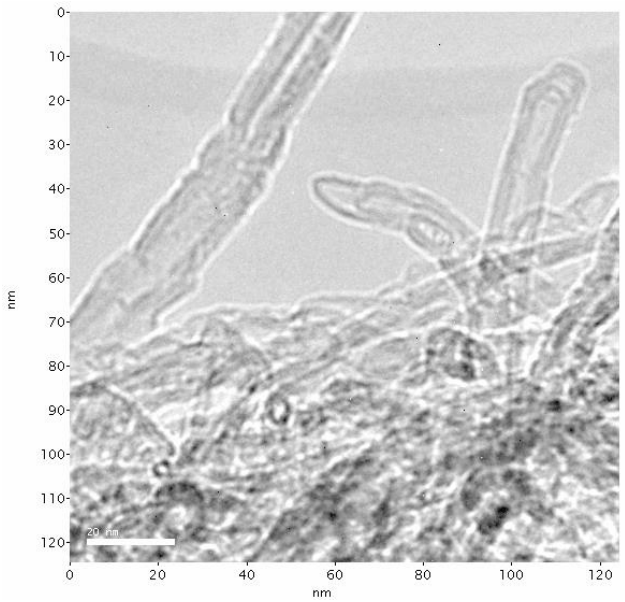

Figure 1- 16 TEM analysis of Baytubes 150HP

SEM studies (**Figure 1- 17**) show that the untreated MWCNT (**A**) are more entangled than the functionalized one (**B**). This proves that the acid treatment performed was effective.

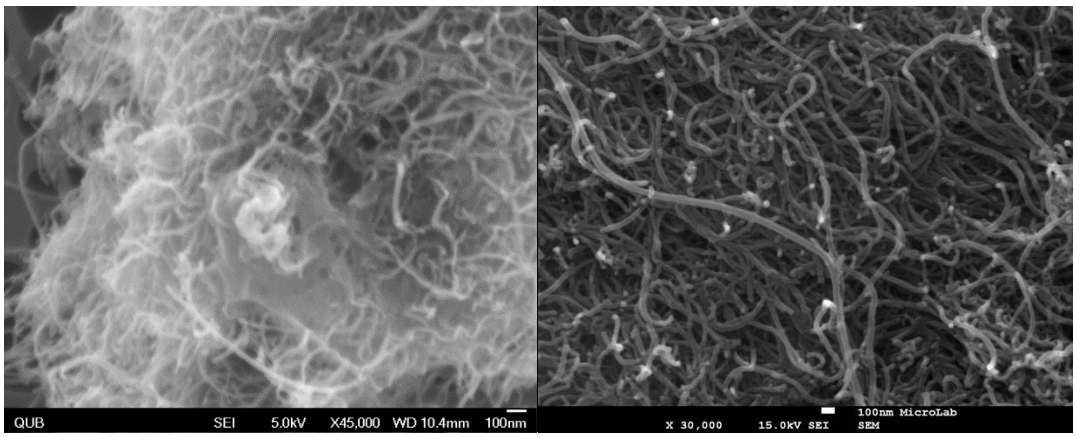

(A) (B)

Figure 1- 17 SEM image of (A) Baytubes 150HP and (B) functionalized MWCNT.

Functionalized MWCNTs produced in this work were also characterized using Raman spectroscopy. Raman spectroscopy is a powerful non-destructive tool to characterize carbonaceous materials, particularly for distinguishing ordered and disordered crystal structure of carbon. The typical features of carbon in Raman spectra are the G band (graphite) around 1582 cm^{-1} and the D band (defect) around 1350 cm^{-1}. The G band is usually assigned to the E_2g photons of C sp^2 atoms, while the D band is a breathing mode of k-point phonons of A_1g symmetry. **Figure 1- 18** shows the Raman spectra of pure MWCNTs and functionalized MWCNTs used in the present work. The Raman spectra were measured using 514.5 nm laser excitation over the Raman shift interval of 1000–2000 cm^{-1}. The D- and G-bands of pure MWCNTs at around 1290 and 1590 cm^{-1}, corresponding to defect and disorder-induced modes, and the in- plane E_2g zone centred mode, are clearly observed in pure MWCNTs.

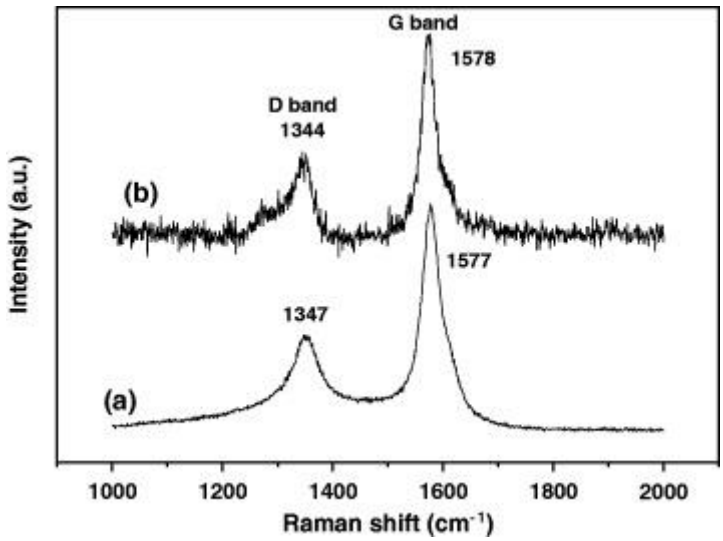

Figure 1- 18 Raman spectra of (a) pure MWCNTs and of (b) factionalized MWCNTs.

Preparation of MWCNT-Rh

The preparation of MWCNT-Rh was a one-step sonochemical synthetic method[17]. Rhodium was supported on the surface of functionalized MWCNT. The carboxylate groups serve as an anchor sites for rhodium nanoparticles on the MWCNT. And the chemical bonding between carboxylate MWCNT and rhodium is –COO-Rh. The TEM images were shown in **Figure 1- 19**. The rhodium nanoparticles are dispersed on the surfaces of carboxylate functionalized MWCNT. As reported in the literature[56], the particle size of rhodium is related to the reducing strength of the reduction agent. In our case, we used a very strong reducing agent which was $NaBH_4$. It produced rhodium nanoparticle on the surfaces of functionalized MWCNT with 10 nm in diameter. The surface of MWCNT-Rh can be observed in **Figure 1- 20**. Rhodium particles were attached to the surface of MWCNT which are the big white dots in the figure. EDS studies (**Figure 1- 21**)show that at the specific position, the loading of rhodium was low and various of elements from reducing agent and raw materials are presented. As we discussed previously, more washing steps are supposed to be necessary to remove them. The silica and titanium elements may come from the other samples.

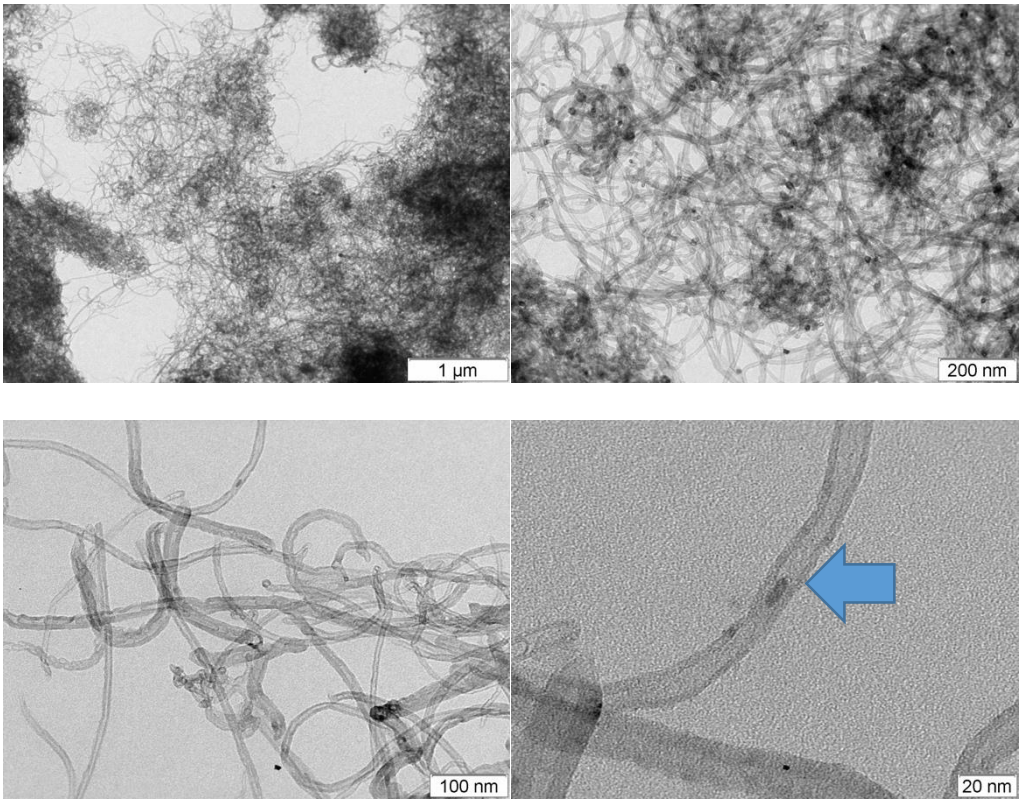

Figure 1- 19 TEM images of MWCNT-Rh nanoparticles. The dark points on the nanotubes surface are rhodium.

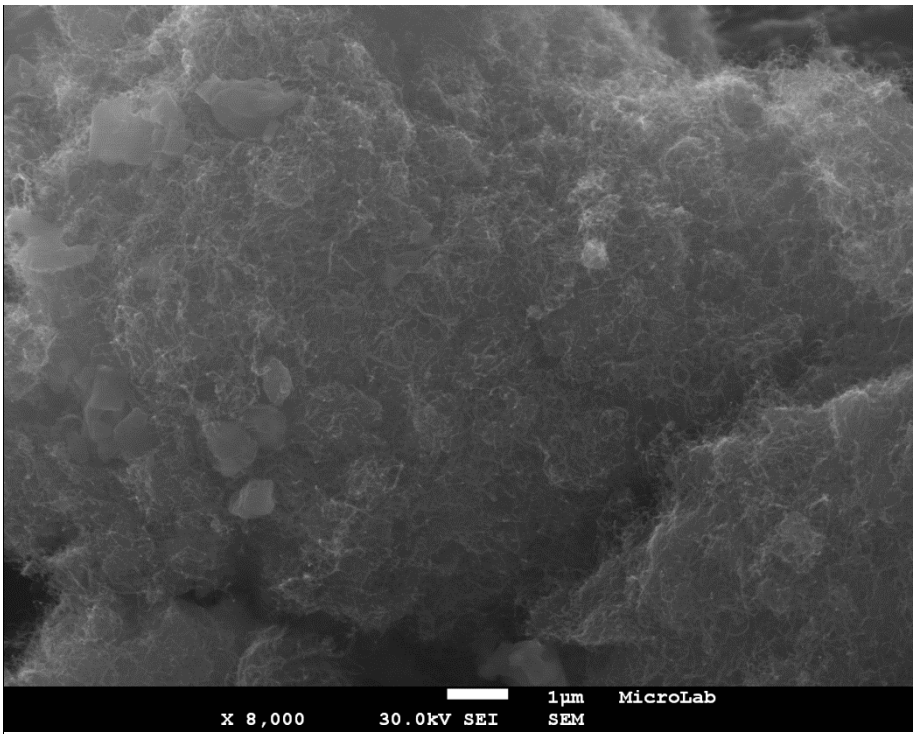

Figure 1- 20 SEM image of MWCNT-Rh nanoparticles.

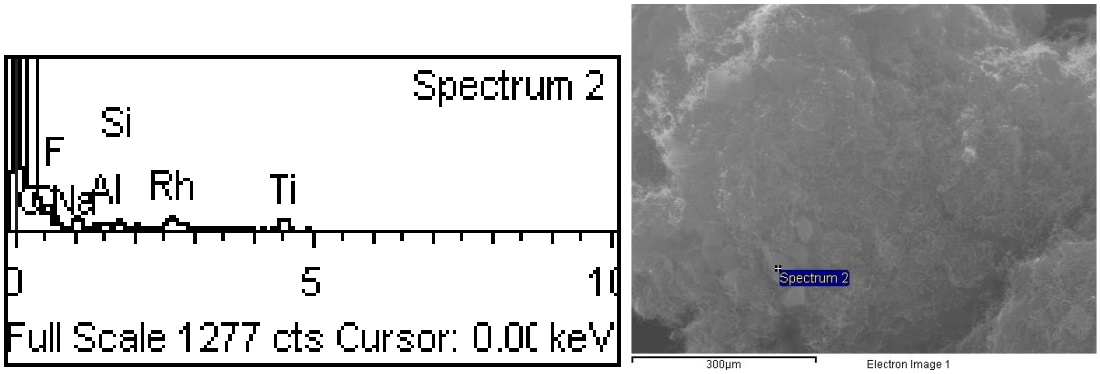

Figure 1- 21 EDS spectrum of MWCNT-Rh nanoparticles.

Preparation of Fe_3O_4@TiO_2-Rh

In the preparation of Fe_3O_4@TiO_2-Rh nanoparticles, rhodium nanoparticles are deposited toTiO_2 (**Scheme 1- 4**). The TEM analysis (**Figure 1- 22**)shows that the size of the particles becomes bigger. The average size stays between 100 nm to 200 nm. In the SEM images (**Figure 1- 23**), from the shape of the core shell nanoparticles, we can find that the particles are easily aggregated to each other. The rhodium is attached to the surface of the core-shell nanoparticles. From the EDS (**Figure 1- 24**), we can find that there are a lot of elements that we don't expect. The purity of Fe_3O_4@TiO_2-Rh is not high. The impurities may come from other samples. The mechanism of this reaction probably is that metallic ion goes into the lattice of TiO_2 and replaces titanium. Thus a distortion of the lattice or a new oxygen vacancy is formed. In our case, Rh^{3+} is mixed with TiO_2 and replaces the Ti^{4+}, which causes the lack of an electron in the lattice of TiO_2. To keep the electrovalence balance, a new oxygen vacancy must be formed nearby. Meanwhile Ti^{4+} is reduced to Ti^{3+}. Oxygen vacancy and Ti^{3+} reducing centre can be the active position for reactions.

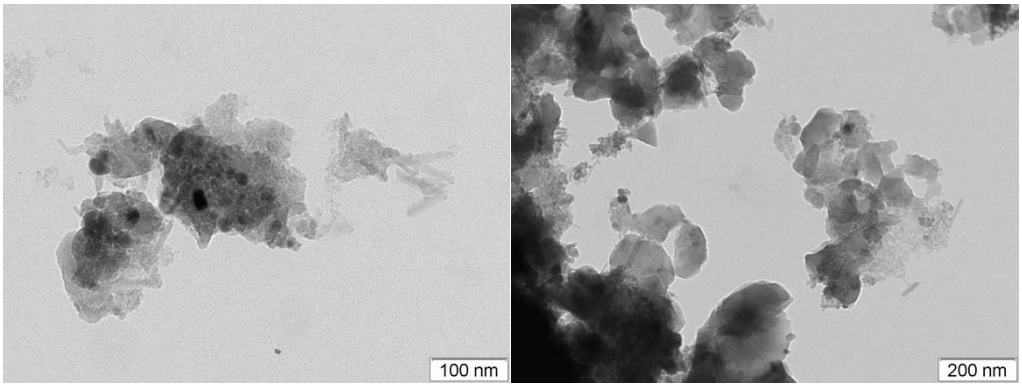

Figure 1- 22 TEM images of Fe_3O_4@TiO_2-Rh nanoparticles.

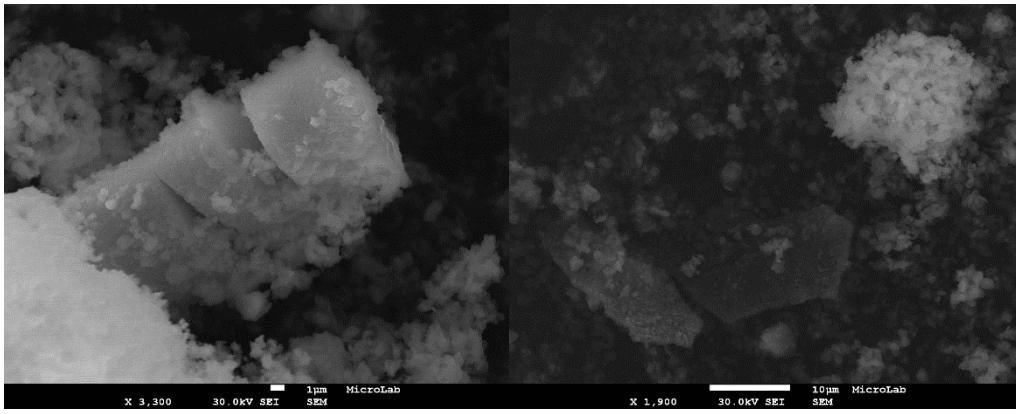

Figure 1- 23 SEM images of Fe_3O_4@TiO_2-Rh nanoparticles.

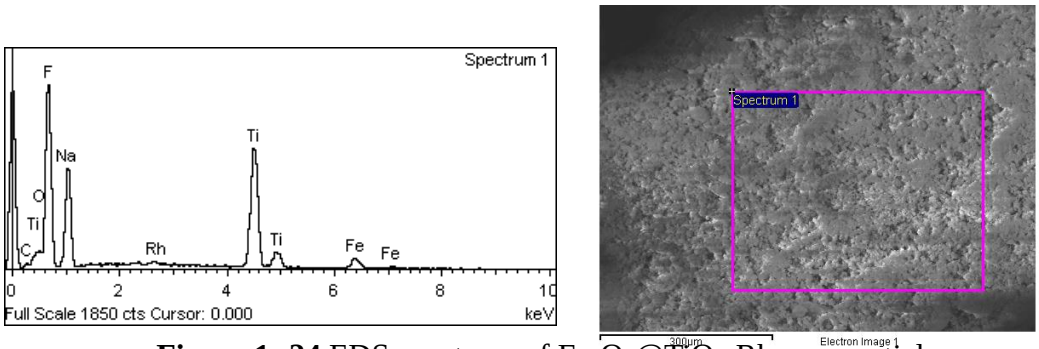

Figure 1- 24 EDS spectrum of Fe_3O_4@TiO_2-Rh nanoparticles.

Preparation of Fe_3O_4@TiO_2-Rh-MWCNT

Our final product is Fe_3O_4@TiO_2-Rh-MWCNT. It combines both MWCNT-Rh and Fe_3O_4@TiO_2. In this complex nanoparticles, MWCNT offers chemical stability and high surface area. Rhodium works as the catalytic active component. TiO_2 gives the ability of corrosion resistance and photo catalysis. For the iron part, Fe_3O_4 is a supermagnetic compound which makes the nanoparticles be easily separated magnetically. As a starting material, after a series of reactions, Fe_3O_4 still maintains its

magnetic property. The Fe_3O_4@TiO_2-Rh-MWCNT also has a strong magnetic property.

From TEM images (**Figure 1- 25**) we can find that the long wired structure of carbon nanotubes are entangled into the surface of the complex. Thus makes an increase in the diameter of the composite. Moreover, from observation of TEM picture we can that the average size of the nanacomposite increased to more than 200 nm. The surface structure (**Figure 1- 26**) of Fe_3O_4@TiO_2-Rh-MWCNT is similar to the structure of MWCNT-Rh. The difference is the size of the particles attached on the surface of MWCNT. Because the size of core-shell system Fe_3O_4@TiO_2 has a bigger average size.

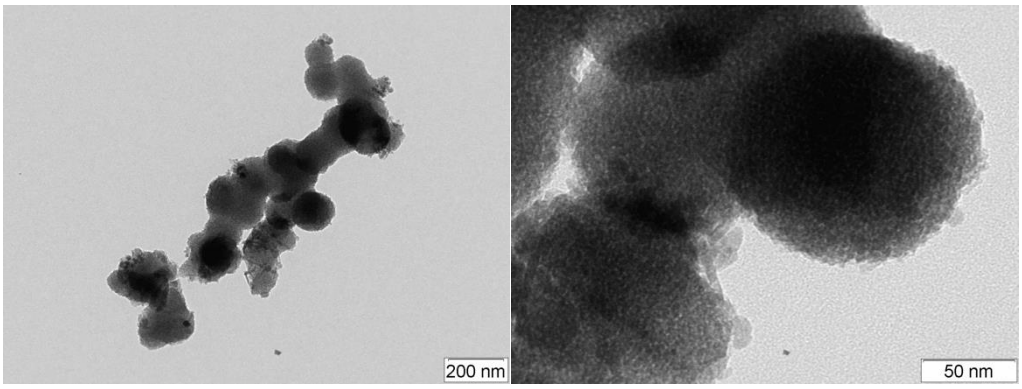

Figure 1- 25 TEM images of Fe_3O_4@TiO_2-Rh-MWCNT nanoparticles.

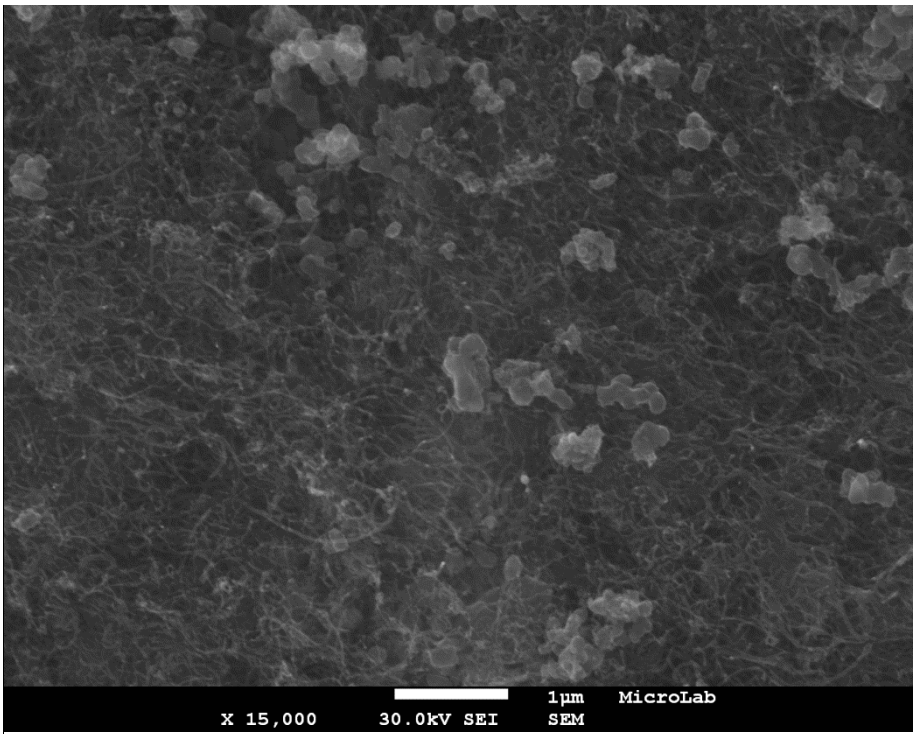

Figure 1- 26 SEM image of Fe_3O_4@TiO_2-Rh-MWCNT nanoparticles.

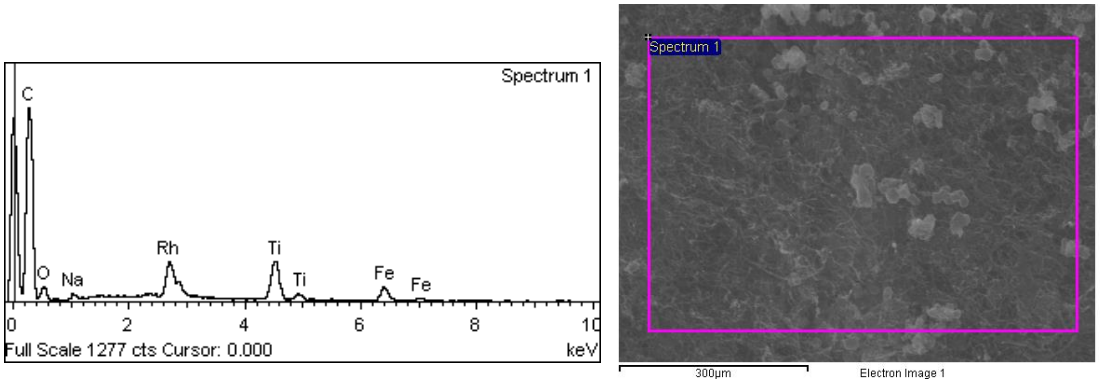

Figure 1- 27 EDS spectrum of Fe_3O_4@TiO_2-Rh-MWCNT nanoparticles.

EDS studies (**Figure 1- 27**) of Fe_3O_4@TiO_2-Rh-MWCNT show that the loading of Rh is high. There are no unexpected elements in the compound.

The synthesized nanoparticles are in the scale of 50 nm to 200 nm in size. Some of the nanoparticles were aggregated to a bigger bulk particles. It is probably because of the drying step in the oven. However if these particles have a different behavior with the bulk particles, we can still regard them as nanoparticles even they are in microscale.

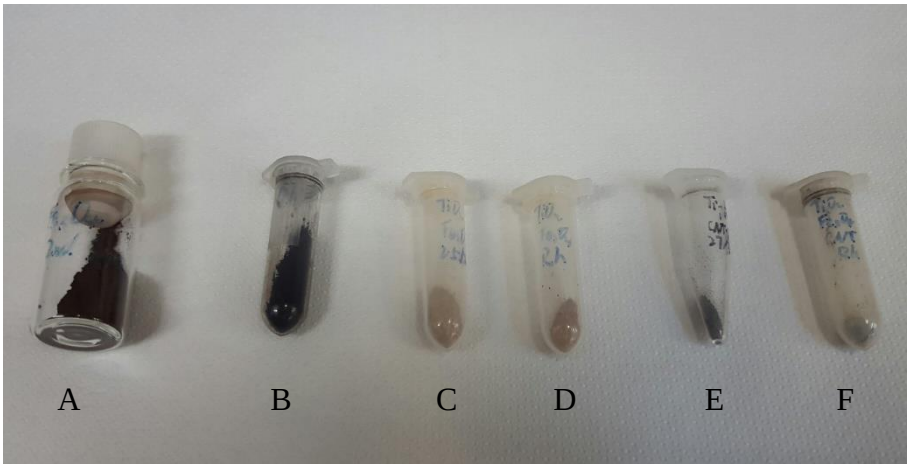

Figure 1- 28 Synthesized nanoparticles, A) Fe_3O_4, B) MWCNT-Rh, C) Fe_3O_4@TiO_2, D) Fe_3O_4@TiO_2-Rh, E) Fe_3O_4@TiO_2-Rh-MWCNT, F) Fe_3O_4@TiO_2-Rh-MWCNT.

3.2 Hydrogenation transfer of nitroarenes and cyclohexene

The results of the hydrogenation transfer of nitroarenes and cyclohexene are shown in **Table 1- 5**.

Table 1- 4 The results of the hydrogenation transfer of cyclohexene and nitroarenes catalyzed by different catalysts. [a]

Entry	Catalyst	Substrate	Yield[b] %	Selectivity %	TOF[c] x10^{-3} (mol.g^{-1}· h^{-1})
1	-	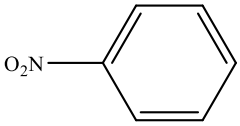 Nitrobenzene	0.9	64.29	
2	Fe_3O_4@TiO_2		2.1	77.78	3
3	MWCNT		1.9	79.17	3
4	MWCNT-Rh		9.5	93.14	14
5	$RhCl_3$		3.0	81.08	5
6	Fe_3O_4@TiO_2-Rh		40.0	97.32	60
7	Fe_3O_4@TiO_2-Rh-MWCNT		49.0	97.22	74
8	-	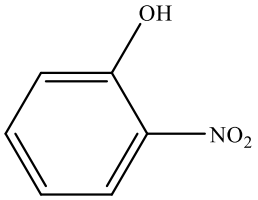 2-Nitrophenol	2.0	86.96	
9	Fe_3O_4@TiO_2		3.7	92.50	6
10	MWCNT		4.8	90.57	7
11	MWCNT-Rh		5.7	95.00	9
12	$RhCl_3$		4.8	97.96	7
13	Fe_3O_4@TiO_2-Rh		38.4	98.21	58
14	Fe_3O_4@TiO_2-Rh-MWCNT		45.2	98.05	68
15	-	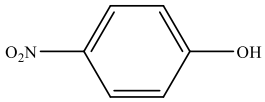 4-Nitrophenol	0	-	
16	Fe_3O_4@TiO_2		4.1	87.23	6
17	MWCNT		0	-	0
18	MWCNT-Rh		7.5	93.75	11
19	$RhCl_3$		5.9	93.65	9
20	Fe_3O_4@TiO_2-Rh		32.1	97.27	48
21	Fe_3O_4@TiO_2-Rh-MWCNT		47.3	97.73	71
22	-	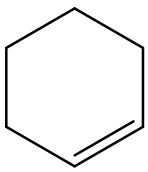 Cyclohexene	0	-	
23	Fe_3O_4@TiO_2		0.3	60.00	0
24	MWCNT		2.0	71.43	3
25	MWCNT-Rh		13.2	97.78	20
26	$RhCl_3$		1.1	91.67	2
27	Fe_3O_4@TiO_2-Rh		25.7	98.09	39
28	Fe_3O_4@TiO_2-Rh-MWCNT		30.3	96.81	45

[a] Reaction conditions,, unless stated otherwise: $[reagent]_0$ = 0.50 mol L^{-1}, $[N_2H_2]_0$ = 2.2 mol L^{-1}, ethyleneglycol up to 2 mL total volume, 80 ℃, 10 min. [b] Based on GC analysis. [c] Number of moles of product per g of metal catalyst per hour

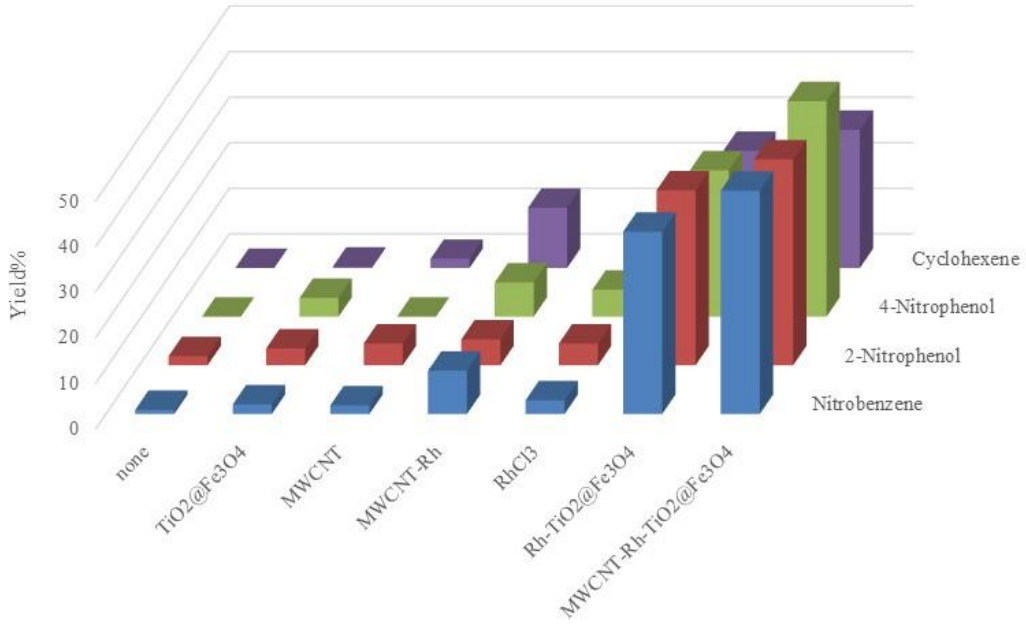

Figure 1- 29 Hydrogenation transfer of cyclohexene and nitroarenes catalyzed by different nanoparticles.

The hydrogenation of nitroarenes and cyclohexene is a prominent reaction in the preparation of pharmaceuticals, agrochemicals and pigments, because the versatile intermediates can be generated through it. The challenging task is the selective reduction of nitro group. As reported before[48], generally high temperature and high loading metal are required for efficient selective hydrogenation in the presence of hydrazine hydrate and metal catalysts.

As can be seen in **Table 1- 5** and **Figure 1- 29**, the hydrogenation of nitrobenzene, 2-nitrophenol, 4-nitrophenol and cyclohexene with the absence of catalyst in the presence of hydrazine hydrate as reducing agent can hardly achieve, which gave yields below 2%. Identically the reactions catalyzed by the support of Fe_3O_4@TiO_2 also gave low yields below 4%. Once the hydrogenation was catalyzed by the rhodium based catalysts, the yields increased significantly. As we expect, the reactions catalyzed by Fe_3O_4@TiO_2-Rh-MWCNT achieved the highest yield to each of the substrates. Because rhodium, which is a transition metal, worked as the kernel of the catalyst that can bind the unsaturated substrate and hydrogen, which comes from the reducing agent, to facilitate the transfer of hydrogen to substrate. Moreover, thanks to the unique structure

of MWCNT[57], on which rhodium is supported, the contact area of the catalyst to the substrate increases. It also promotes the hydrogenation.

Recently Nie and coworkers[58] made a research about the hydrogenation of nitrobenzene to aniline and nitroarenes to amines catalyzed by MWCNT supported Pt. The yield of aniline reached 48.0% after 180 min of reaction at 0 ℃ under 1.0 MPa of atmosphere. The yield of amines is more than 95% after 120 min of reaction at 40 ℃ under 1.0 MPa. Compared with their work, we achieved the similar yield of aniline in much less reaction time at higher temperature, but a lower yield of amines with the assistance of microwave reactor. And with the magnetic property given by Fe_3O_4 our catalysts can be easily separated after the reaction (**Figure 1- 30**).

Figure 1- 30 Separation of catalysts with magnet.

Catalytic recycling of Fe_3O_4@TiO_2-Rh-MWCNT was tested up to 4 consecutive cycles. The results are shown in **Table 1- 5** and **Figure 1- 31**.

Table 1- 5 Catalytic recycling for the MW-assisted hydrogenation (10 min) of nitrobenzene with hydrazine at 80 ℃ catalyzed by Fe_3O_4@TiO_2-Rh-MWCNT.

Entry	Catalyst	Yield %	Selectivity %
7	Fe_3O_4@TiO_2-Rh-MWCNT 1st cycle	49.0	97
29	Fe_3O_4@TiO_2-Rh-MWCNT 2nd cycle	48.1	97
30	Fe_3O_4@TiO_2-Rh-MWCNT 3rd cycle	47.7	97
31	Fe_3O_4@TiO_2-Rh-MWCNT 4th cycle	46.7	97

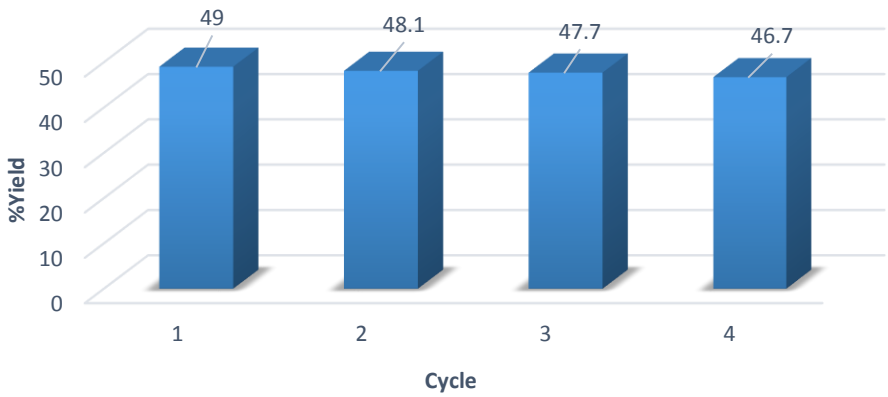

Figure 1- 31 Results of catalytic recycling for the MW-assisted hydrogenation (10 min) of nitrobenzene with hydrazine at 80 ℃ catalyzed by Fe_3O_4@TiO_2-Rh-MWCNT.

In 4 consecutive cycles of hydrogenation, the yield of reactions decreased 5% (from 49.0% to 46.7%). Concerning that, during the separation of catalysts for each of the cycles, there was always a loss in mass of the catalysts. Therefore, we can conclude that Fe_3O_4@TiO_2-Rh-MWCNT nanoparticles are reusable for at least 4 cycles of reactions maintaining their activity.

3.3 Reduction of 2-Nitrophenol

The reduction of 2-nitrophenol was monitored by UV-Vis spectra in a scanning range of 200-700 nm at room temperature with a scan speed of 400 nm per minute. Using acetonitrile as the baseline, the solution of 2-nitrophenol dissolved in acetonitrile showed a peak centred at 351 nm. With the addition of sodium borohydride solution the maximum absorption band shifted to around 444 nm corresponding to 2-aminophenol. The decrease of the absorbance of the peak at 351 nm (or the increase of the absorbance of the peak at 444 nm) was monitored to study the reduction of 2-nitrophenol. The constant rate was calculated by measuring the absorbance at 351 nm at a constant interval of 2 min.

In our study, we used the modified Langmuir Hinshelwood (L-H) kinetic expression to describe the heterogeneous reaction successfully. The reduction reaction follows the

first-order kinetics, which is described by equation:

$$A_t = A_0\, e^{-k_{app}t} \qquad (1)$$

where A_0 is the initial absorbance of the pigment,

A_t is the absorbance of the pigment at time t,

k_{app} is the reaction rate constant (min^{-1}).

The hydrogenation of 2-nitrophenol catalyzed by rhodium complex was investigated in 25 min of reaction. The UV spectrum of reduction of 2-nitrophenol catalyzed by Fe_3O_4@TiO_2-Rh-MWCNT is presented in **Figure 1- 32**. **Figure 1- 33** shows the plot of the maximum absorption vs. time. Then the rate was plotted by the function of ln (A_t/A_0) *vs.* time in **Figure 1- 34**.

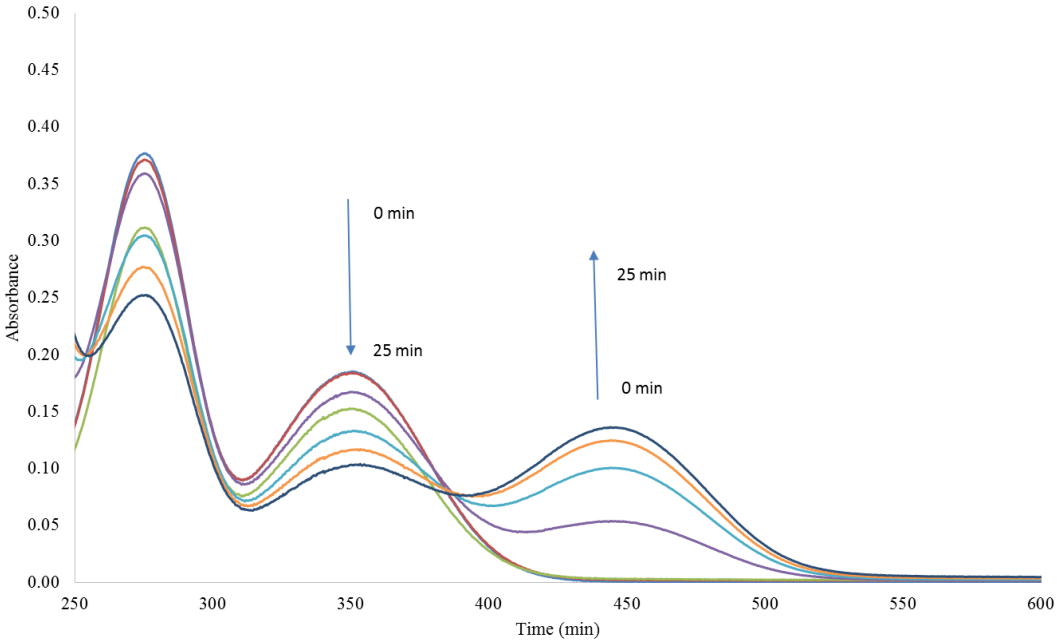

Figure 1- 32 UV-Vis spectra of the reduction of 2-nitophenol catalyzed by Fe_3O_4@TiO_2-Rh-MWCNT.

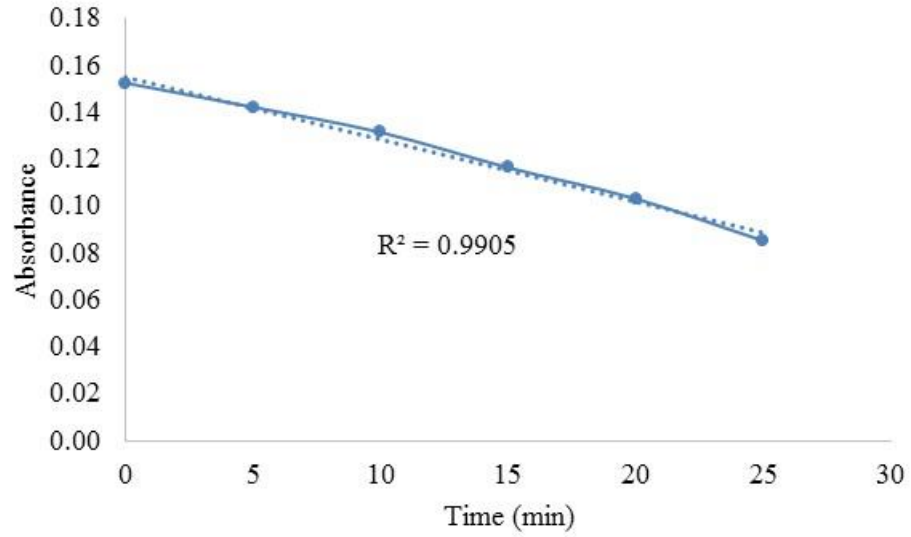

Figure 1- 33 Plot of the absorbance at the peak of 351 nm *vs.* time.

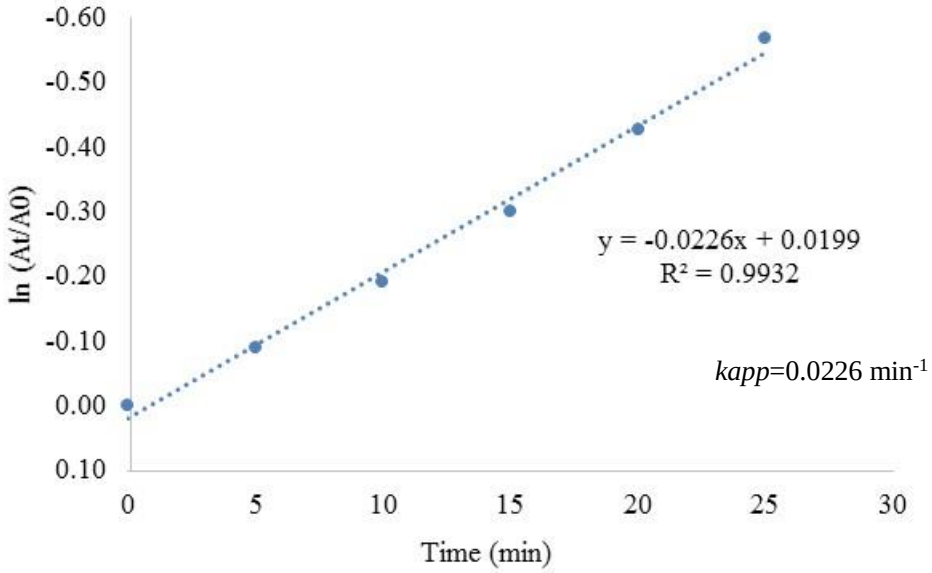

Figure 1- 34 Plot of ln (A_t/A_0) *vs.* time of the reduction of 2-nitrophenol.

After 30 min of reaction, a quantity of orange floc appeared in the solution. Then the reaction was stopped. The UV-Vis spectra was obtained until 25 min of reaction. The expected linear relationship between ln (A_t/A_0) and time was shown in **Figure 1-34**. The rate constant *kapp* is calculated to be 0.0226 min^{-1}.

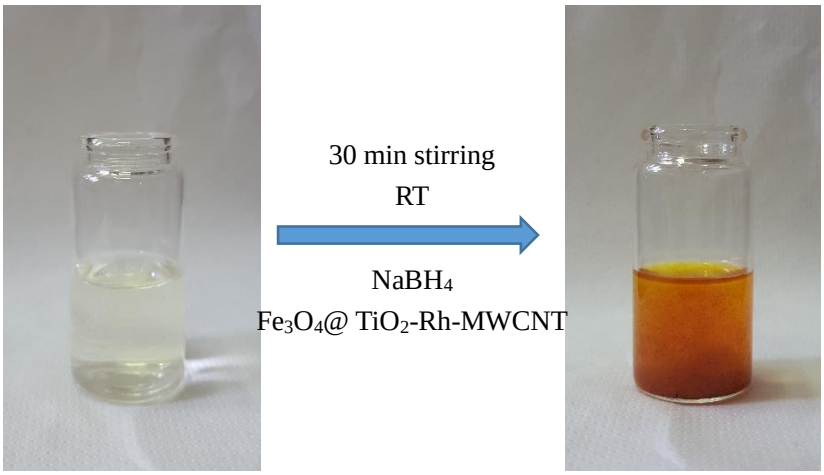

Figure 1- 35 During the reduction, the light yellow color of 2-nitrophenol changed to dark orange. After 30 min of reaction an orange flocculation appeared in the solution.

To make a comparison, we used the same amount of MWCNT-Rh to catalyze the reduction of 2-nitrophenol. Reproducing condition, we got the UV-Vis spectra below (**Figure 1- 36**).

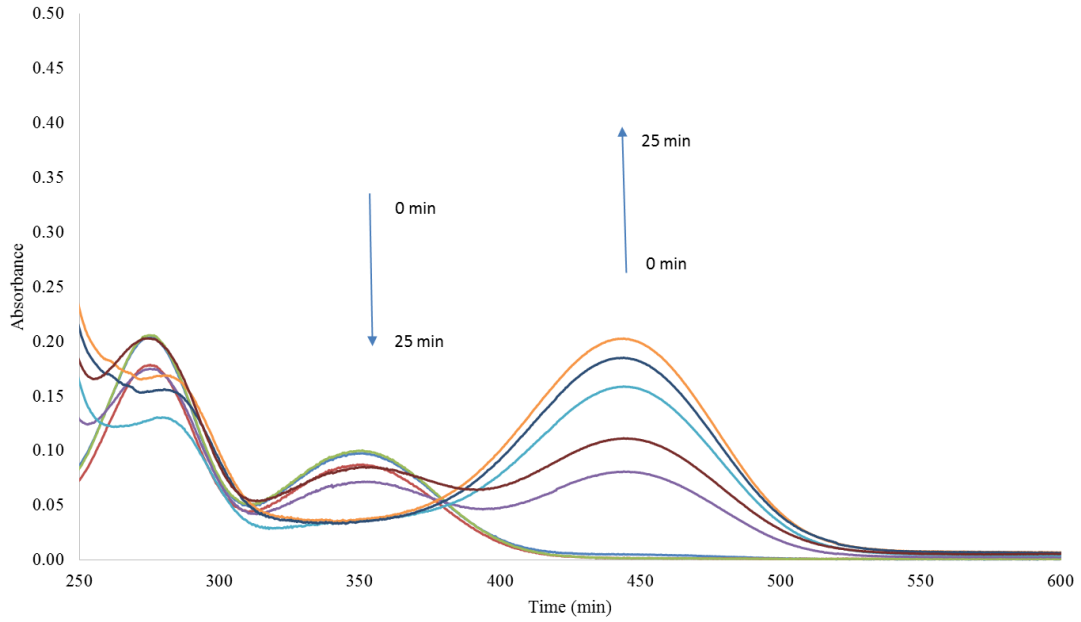

Figure 1- 36 UV-Vis spectra of the reduction of 2-nitrophenol catalyzed by MWCNT-Rh.

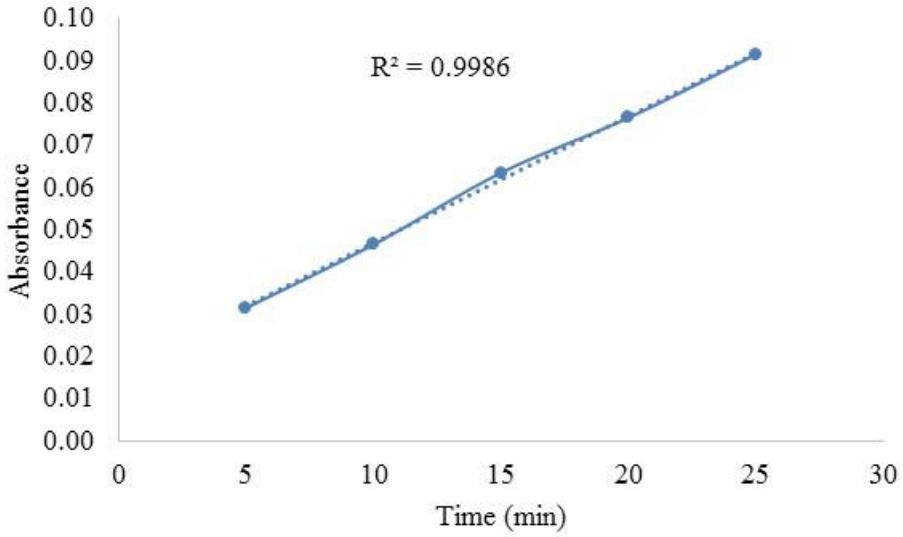

Figure 1- 37 The plot of the absorbance at the peak of 351 nm *vs.* time.

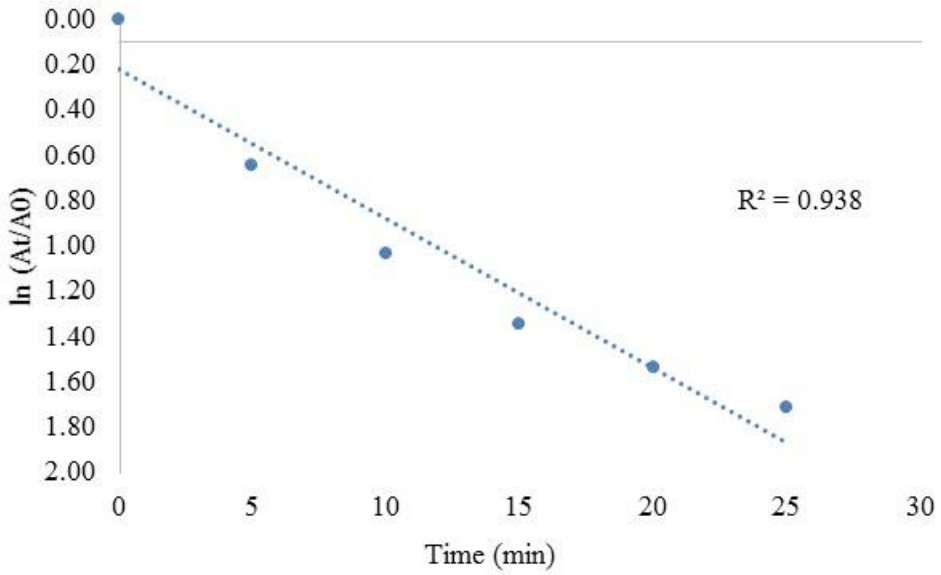

Figure 1- 38 The plot of ln (At/A0) *vs.* time of the reduction of 2-nitrophenol, *kapp* = 0.0659 min^{-1}.

As **Figure 1- 38** shows, the rate constant of Fe_3O_4@TiO_2-Rh-MWCNT catalyzed reduction of 2-nitrophenol is higher than MWCNT-Rh catalyzed reaction. The good catalytic property of Fe_3O_4@TiO_2-Rh-MWCNT is probably attributed to the TiO_2 core, which can release energy under the radiation of UV-Vis device and promote the reduction of 2-nitrophenol. Moreover, after 35 min of reaction, the complex of Fe_3O_4@TiO_2-Rh-MWCNT catalyst was still magnetic with the presence of Fe_3O_4. It gives an advantage of easy separation from the reaction mixture. We can easily separate

the catalyst using a magnet.

3.4 Pigment decoloration

The pigment analysis is used to study the catalytic activity of the catalysts used in pigment decoloration. Moreover it is important to analyze the reaction kinetically. In our study, we used the modified Langmuir Hinshelwood (L-H) kinetic expression to describe the heterogeneous reaction successfully. The degradation of the pigments follows the first-order kinetics, which is described by equation:

$$A_t = A_0\, e^{-k_{app}t} \qquad (2)$$

where A_0 is the initial absorbance of the pigment,

A_t is the absorbance of the pigment at time t,

k_{app} is the reaction rate constant (min^{-1}).

Regarding the pigment analysis, we used three pigments as models to analyze the catalytic activity of the catalysts. We carried out a series of experiment to investigate the catalytic activity of the catalyst in different pigments at different pH value. Visually we can find the changes in color after 10 min of reaction. The shifts of the maximum absorption wavelength are shown in **Table 1- 6**. The color of the pigments are shown in **Table 1- 7.**

Table 1- 6 Maximum absorbance wavelength of the pigments at studied pH value.

Pigment	λ(pH=2) /nm	λ(pH=7) /nm	λ(pH=12) /nm
Amaranth	521	521	494
Tartrazine	427	426	400
Brilliant blue	627	627	627

Table 1- 7 The color of the pigments before and after the decoloration catalyzed by Fe_3O_4@TiO_2-Rh-MWCNT complex in different pH value.

Pigment	pH=2		pH=7		pH=12	
	Before reaction	After reaction	Before reaction	After reaction	Before reaction	After reaction
Amaranth						
Tartrazine						
Brilliant blue						

3.4.1 Decoloration of amaranth

Amaranth dye (C.I. name is Food Red 9) is a dark red that comes from amaranth grain. In spite of the fact that it is banned by FDA since 1976 amaranth pigment remain in use in several other countries. As an anionic dye, it can be applied to fiber synthesis, paper production and leather dying. As an addictive, it is usually used as a trisodium salt. It is soluble in water with a dark red to purple color. And the maximum absorbance is at around 520 nm.

In our study, we tried to decolorize the amaranth dye with the presence of UV irradiation and H_2O_2 catalyzed by Fe_3O_4@TiO_2-Rh-MWCNT.

The decoloration reaction was carried out directly in the 10 mm quartz cell. The color changing is shown in **Figure 1- 39**.

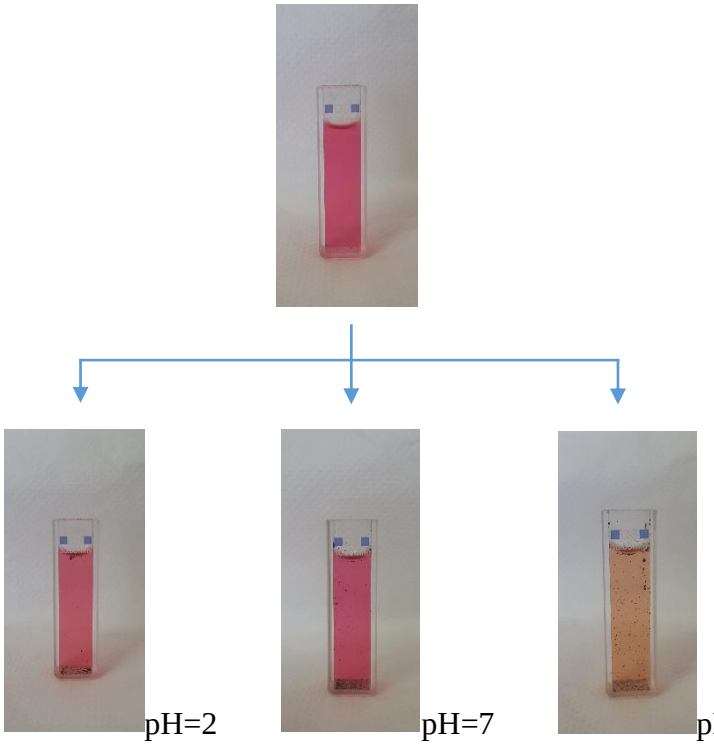

Figure 1- 39 The color changing of amaranth pigment after 5 min of reaction using Fe_3O_4@TiO_2-Rh-MWCNT as catalyst in the cells at different pH value.

Visually the degradation of the amaranth dye in base solution is the highest among the three different pH condition based on **Figure 1- 39**. And the color of the sample in acid condition is lighter than the neutral one. Then the kinetic study of the decoloration was investigated monitored by UV-Vis. And the UV spectra are shown in **Figure 1- 40**.

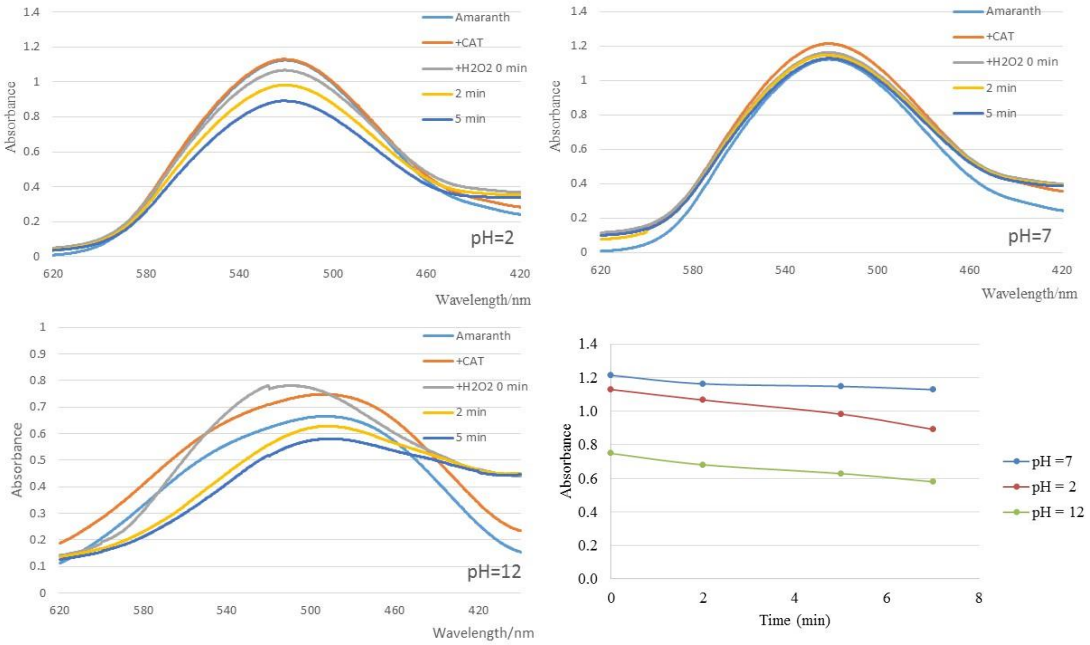

Figure 1- 40 UV spectrum of the amaranth pigment catalyzed by Fe_3O_4@TiO_2-Rh-

MWCNT with the presence of H_2O_2 as oxidant at pH 2, 7 and 12. And the plot of absorbance at maximum absorption wavelength of amaranth pigment to time at pH 2, 7 and 12.

The Fe_3O_4@TiO_2-Rh-MWCNT catalyzed reaction was mild. Once the catalysts were added into the cell, a small number of bubbles, which came from the decomposition of H_2O_2, were generated. The reactions at pH 7 were slow, and there was no big change in color. However this catalyst also has a good activity at pH 2 and pH 12. After 5 mins of reaction, the maximum absorbance decreased from 0.75 to 0.58. The conversion of the pigment was 21.02% at pH 2 and 22.45% at pH 12. **Figure 1- 40** shows the rates for the decoloration of amaranth using Fe_3O_4@TiO_2-Rh-MWCNT complex as catalyst. Rates values and conversion are shown in **Table 1- 9**. The top rate of decoloration appeared at pH 2.

Table 1- 8 Rates and conversion of amaranth decoloration catalyzed by Fe_3O_4@TiO_2-Rh-MWCNT.

pH	k*app* min^{-1}	time min	Conversion %
2	0.0355	7	21.02
7	0.0060	7	7.04
12	0.0316	7	22.45

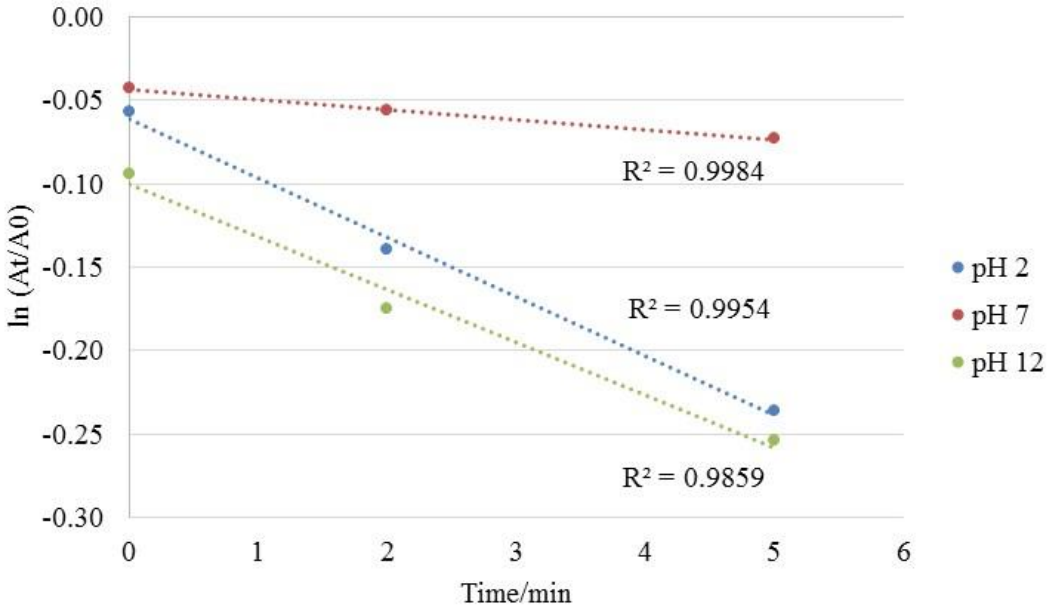

Figure 1- 41 Decoloration rates of amaranth pigment using as catalyst at pH 2, 7 and 12.

Compared with the recent research made by Vinod K. Gupta and coworkers[59], we used the oxidation to decolorize the pigment with the absence of UV lamp. With the presence of H_2O_2 the degradation becomes faster. Our catalyst is more effective in basic solution. Moreover, after 5 mins of reaction our catalyst is still magnetic, which can be easier to recycle and separate for post treatment.

3.4.2 Decoloration of tartrazine

Tartrazine, also known as Yellow Dye No. 5, is a synthetic azo dye. It has been widely used in food and drugs industries. In our study, we decolorize tartrazine using Fe_3O_4@TiO_2-Rh-MWCNT catalysts in presence of H_2O_2 as oxidant. The changing in color before and after reactions at different pH is shown in **Figure 1- 42**.

After 5 mins of reaction, no obvious changing can be observed. The yellow color remained at all of the pH value. Then the spectra in **Figure 1- 43** confirm what is seen in **Figure 1- 42**.

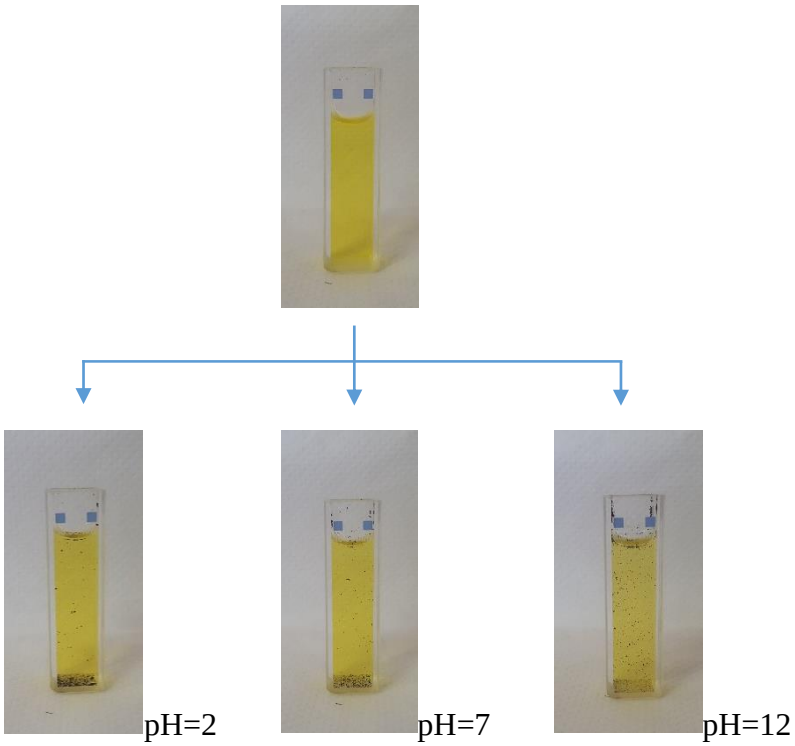

Figure 1- 42 Color changing of tartrazine dye after 5 min of reaction using Fe_3O_4@TiO_2-Rh-MWCNT as catalyst in the cells at different pH value.

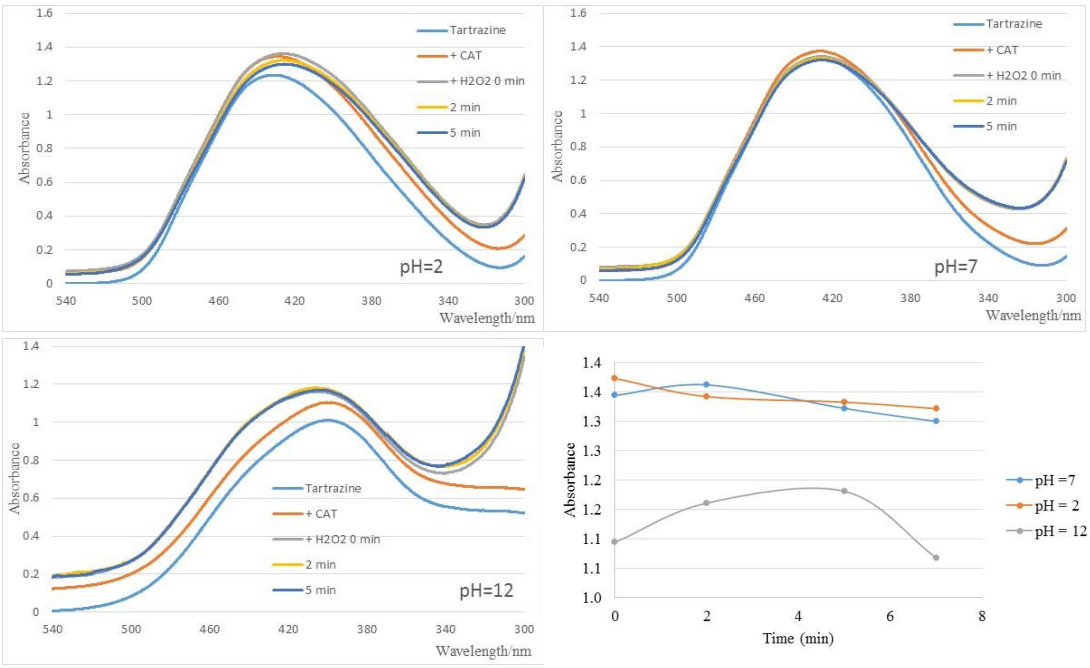

Figure 1- 43 UV-Vis spectrum of tartrazine pigment catalyzed by Fe_3O_4@TiO_2-Rh-MWCNT in presence of H_2O_2 as oxidant at pH 2, 7 and 12. And the plot of absorbance at maximum absorption wavelength of tartrazine pigment to time at pH 2, 7 and 12.

As shown in **Figure 1- 43**, the maximum absorption wavelength shifted from 426 nm to 400 nm at pH 12, and slightly shifted to 427 at pH 2. **Figure 1- 44** shows the rates of the decoloration of tartrazine pigment catalyzed by Fe_3O_4@TiO_2-Rh-MWCNT complex. Rates values and conversion are shown in **Table 1- 10**.

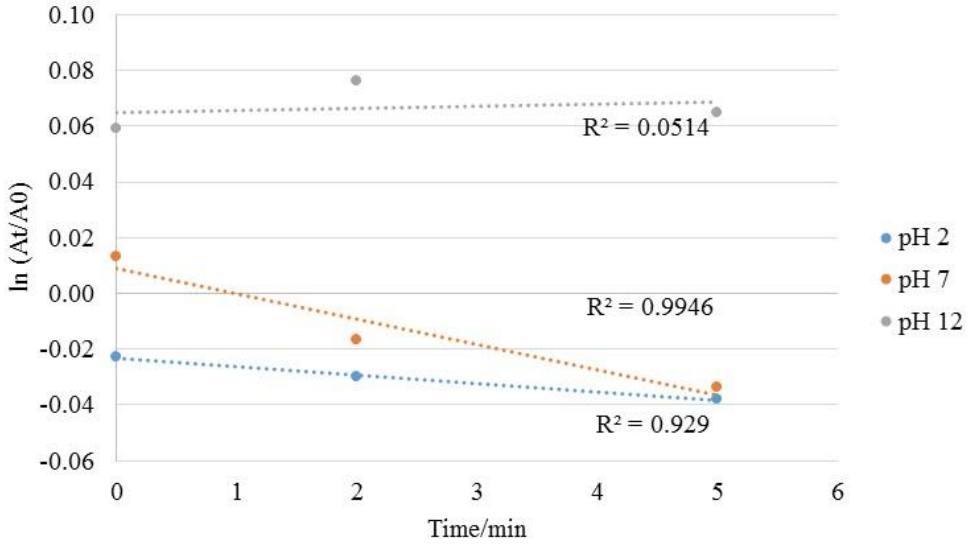

Figure 1- 44 Decoloration rates of tartrazine pigment using Fe_3O_4@TiO_2-Rh-MWCNT as catalyst at pH 2, 7 and 12.

As can be seen in **Figure 1- 44**, the highest rate of decoloration is at acidic pH. It is probably because of the molecule hydrolytic desulfonation, where in ground state the aromatic rings of sulfonic acid molecules are not protonated[60]. Protonation only happens in electronic excitation. The conversion of tartrazine decoloration at all pH values was low. The catalyst is not efficient for tartrazine decoloration.

Table 1- 9 Rate and conversion of tartrazine decoloration catalyzed by Fe_3O_4@TiO_2-Rh-MWCNT.

pH	k*app* min^{-1}	time min	Conversion %
2	0.0091	7	3.74
7	0.0031	7	3.32
12	0.0008	7	2.42

3.4.3 Decoloration of brilliant blue

Brilliant blue, also known as E133, is a colorant for foods such as ice cream, packet soups, sweets and drinks. The appearance of brilliant blue is a reddish blue powder. In our study, we also used Fe_3O_4@TiO_2-Rh-MWCNT to catalyze the decoloration of brilliant blue in the presence of H_2O_2 as oxidant. Kinetic study monitored by UV-Vis was investigated in 5 min of reaction at different pH values. The color difference before and after reactions is shown in **Figure 1- 45**. The UV spectra of the solutions in different pH values are shown in **Figure 1- 46**.

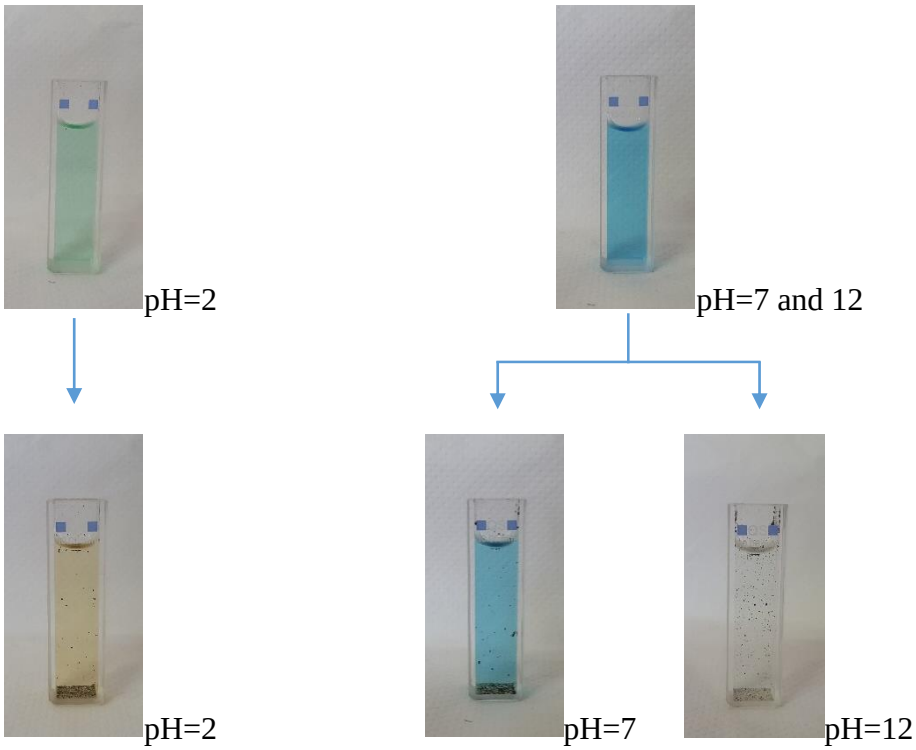

Figure 1- 45 The color changing of brilliant blue after 5 min of reaction using Fe_3O_4@TiO_2-Rh-MWCNT as catalyst in the cells at different pH value.

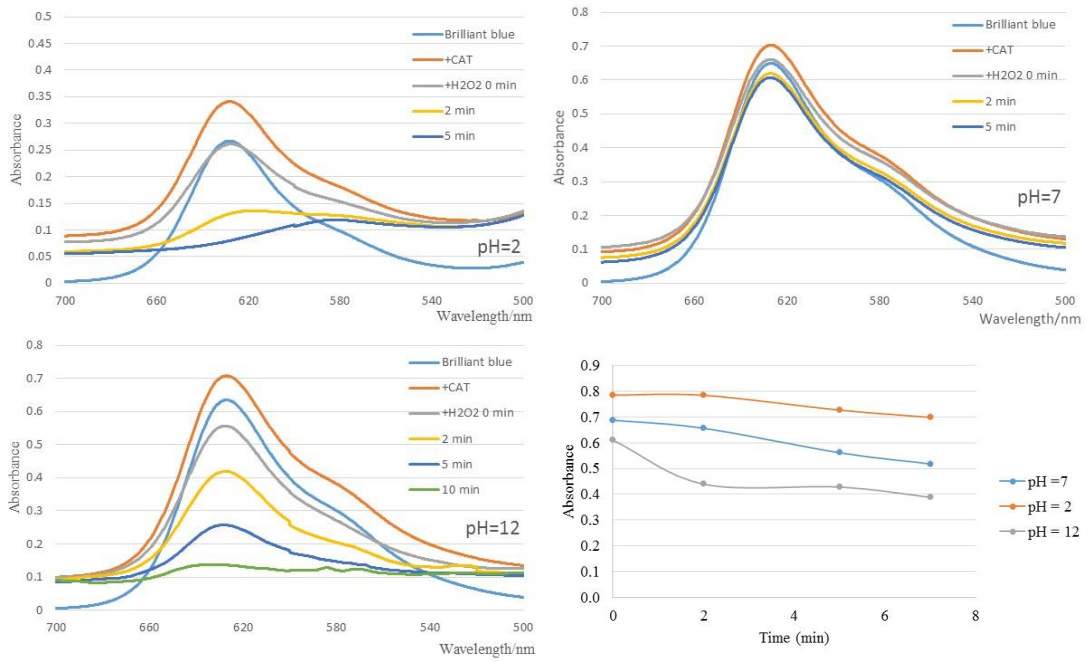

Figure 1- 46 The UV-Vis spectrum of brilliant blue pigment catalyzed by Fe_3O_4@TiO_2-Rh-MWCNT in presence of H_2O_2 as oxidant at pH 2, 7 and 12. And the plot of absorbance at maximum absorption wavelength of brilliant blue pigment to time at pH 2, 7 and 12.

Figure 1- 47 shows the decoloration rate of brilliant blue catalyzed by

Fe_3O_4@TiO_2-Rh-MWCNT complex. Rates values and conversion are shown in **Table 1- 11**.

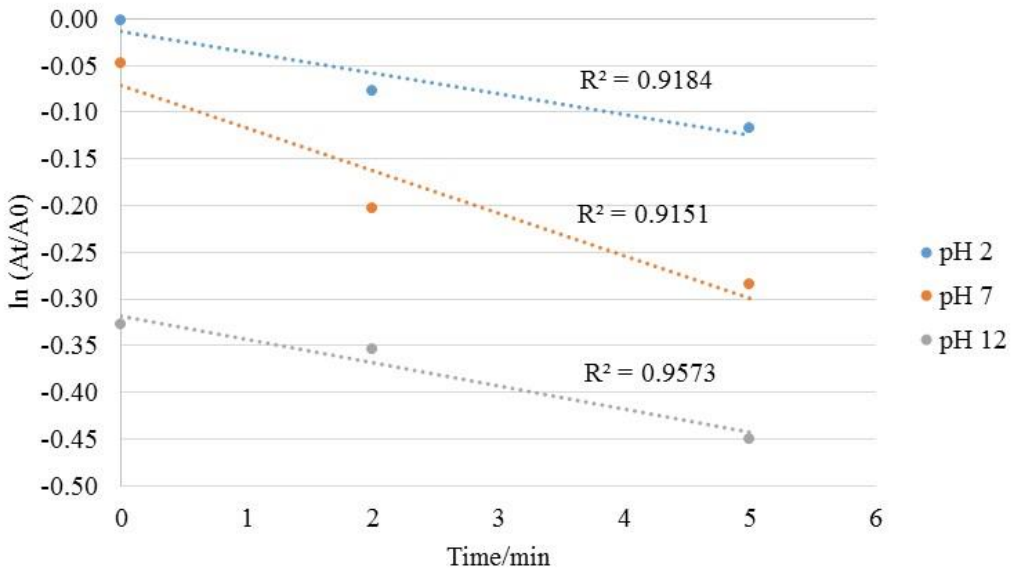

Figure 1- 47 Decoloration rates of brilliant blue pigment using Fe_3O_4@TiO_2-Rh-MWCNT as catalyst at pH 2, 7 and 12.

Table 1- 10 Rate and conversion of brilliant blue decoloration catalyzed by Fe_3O_4@TiO_2-Rh-MWCNT.

pH	k*app* min^{-1}	time min	Conversion %
2	0.0223	7	11.02
7	0.0457	7	24.70
12	0.0250	7	36.21

Fe_3O_4@TiO_2-Rh-MWCNT is efficient for the decoloration of brilliant blue. The highest rate and conversion are at basic condition. After 7 min of reaction, the conversion of brilliant blue reached more than 36%. The coloration efficiency under alkaline conditions increased due to the increase in hydroxyl ions that induce more hydroxyl radical formation. However the perhydroxyl radical can form hydrogen peroxide in acidic condition, which gave rise to the hydroxyl radical[61]. As reported by Tabasom[61] and coworkers, brilliant blue pigment was degradated by surface-modified silver-doped ZnO catalyst. 42.43% of conversion was achieved using 10 mg of catalyst under UV light after 3 h of reaction. As a contrast, in our work, less quantity of catalyst,

less reaction time and no light source were used. But as a result, we achieved a similar conversion. In this case, Fe_3O_4@TiO_2-Rh-MWCNT is more efficient for the decoloration of brilliant blue.

4. Conclusion

In summary, we successfully synthesized rhodium based nanoparticles, which are supported by carbon nanotubes and coated by Fe_3O_4@TiO_2 core-shell system. Fe_3O_4@TiO_2-Rh-MWCNT is an aerobic stable magnetic nano complex. The structure, size and element composition was monitored by SEM and TEM. The catalytic activity for the hydrogenation transfer of nitrobenzene, nitroarenes and cyclohexene and decoloration of pigment was analyzed by GC and UV-Vis.

For the hydrogenation, different catalysts were used to compare the efficiency. A kinetic study of hydrogenation of 2-nitrophenol catalyzed by Fe_3O_4@TiO_2-Rh-MWCNT in the presence of $NaBH_4$ as reducing agent was performed. The results suggest that Fe_3O_4@TiO_2-Rh-MWCNT nanocatalyst is efficient for the hydrogenation reactions. The magnetic strength remains after reactions and profits the separation of the catalysts from the liquid phase.

Regarding the decoloration of pigments, pH values of the solution are considered to be important factor that influence the result. Kinetic studies in different pH values were carried out. The different constant rates indicate that Fe_3O_4@TiO_2-Rh-MWCNT nanocatalyst is efficient at specific pH value for different pigments.

References

[1] Willian, H. W. On a New Metal, Foundin Crude Platina. *Phil. Trans. R. Soc. Lond.* **1804**, *94*, 419–430.

[2] Alain, R.; Jürgen, S.; Henri, P. Reduced Transition Metal Colloids: A Novel Family of Reusable Catalysts? *Chem. Rev.* **2002**, *102*, 3757-3778.

[3] Jongh, L. J. *Physics and Chemistry of Metal Cluster Compounds.* Dordrecht: Kluwer Academic Publishers 1994.

[4] Schmid, G. *Clusters and Colloids, from Theory to Applications.* Weinheim: Wiley-VCH 1994.

[5] Kenneth, J. K. *Nanoscale Materials in Chemistry.* New York: Wiley & Sons 2001.

[6] Rao, C. N. R.; Müller, A.; Cheetham, A. K. *The chemistry of nanomaterials.* WILEY-VCH Verlag GmbH & Co. KGaA, Weinheim 2004.

[7] Schmid, G. *Nanoparticles, from Theory to Applications.* Weinheim: Wiley- VCH 2004.

[8] John, M. T. The Advantages of Exploring the Interface Between Heterogeneous and Homogeneous Catalysis. *Chem. Cat. Chem.* **2010**, *2*, 127- 132.

[9] Didier, A. *Nanoparticles and Catalysis.* Weinheim: Wiley-VCH 2008.

[10] Takeshisa, F.; Kenji. M.; Satoshi, O.; Hiroya, A.; Makio, N.; Kiyoshi, N. Morphology control of Ni–YSZ cermet anode for lower temperature operation of SOFCs. *J. Power Sources*. **2004**, *125*, 17-21.

[11] Pierluigi, B.; Francesca, L. *Heterogenized homogeneous catalysts for fine chemicals production: materials and processes.* Dordrecht: Springer 2010. ISBN 978-90-481-3695-7.

[12] Sergey, S. Z.; Valentine, P. A. $Pd_2(dba)_3$ as a Precursor of Soluble Metal Complexes and Nanoparticles: Determination of Palladium Active Species for Catalysis and Synthesis. Organometallics. **2012**, *31*, 2302-2309.

[13] Osborn, J. A.; Jardine, F. H.; Young, J. F.; Wilkinson, G. The preparation and properties of tris(triphenylphosphine)halogenorhodium(I) and some reactions thereof including catalytic homogeneous hydrogenation of olefins and acetylenes

and their derivatives. *J. Chem. Soc. A*. **1966**, 1711–1732.

[14] Ol ívia, S. G. P. S.; Jos é, J. M. Ó.; Manuel. F. R. P. Nitrate Reduction Catalyzed by Pd–Cu and Pt–Cu Supported on Different Carbon Materials. *Catal. Lett.* **2010**, *139*, 97-104.

[15] Daping, H.; Chao, Z.; Cheng, X.; Niancai, C.; Huaiguang, L.; Shichun, M.; Mu, P. Polyaniline-Functionalized Carbon Nanotube Supported Platinum Catalysts. *Langmuir*. **2011**, *27*, 5582–5588.

[16] Horng-Bin, P.; Chien, M. W. Sonochemical One-Pot Synthesis of Carbon Nanotube-Supported Rhodium Nanoparticles for Room-Temperature Hydrogenation of Arenes. *J. Phys. Chem. C.* **2009**, *113*, 19782-19788.

[17] Horng-Bin, P.; Chien, M. W. One-Step Synthesis of Size-Tunable Rhodium Nanoparticles on Carbon Nanotubes: A Study of Particle Size Effect on Hydrogenation of Xylene. *J. Phys. Chem. C*. **2010**, *114*, 11364-11369.

[18] Innocenzo, G. C.; Michela, C. Highly dispersed rhodium particles on multi-walled carbon nanotubes for the electrochemical reduction of nitrate and nitrite ions in acid medium. *Electrochim. Acta.* **2014**, *138*, 447–453.

[19] Gerardo, A. F. E.; Juan, C. F. G. Participation of linear methoxy species bonded to Ti^{4+} sites in the methanol carbonylation catalyzed by TiO_2-supported rhodium: An infrared investigation. *J. Mol. Catal. A: Chem.* **2012**, *359*, 49–56.

[20] Claudie, H.; Elodie, G. B.; Audrey, D. N.; Alain, R. Rh(0) colloids supported on TiO_2: a highly active and pertinent tandem in neat water for the hydrogenation of aromatics. *Green Chem.* **2011**, *13*, 1766-1771.

[21] Astruc, D.; Lu, F.; Aranzaes, J.R. Nanoparticles as recyclable catalysts: the frontier between homogeneous and heterogeneous catalysis. *Angew. Chem. Int. Ed.* **2005**, *44*, 7852–7872.

[22] Christophe, M. T.; Georg, S. F. Ligand effects in the rhodium-catalyzed carbonylation of methanol. *Coord. Chem. Rev.* **2003**, *243*, 125-142.

[23] Gates, B. C. Supported Metal Clusters: Synthesis, Structure, and Catalysis. *Chem. Rev.* **1995**, *95*, 511–522.

[24] Jason, A. W.; Richard, G. F. A review of soluble transition-metal nanoclusters as

arene hydrogenation catalysts. *J. Mol. Catal. A: Chem.* **2003**, *191*, 187–207.

[25] Alain, R.; Jürgen, S.; Henri, P. Arene Hydrogenation with a Stabilised Aqueous Rhodium(0) Suspension: A Major Effect of the Surfactant Counter-Anion. *Adv. Synth. Catal.* **2003**, *345*, 222–229.

[26] Maxynm, V. V.; Galia, M.; Yonathan, H.; Adina, H.; Ronny, N. Palladium Nanoparticles Stabilized by Alkylated Polyethyleneimine as Aqueous Biphasic Catalysts for the Chemoselective Stereocontrolled Hydrogenation of Alkenes. *Org. Lett.* **2006**, *8*, 5445–5448.

[27] Vincent, M.; Alain, R.; Esther, R.; Karine, P.; Bruno, C. *Adv. Synth. Catal.* **2004**, *346*, 72–76.

[28] Jairton, D.; Gledison, S. F.; Alexandre, P. U.; Paulo, F. P. F.; Sergio, R. T. Transition-Metal Nanoparticles in Imidazolium Ionic Liquids: Recycable Catalysts for Biphasic Hydrogenation Reactions. *J. Am. Chem. Soc.* **2002**, *124*, 4228–4229.

[29] Liane, M. R.; Giovanna, M.; Paulo, F. P. F.; Sergio, R. T. On the Use of Ruthenium Dioxide in 1-n-Butyl-3-Methylimidazolium Ionic Liquids as Catalyst Precursor for Hydrogenation Reactions. *J. Dupont Catal. Lett.* **2004**, *92*, 149–153.

[30] Tilmann, J. G.; Dongbin, Z.; Nikola, C. C.; Gabor, L.; Bernd, W.; Paul, J. D. Biphasic Hydrosilylation in Ionic Liquids: A Process Set for Industrial Implementation. *J. Am. Chem. Soc.* **2006**, *128*, 9773–9780.

[31] Carla, W. S.; Giovanna, M.; Jairton, D.; Paulo, F. P. F.; Sérgio, R. T. Nanoscale Pt(0) Particles Prepared in Imidazolium Room Temperature Ionic Liquids: Synthesis from an Organometallic Precursor, Characterization, and Catalytic Properties in Hydrogenation Reactions. *Inorg. Chem.* **2003**, *42*, 4738–4742.

[32] Alois. F. *Active Metals: Preparation, Characterization, Applications*. VCH, Weinheim 1996.

[33] Niederer, J. P. M.; Arnold, A. B. J.; Holderich, W. F.; Spliethof, B.; Tesche, B.; Reetz, M.; Bönnemann, H. *Top. Catal.* **2002**, *18*, 265–269.

[34] Nanfeng, Z.; Galen, D. S. A General Synthetic Strategy for Oxide-Supported Metal Nanoparticle Catalysts. *J. Am. Chem. Soc.* **2006**, *128*, 14278-14280.

[35] Tae-Jong, Y.; Woo, L.; Yoon-Seuk, O.; Jin-Kyu, L. Magnetic nanoparticles as a catalyst vehicle for simple and easy recycling. *N. J. Chem.* **2003**, *27*, 227–229.

[36] Philip, D. S.; Guifeng, L.; Jinda, F.; Max, Y.; Yong, G. Recycling of homogeneous Pd catalysts using superparamagnetic nanoparticles as novel soluble supports for Suzuki, Heck, and Sonogashira cross-coupling reactions. *Chem. Commun.* **2005**, 4435–4437.

[37] Philip, D. S.; Jinda, F.; Hari, M. R. G.; Max, Y.; Yong, G. Superparamagnetic Nanoparticle-Supported Catalysis of Suzuki Cross-Coupling Reactions. *Org. Lett.* **2005**, *7*, 2085–2088.

[38] Aiguo, H.; Gordon, T. Y.; Wenbin, L. Magnetically Recoverable Chiral Catalysts Immobilized on Magnetite Nanoparticles for Asymmetric Hydrogenation of Aromatic Ketones. *J. Am. Chem. Soc.* **2005**, *127*, 12486–12487.

[39] Miyuki, K.; Takeshi, K.; Kazuya, Y.; Noritaka, M. Ruthenium hydroxide on magnetite as a magnetically separable heterogeneous catalyst for liquid-phase oxidation and reduction. *Green Chem.* **2006**, *8*, 735–741.

[40] Yan, Z.; Philip, D. S.; Yong, G. Magnetic Nanoparticles as an Orthogonal Support of Polymer Resins: Applications to Solid-Phase Suzuki Cross-Coupling Reactions. *J. Org. Chem.* **2006**, *71*, 537–542.

[41] Liane, M. R.; Fernanda, P. S.; Lucas, L. R. V.; Pedro, K. K.; Evandro, L. D.; Rosangela, I.; Richard, L.; Giovanna, M. Superparamagnetic nanoparticle-supported palladium: a highly stable magnetically recoverable and reusable catalyst for hydrogenation reactions. *Green Chem.* **2007**, *9*, 379–381.

[42] Dong, K. Y.; Su, S. L.; Jackie, Y. Y. Synthesis and Applications of Magnetic Nanocomposite Catalysts. *Chem. Mater.* **2006**, *18*, 2459–2461.

[43] Riaz, S.; Bashir, M.; Naseem, S. Iron Oxide Nanoparticles Prepared by Modified Co-Precipitation Method. *IEEE Trans. Magn.* **2014**, *50*, 1-4.

[44] An-Hui, L.; Salabas, E. L.; Ferdi, S. Magnetic Nanoparticles: Synthesis, Protection, Functionalization, and Application. *Angew. Chem. Int. Ed.* **2007**, *46*, 1222 – 1244.

[45] Jian-Qi, M.; Shao-Bo, G.; Xiao-Hua, G.; Hong-Guang, G. Liquid-phase deposition of TiO_2 nanoparticles on core–shell $Fe_3O_4@SiO_2$ spheres: preparation,

characterization, and photocatalytic activity *J. Nanopart. Res.* **2015**, *17*, 307.

[46] Jining, G.; Xinze, R.; Chunmeng, S.; Humin, C.; Tianmin, C.; Yongping, S. One-step solvothermal synthesis of highly water-soluble, negatively charged superparamagnetic Fe_3O_4 colloidal nanocrystal clusters. *Nanoscale*. **2013**, *5*, 7026–7033.

[47] Donia, B.; Rose, A. Novel Photocatalyst: Titania-Coated Magnetite. Activity and Photodissolution. *J. Phys. Chem. B.* **2000**, *104*, 4387–4396.

[48] Sunil, K. S.; Maneet, L.; Lata; Soumya, R. K.; Rakesh, B. M. Synthesis Of Cu/CNTs Nanocomposites for Antimicrobial Activity. *Adv. Nat. Sci.: Nanosci. Nanotechnol.* **2012**, *3*, 045011.

[49] Seyed, M. B.; Maryam, F.; Seyed, M. V.; Mahmood, T. Hydrogenation of arenes, nitroarenes, and alkenes catalyzed by rhodium nanoparticles supported on natural nanozeolite clinoptilolite. *J. Mol. Catal. A: Chem.* **2015**, **407**, 128-136.

[50] He-Yan, J.; Xu-Xu, Z. Phosphine-functionalized ionic liquid-stabilized rhodium nanoparticles for selective hydrogenation of aromatic compounds. *Appl. Catal. A: Gen.* **2015**, *499*, 118-123.

[51] Nüchter, M.; Müller, U.; Ondruschka, B.; Tied, A.; Lautenschläge, W. Microwave-Assisted Chemical Reactions. *Chem. Eng. Technol.* **2003**, *26*, 1207–1216.

[52] Chunxiang, K.; Hisanori, S.; Masao, T. Convenient and stereoselective synthesis of (Z)-1-bromo-1-alkenes by microwave-induced reaction. *Tetrahedron Lett.* **2001**, *42*, 3893-3896.

[53] Poedji, L. H.; Muhammad, F.; Ridwan; Marsi; Dedi, S. Synthesis and Properties of Fe_3O_4 Nanoparticles by Co-precipitation Method to Removal Procion Dye. *Int. J. Environ. Sci. Dev.* **2013**, *4*, 336-340.

[54] Dachipally, P.; Jonnalagadda, S. B. Kinetics of ozone-initiated oxidation of textile dye, Amaranth in aqueous systems. *J. Environ. Sci. Health A Tox. Hazard. Subst. Environ. Eng*. **2011**, *46*, 887-897.

[55] Bin, Z.; Yiting, X.; Yifang, Z.; Lizong, D.; Mingqiu, Z.; Jin, Y.; Yujie, C.; Xudong, C.; Juying, Z. A Facile Synthesis of Polypyrrole/Carbon Nanotube Composites with Ultrathin, Uniform and Thickness-Tunable Polypyrrole Shells. *J. Nanoscale*

Res. Lett. **2011**, *6*, 431.

[56] Pelter, A.; Smith, K.; Brown, H. C. *Borane Reagents.* Academic: New York, 1988.

[57] Charles, C.; Wenzhi, L. A review of application of carbon nanotubes for lithium ion battery anode material. *J. Power Sources.* **2012**, *208*, 74-85.

[58] Rrenfeng, N.; Junhua, W.; Lina, W.; Yu, Q.; Ping, C.; Zhaoyin, H. Platinum supported on reduced graphene oxide as a catalyst for hydrogenation of nitroarenes. *Carbon.* **2012**, *50*, 586 – 596.

[59] Vinod, K. G.; Rajeev, J.; Alok, M.; Tawfik, A. S.; Arunima, N.; Shilpi, A.; Shalini, S. Photo-catalytic degradation of toxic dye amaranth on TiO_2/UV in aqueous suspensions. *Mater. Sci. Eng. C.* **2012**, *32*, 12–17.

[60] Tuane, C. S.; Guilherme, J. Z.; Daniel, A. M.; Gisela, A. U.; Maria, V. B. Z. Assessment of the breakdown products of solar/UV induced photolytic degradation of food dye tartrazine. *Food Chem. Toxicol.* **2014**, *68*, 307–315.

[61] Tabasom, P.; Namratha, K.; Ibrahim, A. I.; Sukhon, P.; Kullaiah, B. Photocatalytic Degradation of Municipal Wastewater and Brilliant Blue Dye Using Hydrothermally Synthesized Surface-Modified Silver-Doped ZnO Designer Particles. *Int. J. Photoenergy*. **2012**, *2012*, 670610.

Chapter 2 MW-assisted oxidation of 1-phenylethanol catalyzed by oxidovanadium(V) complexes supported on nanodiamonds

1. Introduction

Vanadium complexes have been widely used in industrial oxidation catalysis, thanks to their easily interconvertible vanadium oxidation states, coordination numbers, high affinity to oxygen and the Lewis acid character of their centers[1].

Vanadium in +5 oxidation states exist in four different forms, viz., VO^{3+}, VO_2^{+}, $V_2O_3^{4+}$ and $V_2O_4^{2+}$, and exhibits hard acidic character. The hard nature of vanadium centre yielded a rich variety of the oxidovanadium(V) complexes with N, O donors. Many of them effectively catalyze several oxidation processes, namely alkanes[2-9]. They also catalyze[1,9-11] (or co-catalyze) the aerobic (using O_2 as oxidant) oxidation of secondary alcohols with good yields and high selectivities, either in liquid or supported systems as shown in **Scheme 2- 1**.

$\mathbf{R^1}$ = alkyl or aryl; $\mathbf{R^2}$ = H or alkyl

Scheme 2- 1 Aerobic oxidation of alcohols catalyzed by vanadium catalysts[1].

However, the vanadium catalyzed peroxidative (with H_2O_2 or TBHP) oxidation of secondary alcohols is comparatively scarce[1,9-15].

Oxidation of alcohols

The catalytic oxidation of alcohols is one of the most important uses of vanadium complexes. It has attracted much attention in recent years. Now researchers are focused on the development of vanadium(IV) and vanadium(V) complexes for using as catalysts for the oxidation of primary and secondary alcohols[1] under greener conditions.

For example[15], arylhydrazone oxidovanadium compounds, such as the oxidoethoxidovanadium(V) [VO(OEt)L] (H_2L = salicylaldehyde-2-hydroxybenzoylhydrazone), the salt like dioxidovanadium(V) ($NH_3CH_2CH_2OH$) [VO_2L], and the mixed-ligand oxidovanadium(V) [VO(hq)L] (Hhq = 8-hydroxyquinoline) and the vanadium(IV) [VO(phen)L] (phen = 1,10-phenanthroline) complexes have been tested as catalysts for solvent-free microwave-assisted oxidation of aromatic and alicyclic secondary alcohols with *tert*-butylhydroperoxide. An efficient and selective solvent-free synthesis of acetophenone was achieved with yields up to 99% (TON = 497, TOF = 993 h^{-1} for [VO(hq)L]) after only 30 min of low power (25 W) MW irradiation[15]. However, in the homogeneous conditions adopted, the isolation of the catalytic vanadium species was not possible, thus disabling the performance of consecutive catalytic cycles.

In addition, oxidovanadium(V) complexes with three different vanadium motifs (VO^{3+}, VO^{2+} and $V_2O_3^{4+}$) and two aroylhydrazone Schiff bases, [VOL^1(OEt)][VOL^1(OEt)(EtOH)] (**1**), [VOL^2(OEt)] (**2**), [Et_3NH][VO_2L^1] (**3**), [$VO_2(HL^2)$] 2EtOH (**4**), [VOL^1(μ-O)VOL^1] (**5**) and [VOL^2(μ-O)VOL^2] (**6**) (H_2L^1 = 3,5-di-*tert*-butyl-2-hydroxybenzylidene)-2-hydroxybenzohydrazide and H_2L^2 = 3,5-di-*tert*-butyl-2-hydroxybenzylidene)-2-aminobenzohydrazide) (**Scheme 2- 2**) have been very recently synthesized[16] and their catalytic properties studied for the MW-assisted oxidation of 1-phenylethanol (**Scheme 2- 3**) in homogeneous media.

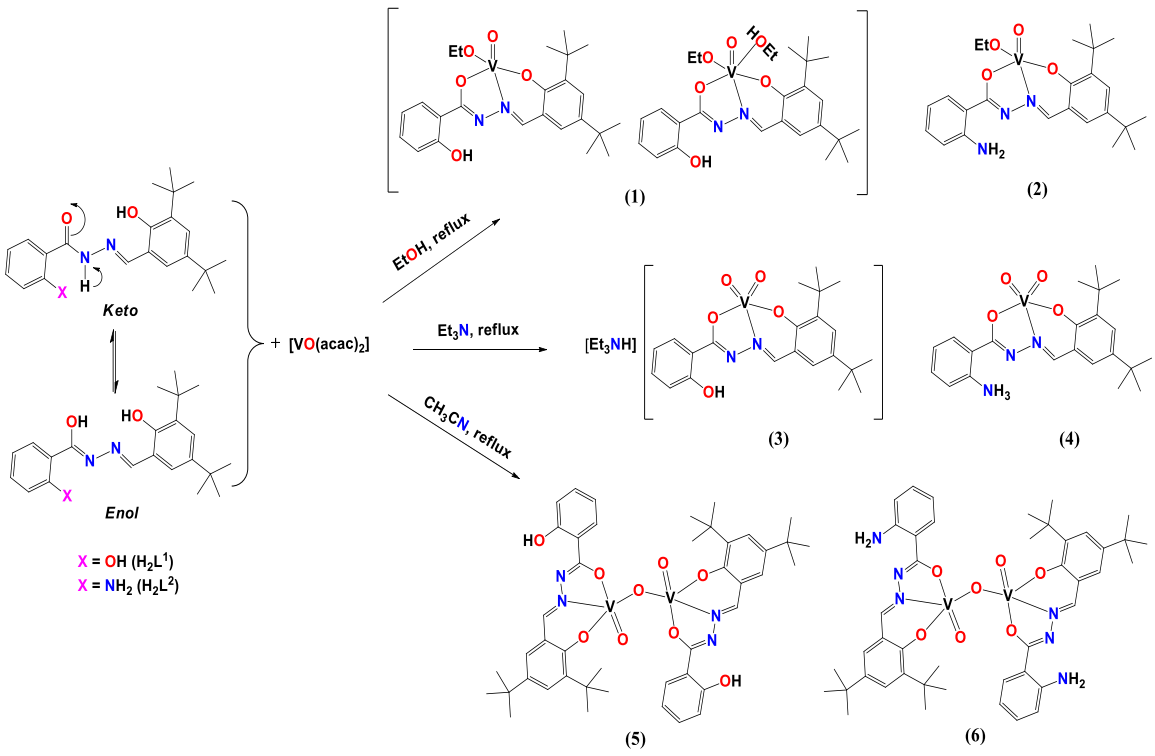

Scheme 2- 2 Synthesis of oxidovanadium(V) complexes **1-6**[16].

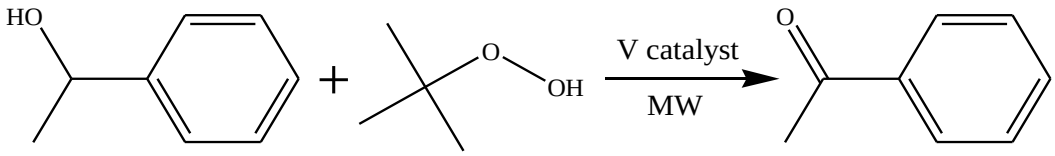

Scheme 2- 3 MW-assisted oxidation of 1-phenylethanol to acetophenone catalyzed by oxidovanadium(V) complexes in the presence of TBHP as oxidant.

In homogeneous and additive-free conditions, almost quantitative conversion, up to 94% (**5**), of 1-phenylethanol in acetophenone was obtained, with a turnover frequency [TOF (moles of acetophenone per mol of catalyst) / hour] of 9.4×10^2 h^{-1}, after 1 h of MW irradiation at 90 ℃ (optimized temperature) and in the presence of 0.1 mol% *vs*. substrate of the oxidovanadium(V) compound. Dinuclear complexes **5** and **6** were the most active, followed by the **1** and **2**. Complexes **3** and **4**, in the same conditions, provided acetophenone yields only up to 28%. [16] Moreover, the isolation of the catalytic vanadium species was not possible, thus disabling their reuse in consecutive catalytic cycles. That is usually easily achieved by the heterogeneous

catalysts. Therefore, the possibility to combine the remarkable properties of homogeneous complexes with the well-known advantages of heterogeneous systems by anchoring them on porous materials is worth to try[1,17].

Other authors immobilized oxidovanadium(IV) acetylacetonate complexes onto polymeric membranes[6], nanostructured ordered carbon material CMK-3[18] and silica nanoparticles[19] and tested them for epoxidation of geraniol. Maurya *et al*.[20] encapsulated oxidovanadium(IV) complexes of tetradentate ligands in zeolite-Y and tested them as catalysts for the oxidation of styrene, cyclohexene and methyl phenyl sulfide. Oxidovanadium(IV) and dioxidovanadium(V) complexes were also immobilized on a polymer support and used for oxo-transfer and amination and oxidation reactions.[21-25] In addition, oxidovanadium(V) complexes were immobilized on a Merrifield and Barlos resin and used for oxygenation of thioanisol to its sulfoxide.[26] In general, the anchored/encapsulated catalysts proved to be significantly more active than their homogeneous counterparts. Their recycle ability and turn over numbers also increased compared to the neat counterparts.

Carbon materials have advantages when used as supports, since their texture and surface chemistry can easily be tuned to fit the desired applications[27-30]. A variety of surface chemical groups can also be added to these materials: carboxylic acids, phenols, carbonyls, lactones, etc.[31,32] Thus, the above oxidovanadium(V) aroylhydrazone complexes **1**-**6** (**Scheme 2- 2**) were immobilized on carbon xerogels, activated carbons and carbon nanotubes, and tested on the selective partial oxidation of 1-phenylethanol, under the same conditions as in homogeneous media. Complexes **3** and **4** were the most difficult to heterogenise. The very low loading thus obtained precluded the catalytic application of these materials on those supports[16,33,34].

In general, compounds **1**, **2**, **5** or **6** supported on the mentioned carbon materials exhibit higher catalytic activity (for the same V load) than the corresponding homogeneous analogues while maintaining the selectivity. In fact, similar acetophenone yields were produced in half of the reaction time with the heterogeneous system under the same reaction conditions[16,33,34].

Therefore, herein we have studied the catalytic activity of complexes **1** – **6**

anchored on a different type of carbon material, the nanodiamonds. The heterogenisation of V complexes on nanodiamonds was tried for the first time in this work[33]. The nanodiamonds were used in their original forms, oxidized with nitric acid, or oxidized with nitric acid and subsequently treated with sodium hydroxide. The chosen catalytic reaction was the microwave-assisted solvent-free peroxidative oxidation of 1-phenylethanol by TBHP.

2. Experimental

2.1 Materials and instruments

Vanadium(V) complexes **1** - **6** (**Scheme 2- 2**) were synthesized and characterized by elemental analysis, IR, ^{1}H NMR, ^{51}V NMR and ESI-Mass spectroscopy techniques by Dr. Manas Sutradhar of Centro de Química Estrutural of Instituto Superior Técnico. The said V-complexes were then heterogenized on nanodiamonds from Sigma Aldrich (<10 nm) by Dr. Sónia Carabineiro from the Faculdade de Engenharia, Universidade do Porto (FEUP). The nanodiamonds were used in their original forms (ND), as purchased; oxidized (NDox); and oxidized with nitric acid and subsequently treated with sodium hydroxide (NDoxNa). The heterogenization protocol was performed in order to achieve 1% wt. of V catalyst per mass of carbon. The loading of V on the nanodiamonds (determined by inductively coupled plasma atomic emission spectroscopy analyses at FEUP) is presented in **Table 2- 1**. The description and characterisation of (powder) nanodiamond samples made by Dr. Sónia Carabineiro is summarized in **Table 2- 2**.

Table 2- 1 V loading (% p/p) on the nanodiamonds.

Carbon Material	**Oxidovanadium(V) complex**					
	1	**2**	**3**	**4**	**5**	**6**
ND	0.51	0.85	0.19	0.19	0.01	1.00
ND-ox	0.41	0.03	0.03	0.10	~0	1.08
ND-ox-Na	0.31	0.44	0.26	0.26	0.36	1.09

Table 2- 2 Description and characterisation of (powder) carbon samples*.

Sample	S_{BET} (m^2/g)	V_p (cm^3/g)	L (nm)	V_{micro} (cm^3/g)	$S_{external}$ (m^2/g)	CO (μmol/g)	CO_2 (μmol/g)
ND	295	1.08	10.6	~0	295	1008	283
ND-ox	253	1.25	14.2	~0	253	1816	1162
ND-ox-Na	238	1.28	11.1	~0	238	1225	1255

*Surface area (S_{BET}), total pore volume (V_p), average mesopore width (L), micropore volume (V_{micro}), external area ($S_{external}$), obtained by adsorption of N_2 at -196 ℃, and amounts of CO and CO_2 desorbed, as determined by TPD.

The 1-phenylethanol (98%), *tert*-butyl hydroperoxide (TBHP, 70% aqueous solution) and benzaldehyde (≥ 99%) were purchased from Sigma-Aldrich and acetonitrile (99.99%) from Fisher Scientific, UK.

The catalytic tests were performed under microwave (MW) irradiation in a focused Anton Paar Monowave 300 microwave reactor fitted with a rotational system and an IR temperature detector, using a 10 mL capacity reaction tube with a 13 mm internal diameter.

Chromatographic analyses of the reaction products were undertaken by using a Fisons Instruments GC 8000 series gas chromatograph with a DB-624 (J&W) capillary column (DB-WAX, column length: 30 m; internal diameter: 0.32 mm), FID detector, and the Jasco-Borwin v.1.50 software in Window XP Operating System. The temperature of injection was 240 ℃. Helium was used as the carrier gas. The products were identified by comparison of their retention times with known reference compounds.

2.2 Experimental procedure

The catalytic tests under MW irradiation were performed in the focused microwave reactor described above. 1-Phenylethanol (2.5 mmol), *tert*-butyl hydroperoxide (70 % aqueous solution, 5.0 mmol) and the heterogeneous V-catalyst (0.8 – 2.5 μmol of the vanadium compound), were introduced in the G10 vessel, which was then placed in the microwave reactor at 10 W power and stirred at 600 rpm at 50 - 150 ℃ for 30 - 90 min. The reaction conditions are indicated in **Table 2- 3**.

Table 2- 3 MW-assisted oxidation of 1-phenylethanol with TBHP catalyzed by vanadium complexes **1-6** supported at nanodiamonds.[a]

Entry	Catalyst	(μmol)	T (℃)
1	**1**@ND	2.5	100
2	**1**@ND	2.5	125
3	**1**@NDox	2.5	100
4	**1**@NDox	1.25	100
5	**1**@NDox	1.25	100
6	**1**@NDoxNa	2.5	100
7	**2**@ND	2.5	100
8	**2**@ND	1.25	125
9	**2**@NDoxNa	2.5	100
10	**3**@ND	2.5	100
11	**3**@ND	2.5	125
12	**3**@NDoxNa	2.5	100
13	**4**@ND	2.5	100
14	**4**@ND	2.5	125
15	**4**@NDox	0.83	100
16	**4**@NDox	0.83	125
17	**4**@NDoxNa	2.5	100
18	**5**@NDoxNa	2.5	100
19	**5**@NDoxNa	2.5	125
20	**6**@ND	2.5	100
21	**6**@ND	2.5	125
22	**6**@NDox	2.5	50
23	**6**@NDox	2.5	75
24	**6**@NDox	2.5	100
25	**6**@NDox	2.5	125
26	**6**@NDox	2.5	150
27	**6**@NDoxNa	2.5	100

[a] The reaction time was 60 min in all experiments, except on **Entry 3** (t=30 min) and **5** (t=90 min).

2.2.1 Products extraction and analysis

After the reaction, the mixture was allowed to cool down to room temperature. 150 μL of benzaldehyde (internal standard) and 2.5 mL of NCMe (to extract the substrate and the organic products from the reaction mixture) were added. The obtained mixture was stirred for *ca.* 10 min and then a sample (1 μL) was taken from the organic phase and analysed by GC after centrifugation and filtering. The internal standard method was used to quantify the organic products. Based on the boiling points of the substrate,

internal standard and product, the program of GC that we set for testing was maintained at 120 ℃ for 1 min, heating from 120 ℃ to 200 ℃ at a rate of 10 ℃/min, holding at 200 ℃ for 1 min and then cooling to 120 ℃.

2.2.2 Recycling experiments

Catalyst recycling of **4**@ND was tested up to 5 consecutive cycles (**Table 2- 4**). On completion of each stage, the products were analysed by GC and the heterogenized catalyst **4**@ND was recovered by filtration, thoroughly washed and dried in the oven at 80 ℃ overnight. It was then reused for a new set of 1-phenylethanol oxidation experiments, keeping constant the molar ratio of substrate to catalyst. The filtrates were also tested in new reactions (by addition of fresh reagents), and no oxidation was detected.

Table 2- 4 Recycling experiments of **4**@ND in consecutive oxidations of 1-phenylethanol.[a]

Entry	Catalyst	m (mg)	Cat.(μmol)
14	**4**@ND 1st cycle	67.0	2.5
28	**4**@ND 2nd cycle	67.0	2.5
29	**4**@ND 3rd cycle	47.3	1.8
30	**4**@ND 4th cycle	32.0	1.2
31	**4**@ND 5th cycle	31.0	1.2

[a]All the reactions were performed for 30 min at 125 ℃.

3. Results and Discussion

Complexes **1**-**6** immobilized on nanodiamonds, used in their original forms (ND), as purchased; oxidized (NDox); and oxidized with nitric acid and subsequently treated with sodium hydroxide (NDoxNa), were tested as heterogeneous catalysts for the microwave-assisted solvent-free peroxidative oxidation of 1-phenylethanol by ^{t}BuOOH. Their catalytic performance is presented in **Table 2- 5**. The nanodiamonds alone (with no complexes anchored) were also tested in the same conditions and revealed no significant catalytic activity (**Table 2- 6**).

Interestingly, complexes **3** and **4** which were reported[16,34] as the most difficult

ones to heterogenise in other carbon materials, led to higher loads on ND materials (see **Table 2- 1**) what allowed to investigate these materials for the MW-assisted oxidation of 1-phenyletahnol under the reaction conditions previously described.

Table 2- 5 Selected data for the MW-assisted oxidation of 1-phenylethanol catalyzed by vanadium complexes **1-6** immobilized on different types of nanodiamonds (ND, NDox and NDoxNa).[a]

Entry	Catalyst	T (℃)	TOF (h^{-1})[b]	Yield%[c]	Selectivity%
1	**1**@ND	100	496	44.7	99
2	**1**@ND	125	676	61.3	97
3	**1**@NDox	100	714	61.2	99
4	**1**@NDox	100	842	40.0	99
5	**1**@NDox	100	519	75.9	99
6	**1**@NDoxNa	100	519	52.5	95
7	**2**@ND	100	611	57.9	99
8	**2**@ND	125	868	75.5	99
9	**2**@NDoxNa	100	292	28.9	93
10	**3**@ND	100	68	6.7	67
11	**3**@ND	125	164	15.3	86
12	**3**@NDoxNa	100	248	23.0	93
13	**4**@ND	100	669	65.9	99
14	**4**@ND	125	1823	91.0	99
15	**4**@NDox	100	610	56.3	99
16	**4**@NDox	125	1458	83.0	98
17	**4**@NDoxNa	100	510	47.8	98
18	**5**@NDoxNa	100	312	29.1	99
19	**5**@NDoxNa	125	537	48.0	99
20	**6**@ND	100	141	13.9	85
21	**6**@ND	125	535	52.9	97
22	**6**@NDox	50	465	44.3	98
23	**6**@NDox	75	83	8.0	88
24	**6**@NDox	100	316	31.7	90
25	**6**@NDox	125	147	14.7	80
26	**6**@NDox	150	678	75.1	96
27	**6**@NDoxNa	100	412	41.0	95

[a] Reaction conditions unless stated otherwise: 5 mmol of 1-phenylethanol, 10 mmol of TBHP (2 eq., 70% in H_2O), 0.5 h of MW irradiation (10 W power). [b] Turnover frequency = number of moles of acetophenone per mole of V-complex loaded on the carbon material, per hour. [c] Moles of acetophenone per 100 mol of 1-phenylethanol.

Table 2- 6 MW-assisted solvent-free oxidation of 1-phenylethanol in the presence of the nanodiamonds ND, ND-ox and ND-ox-Na.[a]

Entry	Material	Temperature (℃)	Yield[b] (%)
32	ND	90	5
33	ND	125	1
34	NDox	90	3
35	NDox	125	7
36	NDoxNa	90	2
37	NDoxNa	125	3

[a] Reaction conditions unless stated otherwise: 5 mmol of 1-phenylethanol, 10 mmol of TBHP (2 eq., 70% in H_2O), 0.5 h of MW irradiation (10 W power). [b] Moles of acetophenone per 100 mol of 1-phenylethanol.

In general, complexes **1**, **2**, **5** and **6** immobilized on nanodiamonds exhibit similar to or better catalytic activity (**Figure 2- 1**) than the previously found[16,33,34] for the corresponding analogues immobilized on carbon nanotubes, carbon xerogels or activated carbons. The very low loading of complexes **3** and **4** obtained in the heterogenization process precluded the catalytic application of these materials on those supports[16,33,34].

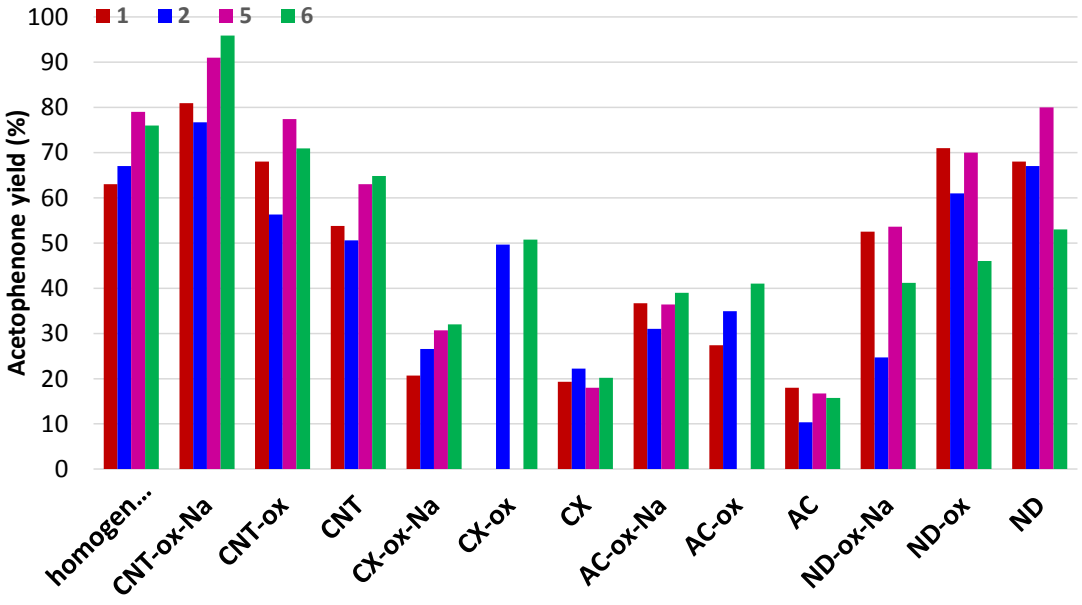

Figure 2- 1 Acetophenone yields produced by MW-assisted and solvent-free oxidation of 1-phenylethanol catalyzed by vanadium complexes **1**, **2**, **5** and **6** in homogeneous conditions and immobilized in twelve different carbon materials: CX, AC, CNT and ND with different treatments. The data concerning CX, AC and CNT was obtained from references [16] and [33]. Some of the samples are not shown in this figure, because the vanadium loading is very low.

However, we found that to reach acetophenone yields up to 91% (with 99% selectivity) in 0.5 h reaction time, 125 ℃ are required (**Entry 14**, **Table 2- 5**). In fact, the temperature range screening using **6**@NDox as catalyst revealed that 125 ℃ was the best temperature to obtain the maximum yield of acetophenone under the above described reaction conditions (**Figure 2- 2**).

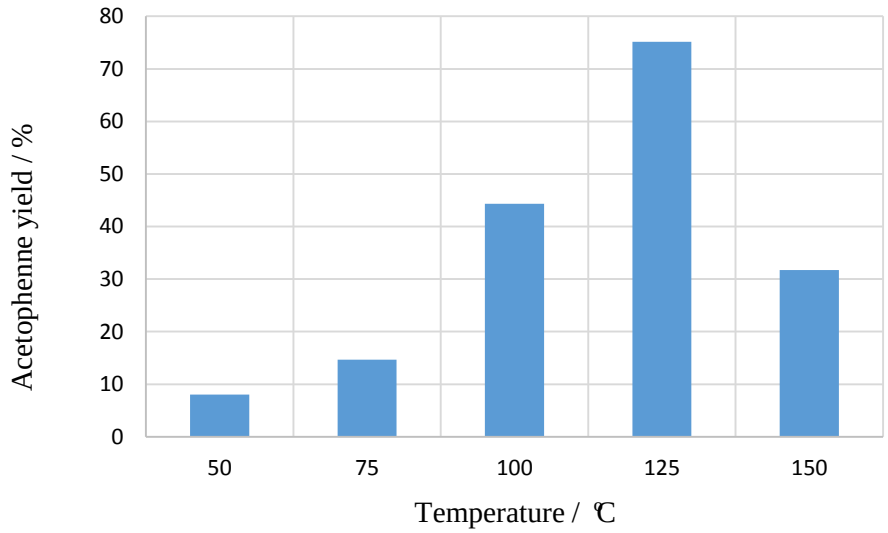

Figure 2- 2 Effect of the temperature on the acetophenone yield produced by oxidation of 1-phenylethanol in the presence of **6**@NDox after 0.5 h of MW (10 W power) irradiation.

Complexes **3** and **4** provide the most active catalytic systems with nanodiamonds. The anchorage of these complexes seems to be more favorable in supports with neutral groups, such as the pristine ND and NDox than on anionic NDoxNa. Thus the groups contained in the graphitic layer that NDs have,[36] seem more favorable to anchor the complexes.

We also found that the oxidative treatment on ND did not improve the catalytic activity of the resulting materials @NDox (**Figure 2- 3**), as found (and previously reported[16,33,34]) for the other carbon materials tested (AC, CX and CNT). Indeed, the most active ND system was **4**@ND (TOF values, considered as moles of acetophenone per mole of V-complex loaded on the nanodiamond, per hour, up to 1.82 x 10^3, **Figure 2- 3**, **Table 2- 5**) with a maximum yield of 91%.

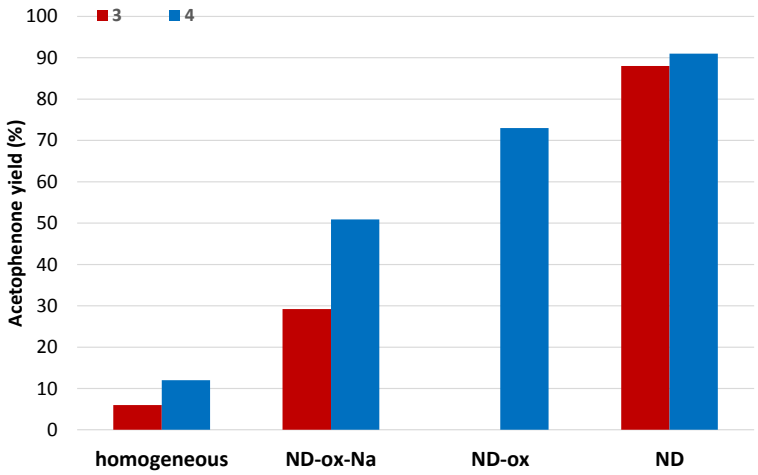

Figure 2- 3 Yield of acetophenone produced by MW-assisted oxidation of 1-phenylethanol (0.5 h) catalyzed by compounds **3** or **4** in homogeneous conditions or supported on nanodiamond materials with different treatments.

Catalyst recycling of **4**@ND was tested up to 5 consecutive cycles as described above. In a second, third, fourth and fifth run, the observed activity was 97%, 74%, 67% and 61% of the initial one, being the selectivity maintained. **Figure 2- 4** and **Table 2- 7** present the recyclability of the system **4**@ND.

Table 2- 7 Effect of the catalyst recycling on the yield of acetophenone for the MW-assisted oxidation (0.5 h) of 1-phenylethanol with TBHP, at 125 ℃ catalyzed by **4**@ND.

Entry	Catalyst	Conversion%	TOF (h^{-1})	Yield%
14	**4**@ND 1st cycle	91.9	1822	91.0
28	**4**@ND 2nd cycle	90.7	1764	88.2
29	**4**@ND 3rd cycle	68.7	1346	67.3
30	**4**@ND 4th cycle	62.3	1220	61.0
31	**4**@ND 5th cycle	55.9	1102	55.1

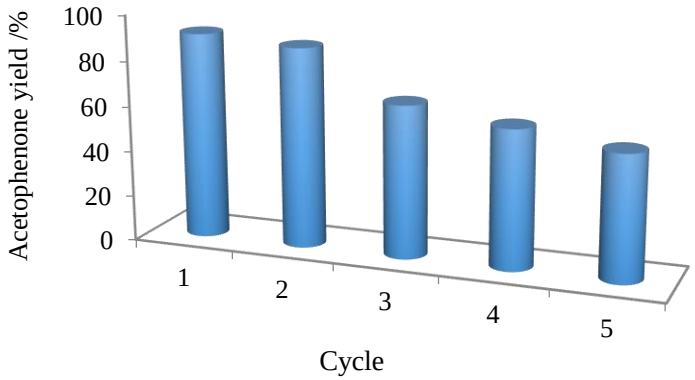

Figure 2- 4 Effect of the catalyst recycling on the yield of acetophenone for the MW-assisted oxidation (0.5 h) of 1-phenylethanol with TBHP, at 125 ℃ catalysed by **4**@ND.

In a recent research Sarmah and coworkers[36] showed that the oxidation of 1-phenylethanol by TBHP was catalyzed by vanadyl sulfate ($VOSO_4$) in MeCN and yielded acetophenone up to 90% after 8 h of reaction at room temperature. Our catalysts have a better performance than those reported.

4. Conclusion

This study contributes towards the development of the still unexplored application of oxidovanadium complexes as catalysts for the microwave-assisted solvent-free oxidation of secondary alcohols under mild conditions.

The immobilization of the oxidovanadium complexes onto the nanodiamonds supports appeared to be rather favorable for their catalytic activity. These heterogeneous systems also offered practical advantages of recycling, allowing successive cycles (up to 5) with a rather high selectivity to acetophenone.

Comparison of the catalytic behavior of different types of oxidovanadium(V) complexes under homogeneous and heterogeneous conditions widen the chemistry of vanadium in the field of oxidation catalysis.

References

[1] Sutradhar, M.; Martins, L. M. D. R. S.; Guedes da Silva, M. F. C.; Pombeiro, A. J. L. Vanadium complexes: Recent progress in oxidation catalysis. *Coord. Chem. Rev*. **2015**, *301-302*, 200-239.

[2] Sutradhar, M.; Kirillova, M. V.; Guedes da Silva, M. F. C.; Martins, L. M. D. R. S.; Pombeiro, A. J. L. A Hexanuclear Mixed-Valence Oxovanadium(IV,V) Complex as a Highly Efficient Alkane Oxidation Catalyst. *Inorg. Chem*. **2012**, *51*, 11229-11231.

[3] Silva, T. F. S.; Alegria, E. C. B. A.; Martins, L. M. D. R. S.; Pombeiro, A. J. L. Half-Sandwich Scorpionate Vanadium, Iron and Copper Complexes: Synthesis and Application in the Catalytic Peroxidative Oxidation of Cyclohexane under Mild Conditions. *Adv., Synth. Cat.* **2008**, *350*, 706-716.

[4] Mishra, G. S.; Silva, T. F. S.; Martins, L. M. D. R. S.; Pombeiro, A. J. L. Scorpionate complexes of vanadium(III or IV) as catalyst precursors for solvent-free cyclohexane oxidation with dioxygen. *Pure Appl. Chem*. **2009**, *81*, 1217-1227.

[5] Silva, T. F. S.; Luzyanin, K. V.; Kirillova, M. V.; Guedes da Silva, M. F. C.; Martins, L. M. D. R. S.; Pombeiro, A. J. L. Novel Scorpionate and Pyrazole Dioxovanadium Complexes, Catalysts for Carboxylation and Peroxidative Oxidation of Alkanes. *Adv., Synth. Cat*. **2010**, *352*, 171-187.

[6] Silva, T. F. S.; Mac Leod, T. C. O.; Martins, L. M. D. R. S.; Guedes da Silva, M. F. C.; Schiavon, M. A.; Pombeiro, A. J. L. Pyrazole or tris(pyrazolyl)ethanol oxo-vanadium(IV) complexes as homogeneous or supported catalysts for oxidation of cyclohexane under mild conditions. *J. Mol. Cat. A: Chem*. **2013**, *376*, 52-60.

[7] Kirillova, M. V.; Kuznetsov, M. L.; Reis, P. M.; Silva, J. A. L.; Fraústo da Silva, J. J. R.; Pombeiro, A. J. L. Direct and Remarkably Efficient Conversion of Methane into Acetic Acid Catalyzed by Amavadine and Related Vanadium Complexes. A Synthetic and a Theoretical DFT Mechanistic Study. *J. Am. Chem. Soc*. **2007**, *129*, 10531-10545.

[8] Silva, J. A. L.; Fraústo da Silva, J. J. R.; Pombeiro, A. J. L. Oxovanadium

complexes in catalytic oxidations. *Cord. Chem. Rev*. **2011**, *255*, 2232-2248.

[9] Silva, J. A. L.; Fraústo da Silva, J. J. R.; Pombeiro, A. J. L. Amavadin, a vanadium natural complex: Its role and applications. *Cord. Chem. Rev.* **2013**, *257*, 2388-2400.

[10] Sutradhar, M.; Pombeiro, A. J. L. Coordination chemistry of non-oxido, oxido and dioxidovanadium(IV/V) complexes with azine fragment ligands *Cord. Chem. Rev*. **2014**, *265*, 89-124.

[11] Valeria, C.; Alessia, C.; Barbara, F.; Giulia, L.; Cristiano, Z. Mechanistic aspects of vanadium catalysed oxidations with peroxides. *Coord. Chem. Rev*. **2011**, *255*, 2165-2177.

[12] Giulia, L.; Valeria, C.; Alessia, C.; Miriam, M.; Cristiano, Z. Recent advances in vanadium catalyzed oxygen transfer reactions. *Coord. Chem. Rev.* **2011**, *255*, 2345-2357.

[13] Baokuan, C.; Xianqiang, H.; Bo, W.; Zhengguo, L.; Jufang, H.; Yingnan, C.; Changwen, H. Three New Imidazole-Functionalized Hexanuclear Oxidovanadium Clusters with Exceptional Catalytic Oxidation Properties for Alcohols. *Chem. Eur. J*. **2013**, *19*, 4408-4413.

[14] Bethany, N. W.; Michael, L. D.; Thomas, R. C.; David, L. T.; Susan, K. H.; Susannah, L. S. A Biomimetic Pathway for Vanadium-Catalyzed Aerobic Oxidation of Alcohols: Evidence for a Base-Assisted Dehydrogenation Mechanism. *Chem. Eur. J.* **2012**, *18*, 14981-14988.

[15] Sutradhar, M.; Martins, L. M. D. R. S.; Guedes da Silva, M. F. C.; Pombeiro, A. J. L. Oxidovanadium complexes with tridentate aroylhydrazone as catalyst precursors for solvent-free microwave-assisted oxidation of alcohols. *Appl. Catal. A: Gen*. **2015**, *493*, 50-57.

[16] Guedes da Silva, M. F. C.; Sutradhar, M.; Martins, L. M. D. R. S.; Alegria, E.; Carabineiro, S. A. C.; Figueiredo, L.; Pombeiro, A. J. L. *Oxido-vanadium Complexes as Homogeneous and Supported Catalysts for the Microwave Assisted Oxidation of Alcohols*, 9th International Vanadium Symposium, Padova, Itália, 2014.

[17] Martins, L. M. D. R. S.; Pombeiro, A. J. L. Tris(pyrazol-1-yl)methane metal

complexes for catalytic mild oxidative functionalizations of alkanes, alkenes and ketones. *Coord. Chem. Rev.* **2014**, *265*, 74-88.

[18] Dorbes, S.; Pereira, C.; Andrade, M.; Barros, D.; Pereira, A. M.; Rebelo, S. L. H.; Araújo, J. P.; Pires, J.; Carvalho, A. P.; Freire, C. Oxidovanadium(IV) acetylacetonate immobilized onto CMK-3 for heterogeneous epoxidation of geraniol. *Microporous Mesoporous Mater*. **2012**, *160*, 67-74.

[19] Clara, P.; José, F. S.; André, M. P.; João, P. A.; Ginesa, B.; Jose, M. P.; Cristina, F. $[VO(acac)_2]$ hybrid catalyst: from complex immobilization onto silica nanoparticles to catalytic application in the epoxidation of geraniol. *Catal. Sci. Tech.* **2011**, *1*, 784-793.

[20] Maurya, M. R.; Priyanka, S.; Amit, K.; João, C. P. Oxidovanadium(IV) Complexes of Tetradentate Ligands Encapsulated in Zeolite-Y as Catalysts for the Oxidation of Styrene, Cyclohexene and Methyl Phenyl Sulfide. *Eur. J. Inorg. Chem*. **2011**, *2011*, 4846-4861.

[21] Maurya, M. R.; Umesh, K.; Manikandan, P. Synthesis and Characterisation of Polymer-Anchored Oxidovanadium(IV) Complexes and Their Use for the Oxidation of Styrene and Cumene. *Eur. J. Inorg. Chem.* **2007**, *2007*, 2303-2314.

[22] Maurya, M. R.; Kumar, U.; Isabel, C.; Pedro, A.; João, C. P. A Polymer-Bound Oxidovanadium(IV) Complex Prepared from an L-Cysteine-Derived Ligand for the Oxidative Amination of Styrene. *Eur. J. Inorg. Chem.* **2008**, *2008*, 577-587.

[23] Maurya, M. R.; Aarti, A.; Amit, K.; João, C. P. Polystyrene bound oxidovanadium(IV) and dioxidovanadium(V) complexes of histamine derived ligand for the oxidation of methyl phenyl sulfide, diphenyl sulfide and benzoin. *Dalton Trans.* **2009**, *2009*, 2185-2195.

[24] Maurya, M. R.; Aarti, A.; Umesh, K.; Amit, K.; Fernando, A.; João, C. P. Polymer-bound oxidovanadium(IV) and dioxidovanadium(V) complexes: synthesis, characterization and catalytic application for the hydroamination of styrene and vinyl pyridine. *Dalton Trans.* **2009**, *2009*, 9555-9566.

[25] Maurya, M. R. Structural models of vanadate-dependent haloperoxidases, their reactivity, immobilization on polymer support and catalytic activities. *J. Chem. Sci.*

2011, *123*, 215-228.

[26] Pingsong, W.; Cem, C.; Gabriella, S.; Jérome, D.; Dieter, R. Sulfoxygenation Catalysed by Oxidovanadium Complexes. *Eur. J. Inorg. Chem.* **2008**, *2008*, 5203-5213.

[27] Figueiredo, J. L.; Pereira, M. F. R.; Freitas, M. M. A.; Órfão, J. J. M.Modification of the surface chemistry of activated carbons. *Carbon*. **1999**, *37*, 1379-1389.

[28] Figueiredo, J. L.; Pereira, M. F. R.; Freitas, M. M. A.; Órfão, J. J. M.Characterization of Active Sites on Carbon Catalysts. *Ind. Eng. Chem. Res.* **2007**, *46*, 4110-4115.

[29] Figueiredo, J. L. *J. Mater.* Functionalization of porous carbons for catalytic applications. *Chem. A.* **2013**, *1*, 9351-9364.

[30] Figueiredo, J. L.; Pereira, M. F. R. Synthesis and functionalization of carbon xerogels to be used as supports for fuel cell catalysts. *J. Energy Chem*. 2013, 22, 195-201.

[31] Figueiredo, J. L.; Pereira, M. F. R. The role of surface chemistry in catalysis with carbons. *Catal. Today*. **2010**, *150*, 2-7.

[32] Carabineiro, S. A. C.; M. Fernando, R. P.; José, J. M. Ó.; José L. F. *Surface Chemistry of Activated Carbons*, ed. J. F. Kwiatkowski, Nova Science Pub Inc., New York, **2011**, 125-168.

[33] Carabineiro, S. A. C.; Jiawei, W.; Sutradhar, M.; Martins, L. M. D. R. S.; Guedes da Silva, M. F. C.; Buijnsters, J. G.; Armando. J. L. P.; Figueiredo, J. L. *Oxido-vanadium complexes heterogenised on carbon materials as catalysts for the oxidation of alcohols*, Encontro Luso-Galego de Química, Porto, **2014**, QI/CAT25, 61.

[34] Carabineiro, S. A. C.; Sutradhar, M.; Martins, L. M. D. R. S.; Guedes da Silva, M. F. C.; Buijnsters, J. G.; Armando. J. L. P.; Figueiredo, J. L. Oxidovanadium complexes anchored on carbon materials for oxidation reactions, XXIV Encontro Nacional da Sociedade Portuguesa de Química, Universidade de Coimbra, **2015**, OC2, 24.

[35] Luísa, M. P. M.; Sergio, M. T.; Carabineiro, S. A. C.; Josephus, G. B.; Joaquim, L.

F.; Figueiredo, J. L.; Adrián, M. T. S. Nanodiamond–TiO_2 Composites for Heterogeneous Photocatalysis. *ChemPlusChem.* **2013**, *78*, 801-807.

[36] Gayatri, S.; Saitanya, K. B.; Anindita, D.; Ankur, G.; Utpal, B. An efficient and reusable vanadium based catalytic system for room temperature oxidation of alcohols to aldehydes and ketones. *Tetrahedron Lett.* **2014**, *55*, 5029-5032.

Chapter 3 MW-assisted oxidation of 1-phenylethanol catalysed by gold nanoparticles supported on different materials

1. Introduction

Gold has been widely used in various fields because of its unique chemical and physical properties. However, for a long period of time gold was considered as the most inert metal element. Researchers tried to study catalysis of gold particles but the result was not as expected. Until 1987, a Japanese researcher Haruta[1] prepared highly dispersed gold catalyst by coprecipitation method to oxidize carbon monoxide at low temperature, gold catalysts got a fully development up to now.

Compared with bulk materials, nanoparticles in small scale afford totally different properties. The small dimensions of gold nanoparticles (AuNPs) provide high electron density, dielectric properties and catalysis action. AuNPs can be combined with a variety of biological macromolecules without destroying the bioactivity. A lot of applications was exploited such as drug delivery carriers[2,3], labelling technique[4], biosensors[5], reduction[6] and oxidation[7] catalysts and so on. The current interest in AuNPs arises from these applications especially the catalysts one.

Gold catalysts can be used for oxidation of alkanes and alcohols. For instance, Dr. Mosaed Alhumaimess and coworkers[8] synthesized gold nanoparticles supported on MnO_2 nanowires to selectively oxidize benzyl alcohol. The oxidation products were formed in low conversion (8.8%), while a good selectivity (98.5-100%) was achieved in 4h of reaction. On the other hand, AuNPs are also helpful for hydrogenation of butadiene and unsaturated aldehydes. Milone and coworkers[9] reported a method of the selective hydrogenation of citral using $Au@Fe_2O_3$ as catalysts in liquid phase. At the same time, Fe_2O_3 worked as the carrier and cocatalyst to promote the activation of C=O bond to enhance hydrogenation activity. In the certain reaction conditions, the conversion achieved 100% and the selectivity of geraniol and nerol was beyond 95%.

A solid support for AuNPs is a normal strategy to form immobilized structure and contain both homogeneous and heterogeneous advantages. To reach a high catalytic activity for different reaction system, gold catalysts can be carried by Carbon nanotubes (CNT), Fe_2O_3, Fe_3O_4, TiO_2, Al_2O_3, SiO_2, NiO and so on. However no matter what the carrier is, the catalysts show high catalytic properties only when the size of gold particles is in low nanoscale (5~10 nm). Liang and coworkers[10] synthesized gold nanoparticles supported by TiO_2 to catalyze the hydration of alkynes. The TiO_2-Au/morpholine system is compatible and weakly basic with acid sensitive functional group. The supported catalyst can also be recycled in flow reactors without losing activity. Hutchings and coworkers[11] studied the oxidation of benzyl alcohol using supported gold palladium catalysts. 1%(Au-Pd)/TiO_2 catalyst was synthesized by a sol-immobilisation method for oxidation of benzyl alcohol. Ultimately, the benzyl alcohol conversion reached 70%, and the product mixture contained benzaldehyde (75%) toluene (23-24%) and petite amount of benzoic acid. Also a recent research about the gold catalyst supported on metal oxide was reported by Wei and coworkers[12]. They prepared gold nanoparticles supported on CeO_2, ZrO_2, TiO_2, HT and Al_2O_3 and tested the catalytic activity by the oxidation of benzyl alcohol[13]. With the presence of dioxygen as oxidant, the alcohols formed esters at mild conditions catalyzed by supported gold nanocatalysts.

In this chapter, we studied the catalytic properties of gold nanoparticles supported at carbon, Fe_2O_3, Al_2O_3, ZnO and TiO_2 in the oxidation reaction of 1-phenylethanol in the presence of TBHP (*tert*-butyl hydroperoxide) as oxidant. The reactions were assisted by microwave. Gas chromatography (GC) was used for testing the yield.

We chose the oxidation of 1-phenylethanol as a model reaction because of its importance in industrial organic synthesis[14]. Considering the cheapest and waste-free oxidant, hydrogen peroxide should be the most suitable oxidant. But because of the low stability of hydrogen peroxide, inert condition is always necessary for H_2O_2 oxidized reactions[15]. Instead of H_2O_2, TBHP, due to its high selectivity and stability, was chosen to be an effective oxidant for the selective oxidation of 1-phenylehthanol.

1.1 Main factors that affect the catalytic activity of gold

1.1.1 Size of gold nanoparticles

The size of gold nanoparticles is the most important factor that affects the catalytic activity of gold nanoparticles[16]. Generally, when the size of gold is below 5 nm, the gold nanoparticles show a high catalytic activity. But when the size increases above 10 nm, the catalytic activity decreases significantly.

There are two main reasons that can explain why the gold nanoparticles obtain high catalytic activity. On the one hand, gold nanoparticles have a high surface and interface effect. Because of the small size of gold nanoparticles and large specific surface area, a large ratio of atoms located on the surface. With decreasing of particle size, the specific surface area increases rapidly. The ratio of the atoms on the surface becomes higher and higher. A large amount of atoms appear on the edge and corner. Then because of the lack of coordination neighboring atoms, the atoms on the surface become extremely unstable and easily combined with other atoms, which shows a high catalytic activity. On the other hand, quantum size effect also influences the catalytic activity. Once gold particles are in nano scale, gold atoms change continuous metallic state to independent dispersing state. Therefore gold nanoparticles provide much more position to attach to substrate, which makes gold nanoparticles higher activity than the bulk particles. For instance, CO cannot be absorbed by smooth gold particles in room temperature [17]. But it can only be absorbed at the edge or corner of the gold crystals. While nanoparticles can provide much more such positions for CO. So the gold nanoparticles have a better catalytic activity.

1.1.2 The effect of carriers

The specific surface area, humidity of carriers and the forces between carriers and catalysts influence the catalytic activity of catalysts. Carried with particles that maintain large specific area, gold nanoparticles can reach a high dispersing degree. And with a highly humid carrier, gold will aggregate to bulk particles, which will decrease the catalytic activity. What's more, the catalytic activity of gold nanoparticles increases

with an increasing connection force between carriers.

The shape of gold nanoparticles will be half ball when attached to the surface of carriers with a strong connection force[18]. Gold nanoparticles in this form have a higher free energy, which are easier to attach to the media of the reaction so as to decrease the free energy.

In addition, the force between gold and carrier can change the structure of electron around gold atoms. Normally gold atoms' d orbit is totally full. But once the support system is formed, the d electron on the last orbit will transport to the carrier. Then the electron orbit of gold will be similar to platinum, of which the last d orbit is not full[19]. This is the reason why inert metal gold maintain a very high catalytic activity.

1.1.3 The effect of load size of gold

When supported by the carrier with a low specific surface area, the load size of gold decides the diameter of the particles. With a bigger load size, the diameter becomes larger also. When the load size of gold (mass ratio) is high (higher than 10%), gold is easily aggregated to bulk particles[20].

While using a carrier with a high specific surface area, although the load size is very high, gold can also reach to particles in nano scale.

2. Experimental

2.1 Materials and instruments

Four different types of carbon materials were used as supports: activated carbon (AC) from Sigma-Aldrich Norit® RO 0.8, multiwalled carbon nanotubes (MWCNTs) from Nanocyl™ NC3100, and carbon xerogel (CX) prepared by condensation of resorcinol and formaldehyde at pH 6, as described elsewhere[21 - 24]. Four different types of oxides were used: aluminium oxide (Al_2O_3) from Aldrich (< 50 nm), iron oxide (Fe_2O_3) from Sigma Aldrich (powder), zinc oxide (ZnO) from Evonik Degussa (AdNano VP 20), titanium dioxide (TiO_2) from Evonik Degussa. The 1-phenylethanol (98%), *tert*-butyl hydroperoxide (TBHP, 70%) and benzaldehyde (≥ 99%) were from

Sigma-Aldrich. The acetonitrile (99.99%) was from Fisher Scientific, UK.

Gas chromatographic (GC) measurements were carried out by the Fisons Instruments GC 8000 series gas chromatograph. The FID detector was a DB-624 (J&W) capillary column. The software was JascoBorwin v.1.50 in Window XP Operating System. Microwave reactor Anton Paar Monowave 300 was used for the MW-assisted oxidation of 1-phenylethanol.

2.2 Experimental procedure

The gold on carbon and gold on oxide supports were prepared and characterised by Dr. Sónia Carabineiro from the University of Porto. HRTEM characterisations of the oxide materials were performed in the University of Granada, Spain (Prof. Francisco Maldonado-Hodar), while carbon materials were analysed at the Instituto Potosino de Investigación Científica y Tecnológica, Mexico (Dr. Miguel Avalos-Borja).

2.2.1 Gold loading

Gold was loaded on the carbon supports (1% wt.) by the colloidal method[21], which is known to be the most adequate for this type of materials[25, 26]. The gold precursor, $HAuCl_4 \cdot 3H_2O$ (Alfa Aesar), was dissolved in water, with addition of polyvinyl alcohol (Aldrich) and $NaBH_4$(Aldrich), resulting in a ruby red sol to which the powder support was added under stirring. After a few days the solution started to loose colour, as Au was deposited on the support. The colourless solution was filtered, the catalyst washed thoroughly with distilled water and dried at 110 ℃ overnight. The organic scaffold was removed from the support by a heat treatment under nitrogen flow for 3 h at 350 ℃, and then, the catalyst was activated by further treatment under hydrogen flow for 3 h also at 350 ℃.

Gold was deposited on the oxide supports (1% wt.) by deposition-precipitation[27], which is a common procedure for gold deposition on oxides[25, 26]. A solution of NaOH (1 M) was added to an aqueous solution of $HAuCl_4$ (5×10^{-3}M) in order to rise the pH of the solution to 9. The support was then added with stirring at room temperature (1 g per 50 ml of solution). The resulting suspension was stirred for 1 h and the solid

obtained was filtered, thoroughly washed and then dried at 110 ℃ overnight.

2.2.2 MW-assisted 1-phenylethanol oxidation

In this procedure the catalyst (0.5 mmol), the substrate (2.5 mmol, 300 μL 1-Phenylethanol) and the oxidant agent (5 mmol, 345 μL 70% aqueous solution TBHP) were added in G10 vessel. The mixture was stirred 600 RPM at 100 ℃ for 60 min in microwave reactor. After reaction the sample was extracted with the solvent (2.5 mL MeCN), and internal standard (150 μL benzaldehyde) was added.

The support of catalyst was used in different quantity to be a reference of the reactions.

Table 3- 1 The oxidation of 1-phenylethanol catalyzed by the support materials.[a]

Entry	Support	m (mg)	n (mmol)
1	Fe_2O_3	8.0	0.05
2	Fe_2O_3	80.0	0.5
3	Al_2O_3	5.1	0.05
4	Al_2O_3	51.0	0.5
5	ZnO	4.1	0.05
6	ZnO	40.7	0.5
7	TiO_2	4.0	0.05
8	TiO_2	40.0	0.5
9	C	1.2	0.1
10	C	6.0	0.5

[a] Reactions were carried out at 100 ℃ for 60 min.

Then the reactions were carried out by using gold nanoparticles in different conditions of temperature and quantity.

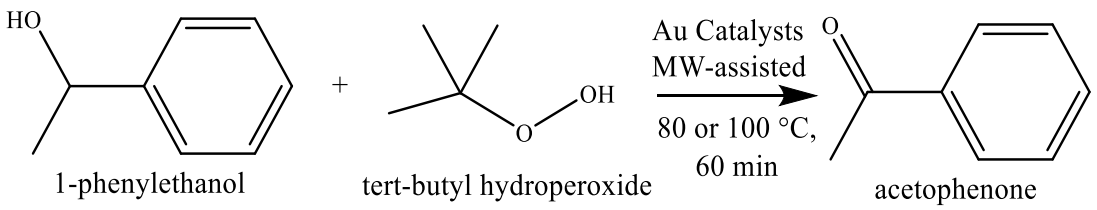

Scheme 3- 1 MW-assisted oxidation of 1-phenylethanol catalyzed by Au nanoparticles supported at different materials.

Table 3- 2 The oxidation of 1-phenylethanol catalyzed by supported gold nanoparticles.

Entry	Catalyst	m (mg)	Cat.(μmol)	T (℃)	t (min)
11	1% Au @ Fe_2O_3	80.1	4.1	100	60
12	1% Au @ Fe_2O_3	41.0	2.1	100	60
13	1% Au @ Fe_2O_3	41.0	2.1	80	60
14	1% Au @ Al_2O_3	51.5	2.6	100	60
15	1% Au @ Al_2O_3	41.0	2.1	100	60
16	1% Au @ Al_2O_3	41.0	2.1	80	60
17	1% Au @ ZnO	41.0	2.1	100	60
18	1% Au @ ZnO	41.0	2.1	80	60
19	1% Au @ TiO_2	41.0	2.1	100	60
20	1% Au @ TiO_2	41.0	2.1	80	60
21	1% Au @ C	6.9	0.35	100	60
22	1% Au @ C	41.0	2.1	100	60
23	1% Au @ C	41.0	2.1	80	60

2.2.3 Recycling Experiment

After all the reactions done, we chose one supported gold catalyst with the highest catalytic activity to test the recycling properties. Two strategies for recycle the catalysts were used. The first strategy is to filter the solid phase, wash and dry in compressed air. And then the catalysts were used for another cycle. The other strategy is to take out all the liquid phase as much as possible from the G10 vessel. And then the reaction was performed again directly with adding substrate and solvent. In this case, the loss of catalyst was lower than the first one.

Table 3- 3 The oxidation of 1-phenylethanol catalyzed by recycling gold nanoparticles.

Entry	Catalyst	m (mg)	Cat.(μmol)	T (℃)	t (min)
19	1% Au @ TiO_2 1st cycle	41	2.1	100	60
24	1% Au @ TiO_2 2nd cycle	41	2.1	100	60
25	1% Au @ TiO_2 3rd cycle	41	2.1	100	60
26	1% Au @ TiO_2 4th cycle	41	2.1	100	60
27	1% Au @ TiO_2 1st cycle CA*	41	2.1	100	60
28	1% Au @ TiO_2 2nd cycle CA	41	2.1	100	60
29	1% Au @ TiO_2 3rd cycle CA	41	2.1	100	60

*CA refers to the catalysts dried under compressed air after reaction.

2.3 GC analysis

The samples were analyzed by GC after centrifugation and filtering. The program of GC that we set for testing was maintained at 120 ℃ for 1 min, heating from 120 ℃ to 200 ℃ at a rate of 10 ℃/min, holding at 200 ℃ for 1 min and then cooling to 120 ℃. The yield and selectivity were calculated from GC data with area of each peak. Finally, the comparison was performed with previous samples under different conditions.

3. Results and Discussion

3.1 Characterization

3.1.1 BET surface area

The Brunauer-Emmett-Teller (BET) is a widely-used and well-behaved method for characterizing the surface areas of the nanoparticles from isotherm data[28].

The materials were characterised by N_2 adsorption at -196 ℃ in a Quantachrome Nova 4200e apparatus, using the multi-point BET theory for specific surface area determination. The results are shown in **Table 3- 4**.

Table 3- 4 BET surface area of supports*.

Samples	BET surface area (m^2/g)
Al_2O_3	210
Fe_2O_3	10
ZnO	26
TiO_2	51
AC	974
CNT	257
CX	611

*Adding Au to the supports does not change much the BET surface area.

From **Table 3- 4** we can conclude that all the supports have a big surface area. Because of the unique structure of the carbon materials, the surface area of activated carbon, carbon nanotubes and carbon xerogel is much bigger than the metal oxide supports, especially the activated carbon of which the surface area reaches 974 m^2/g.

Since the supported gold nanoparticles have the similar surface area as their supports, the AC supported gold nanoparticles have the biggest surface area. As we discussed previously, a big surface area may lead a high activity of the catalysts.

3.1.2 HRTEM images

High-resolution transmission electron microscopy (HRTEM) images of oxides were obtained by means of a Phillips CM-20 electron micro-scope (Granada University). Carbon materials were analysed by HRTEM on a FEI Tecnai F30 instrument (IPICyT, Mexico).

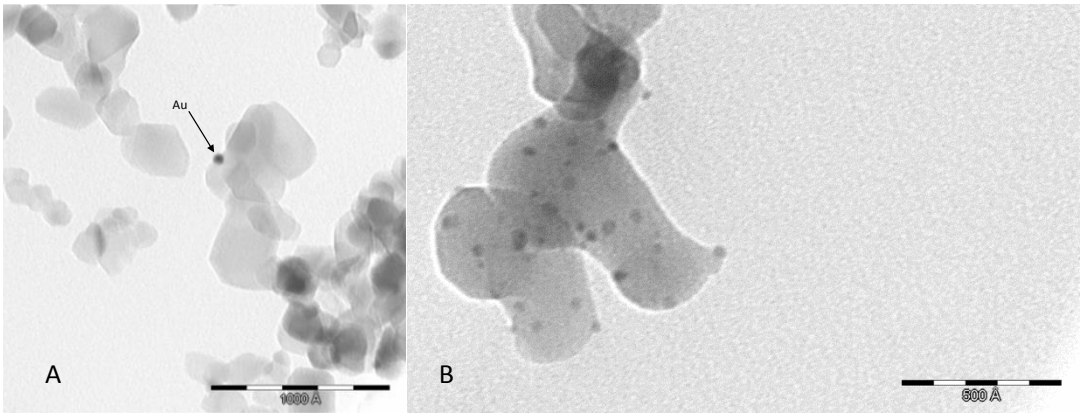

Figure 3- 1 HRTEM image of A) Au@TiO_2, B) Au@Fe_2O_3 (gold nanoparticle seen as darker spots).

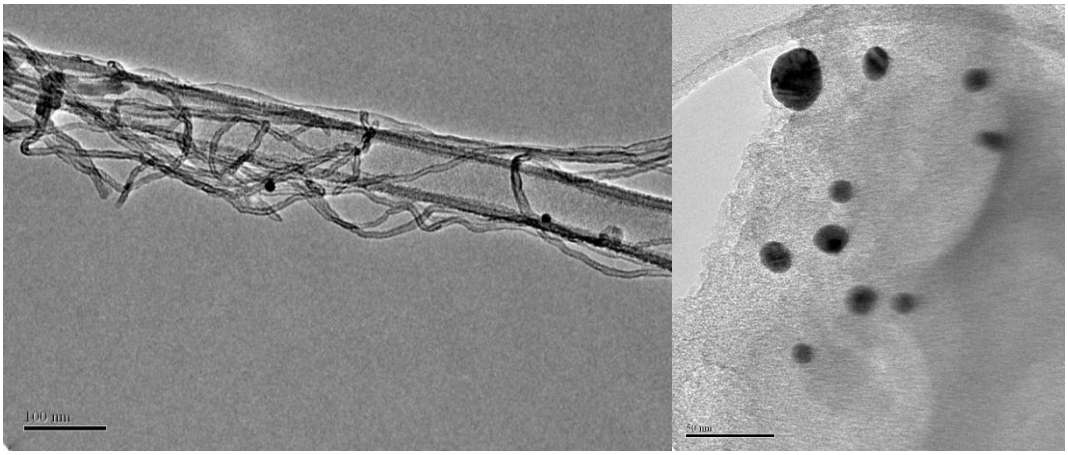

Figure 3- 2 HRTEM image of A) Au@CNT, B) Au@AC (gold nanoparticles seen as darker spots).

As seen in **Figure 3- 1** and **Figure 3- 2**, gold nanoparticles were evenly distributed on the surface of the supports. The gold nanoparticles did not change the size or the

surface area of the supports. The average sizes of the supported gold nanoparticles were still in nano scale.

3.1.3 EDS analysis

The presence of gold was confirmed by Energy-dispersive X-ray spectroscopy (EDS). Samples were mounted on a carbon polymer supported copper micro-grid. A few droplets of a suspension of the ground catalyst in isopropyl alcohol were placed on the grid, followed by drying under ambient conditions. The average gold particle size was determined from measurements made on about 300–500 particles, depending on the sample.

The results of EDS is shown in **Table 3- 5**.

Table 3- 5 Characterization of the supported gold nanoparticles by EDS.

Samples	Average particle size
Au@Al_2O_3	26
Au@Fe_2O_3	2.3
Au@ZnO	5.5
Au@TiO_2	2.2
Au@AC	6.8
Au@CNT	5.1
Au@CX	4.4

Usually the catalytic activity is related with gold nanoparticle size (the smaller the more active), however many other factors can contribute, like the characteristics of the support, and the interaction of the support with gold[23, 24].

3.2 Oxidation of 1-phenylethanol

The results of the oxidation of 1-phenylethanol are shown below in **Table 3- 6**. The TOF (turnover frequency, turnover per hour) and yield are calculated to study the catalytic activity of the catalysts.

Table 3- 6 MW-assisted catalytic oxidation of 1-phenylethanol catalyzed by supports and gold nanoparticles.[a]

Entry	Catalyst	T (℃)	TOF (h^{-1})	Yield[b]%	Selectivity%
1	Fe_2O_3	100	4.5	6.6	17.0
2	Fe_2O_3	100	1.1	21.8	34.8
3	Al_2O_3	100	4.1	5.4	14.2
4	Al_2O_3	100	0.2	4.2	50.6
5	ZnO	100	2.6	4.7	66.2
6	ZnO	100	0.2	3.9	57.4
7	TiO_2	100	3.8	5.9	38.8
8	TiO_2	100	0.3	5.0	90.9
9	C	100	2.6	7.3	28.2
10	C	100	0.5	9.4	77.7
11	Au @ Fe_2O_3	100	614.4	81.8	91.6
12	Au @ Fe_2O_3	100	983.2	80.3	88.9
13	Au @ Fe_2O_3	80	520.9	43.1	59.5
14	Au @ Al_2O_3	100	764.5	77.8	99.4
15	Au @ Al_2O_3	100	825.0	69.3	98.2
16	Au @ Al_2O_3	80	469.5	38.1	98.2
17	Au @ ZnO	100	981.7	84.8	98.8
18	Au @ ZnO	80	826.4	67.8	99.1
19	Au @ TiO_2	100	1095.4	91.1	99.7
20	Au @ TiO_2	80	879.8	74.2	98.3
21	Au @ C	100	663.1	9.0	90.9
22	Au @ C	100	280.2	22.9	95.0
23	Au @ C	80	124.8	10.6	70.2
24	Au @ TiO_2 2^{nd} cycle	100	916.6	72.4	98.0
25	Au @ TiO_2 3^{rd} cycle	100	684.9	52.4	98.7
26	Au @ TiO_2 4^{th} cycle	100	694.5	51.9	99.2
27	Au @ TiO_2 1^{st} cycle CA	100	1052.4	88.9	99.4
28	Au @ TiO_2 2^{nd} cycle CA	100	897.4	71.6	98.9
29	Au @ TiO_2 3^{rd} cycle CA	100	549.5	44.3	99.8

[a] Reaction time is always 1 h. [b] Yield based on 1-phenylethanol.

3.2.1 Influence of the supports

The main product of the oxidation of 1-phenylethanol is acetophenone. Regarding the reactions with the supports, the yield of the product is very low. Also the selectivity and activity are not high. In the case of the gold nanoparticles with various supports, significantly different yields were attained.

Table 3- 7 The oxidation of 1-phenylehtanol catalyzed by supported gold nanoparticles and only the support.

Entry	Catalyst	T (℃)	t (min)	%conv	TOF (h^{-1})	%Yield
2	Fe_2O_3	100	60	62.7	1.1	21.8
12	Au @ Fe_2O_3	100	60	90.3	983.2	80.3
4	Al_2O_3	100	60	-2.4	0.2	4.2
15	Au @ Al_2O_3	100	60	70.6	825.0	69.3
6	ZnO	100	60	6.8	0.2	3.9
17	Au @ ZnO	100	60	85.8	981.7	84.8
8	TiO_2	100	60	6.5	0.3	5.0
19	Au @ TiO_2	100	60	91.4	1095.4	91.1
9	C	100	60	12.1	0.5	9.4
22	Au @ C	100	60	24.1	280.2	22.9

From the figure below, it is easy to find that the yield of reactions with gold nanoparticles are much higher than the ones with only the support. The catalytic activity of supported gold is very high. And between the supported catalysts, Au@TiO_2 gives the best results.

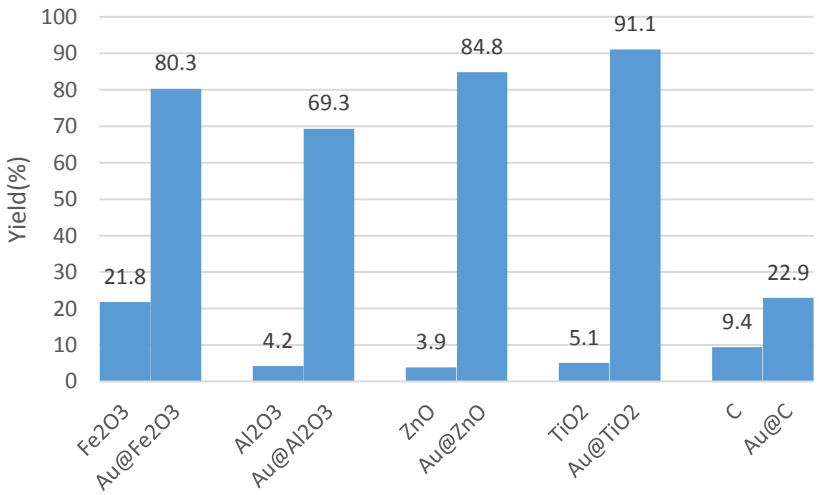

Figure 3- 3 The yield of acetophenone catalyzed by the supports and supported gold nanoparticles. Condition: 100 ℃, 60 min, 600 rpm, microwave reactor, 10W.

3.2.2 Influence of temperature

We investigated the influence of the temperature on the product yield by comparing the yields of the reactions catalyzed by the supported gold nanoparticles in different reaction temperature (80 ℃ and 100 ℃). The results are shown in **Table 3- 8**.

Table 3- 8 The oxidation of 1-phenylethanol catalyzed by gold nanoparticles in different reaction temperature.

Entry	Catalyst	T (℃)	TOF (h^{-1})	Yield%	Selectivity%
12	Au @ Fe_2O_3	100	983.2	80.3	88.93
13	Au @ Fe_2O_3	80	520.9	43.1	59.53
15	Au @ Al_2O_3	100	825.0	69.3	98.16
16	Au @ Al_2O_3	80	469.5	38.1	98.20
17	Au @ ZnO	100	981.7	84.8	98.83
18	Au @ ZnO	80	826.4	67.8	99.12
19	Au @ TiO_2	100	1095.4	91.1	99.67
20	Au @ TiO_2	80	879.8	74.2	98.28
22	Au @ C	100	280.2	22.9	95.02
23	Au @ C	80	124.8	10.6	70.20

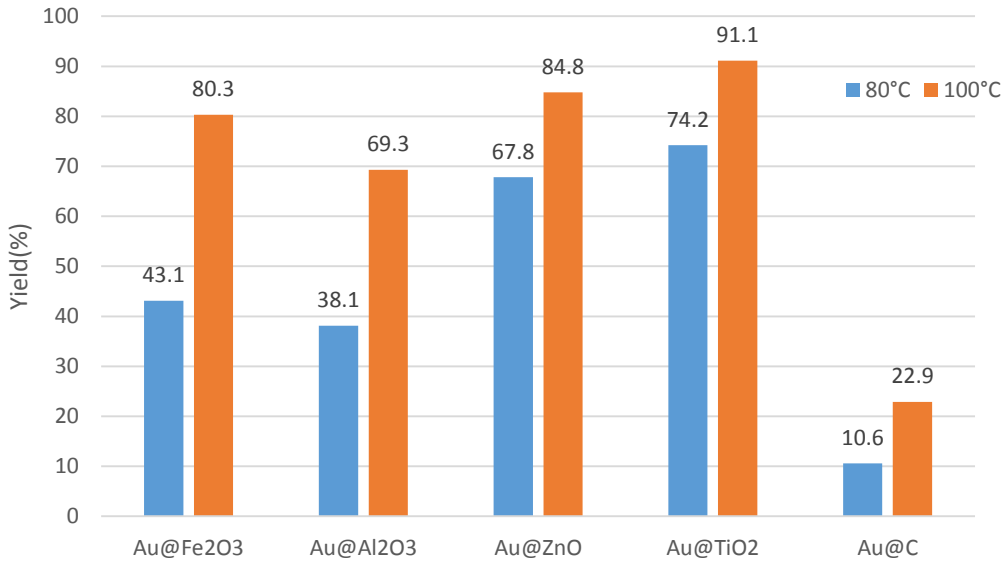

Figure 3- 4 Effect of different temperature in catalytic oxidation of 1-phenylethanol.

From **Figure 3- 4**, we can find that the reaction temperature has an important effect on the MW-assisted oxidation of 1-phenylethanol. With a 20 ℃ of increasing in temperature, the yield increased a lot, especially the Au@Fe_2O_3 and Au@Al_2O_3. So we can figure out that the gold nanoparticles have a higher activity at 100 ℃ than at 80 ℃

for the MW-assisted oxidation of 1-phenylehthanol. And we chose 100 ℃ as the ideal reaction temperature to continue discussing other effects.

3.2.3 Influence of quantity of catalyst

In this section, we chose the reactions catalyzed by Fe_2O_3 supported gold nanoparticles (**Entry 11**, **12**) to discuss the influence of quantity of catalyst. Under the same reaction temperature and time, but almost double quantity of the catalysts, the yield didn't change a lot. In this case, the lower quantity of catalysts was regarded as a better condition for the oxidation of 1-phenylethanol.

3.3 Recycling Experiment

First of all, it is worth mentioning that we removed the liquid phase directly from the vessel and dried in two different methods. We considered that no catalysts were lost during the separating and drying steps. Then for the next cycle of reaction, we added the substrate into the same vessel as the previous cycle. There might be some errors during this method. But we believe the errors were controlled in an acceptable scope. The recycling tests results are shown in **Table 3- 9** and **Figure 3- 5**.

Table 3- 9 The results of the recycling tests catalyzed by TiO_2 supported gold nanoparticles in different recycling methods[a].

Entry	Catalyst	conversion%	TOF (h^{-1})	Yield%
19	Au @ TiO_2 1st cycle	91.4	1095.4	91.1
24	Au @ TiO_2 2nd cycle	71.9	916.6	72.4
25	Au @ TiO_2 3rd cycle	50.1	684.9	52.4
26	Au @ TiO_2 4th cycle	48.3	694.5	51.9
27	Au @ TiO_2 1st cycle CA	89.4	1052.4	88.9
28	Au @ TiO_2 2nd cycle CA	71.4	897.4	71.6
29	Au @ TiO_2 3rd cycle CA	44.4	549.5	44.3

[a] Reaction condition: 100 ℃, 60 min, 600 rpm.

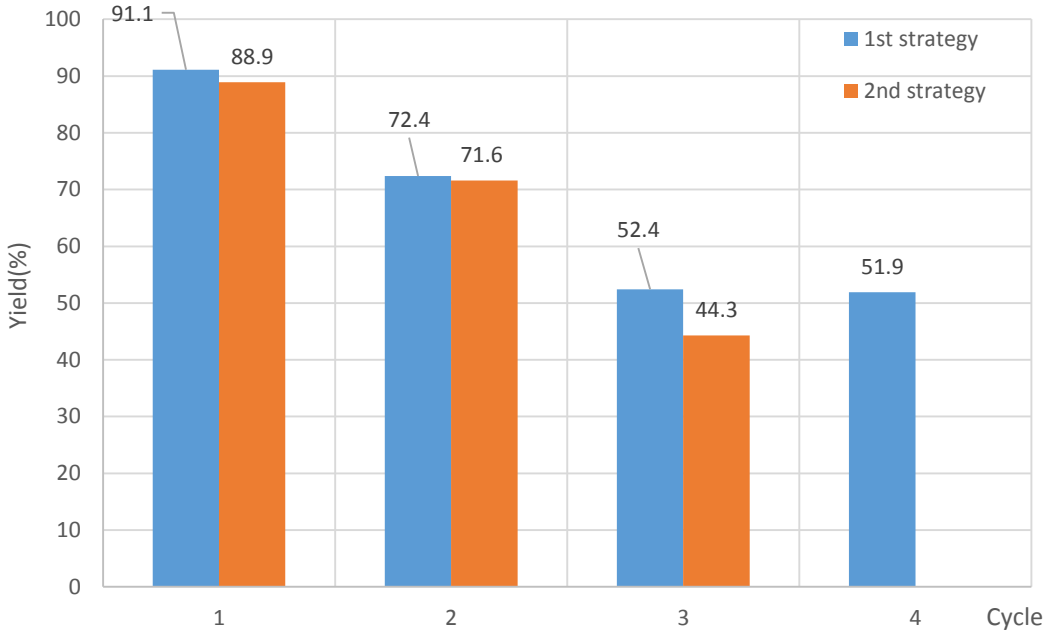

Figure 3- 5 The plot of yields of cycling test reactions to cycles.

The catalytic activity of the gold nanoparticles remains a high level in the first two cycles. For both strategies, a high recycling efficiency was obtained in first two cycles. And it decreases very fast till 3rd cycle. And after 3 cycles, the yield tend to be around 50%.

4. Conclusion

In summary, the supported gold nanoparticles were synthesized successfully. BET, TEM and EDS were used to monitor the surface structure and size. The average sizes of each gold catalyst are in nanoscale. The catalytic activity was analysed by GC through the oxidation of 1-phenylethanol. Our results indicated that gold nanoparticles were activated on the support of metal oxide. Our results also demonstrated that the gold nanoparticles supported on TiO_2 had a good recyclability. Compared with the vanadium catalysts, the highest yield of acetophenone is the same, but vanadium catalysts can be used for more cycles to achieve higher than 50% of yield and the yield of second cycle is higher than gold catalyst. These results have a very important implication on the design of gold catalysts and the industrial producing of acetophenone.

References

[1] Haruta, M.; Yamada, N.; Kobayashi, T. Gold catalysts prepared by coprecipitation for low-temperature oxidation of hydrogen and of carbon monoxide. *J. Catal.* **1989**, *115*, 301-309.

[2] Camila, R. S.; Henrique, R. O.; Wagner, M. P.; Lubhandwa, S. B.; Ricardo, B. A.; Anderson, J. G.; Claure, N. L. Gold Nanoparticle and Berberine Entrapped into Hydrogel Matrix as Drug Delivery System. *J. Biomater. Nanobiotechnol.* **2015**, *6*, 53-63.

[3] Mariangela, B.; Silvia, B.; Francesco, R.; Lorenzo, G.; Paola, F.; Marco, L.; Paolo, P.; Lucia, P. Gold nanoparticles as drug carriers: a contribution to the quest for basic principles for monolayer design. *J. Mater. Chem. B.* **2015**, *3*, 432-439.

[4] James, F. H.; Richard, D. P. New Frontiers in Gold Labeling. *J. Histochem. Cytochem.* **2000**, *48*, 471-480.

[5] Hutter, E.; Maysingere, D. Gold-nanoparticle-based biosensors for detection of enzyme activity. *Trends Pharmacol. Sci.* **2013**, *34*, 497-507.

[6] Shengzong, L.; Jacek, J.; Gerald, B. H.; Bo, X. Supported Gold Nanoparticle-Catalyzed Hydration of Alkynes under Basic Conditions. *J. Org. Lett.* **2015**, *17*, 162-165.

[7] Graham, J. H. Selective oxidation using supported gold bimetallic and trimetallic nanoparticles. *J. Catal. Today.* **2014**, *238*, 69-73.

[8] Mosaed, A.; Zhongjie, L.; Qian, H.; Li, L.; Nickolaos, D.; Nicholas, F. D.; Marco, C.; Stuart, H. T.; Jonathan, K. B.; Christopher, J. K.; Graham, J. H. Oxidation of benzyl alcohol and carbon monoxide using gold nanoparticles supported on MnO_2 nanowire microspheres. *J. Chem.* **2014**, *20*, 1701-1710.

[9] Milone, C.; Tropeano, M. L.; Gulino, G.; Neri, G.; Ingoglia, G.; Galvagno, S. Selective liquid phase hydrogenation of citral on Au/Fe2O3 catalysts. *Chem. Commun. (Camb).* **2002**, *8*, 868-869.

[10] Shengzong, L.; Jacek, J.; Gerald, B. H.; Bo, X. Supported Gold Nanoparticle-Catalyzed Hydration of Alkynes under Basic Conditions. *Org. Lett.* 2015, 17, 162-

165.

[11] Graham, J. H. Nanocrystalline gold and gold palladium alloy catalysts for chemical synthesis. *Chem. Commun.* **2008**, 1148-1164.

[12] Huili, W.; Jingyi, L.; Jing, Y.; Jianwei, Z.; Haiquan, S.; Xiaojing, W. Gold nanoparticles supported on metal oxides as catalysts for the direct oxidative esterification of alcohols under mild conditions. *Inorg. Chim. Acta.* **2015**, *427*, 33–40.

[13] Antonio, B.; Annarita, N.; Alfonso, G. Highly Efficient Direct Aerobic Oxidative Esterification of Cinnamyl Alcohol with Alkyl Alcohols Catalysed by Gold Nanoparticles Incarcerated in a Nanoporous Polymer Matrix: A Tool for Investigating the Role of the Polymer Host. *Chem. Eur. J.* **2014**, *20*, 5478-5486.

[14] Alessandra, S.; Martins, L. M. D. R. S.; Kamran, T. M.; Maximilian, N. K.; Michael, G. B. D.; Claudio, P.; Pombeiro, A. J. L. Microwave-assisted and solvent-free peroxidative oxidation of 1-phenylethanol to acetophenone with a Cu^{II}–TEMPO catalytic system *Catal. Commun.* **2014**, *48*, 69–72.

[15] Gayatri, S.; Saitanya, K. B.; Anindita, D.; Ankur, G.; Utpal, B. An efficient and reusable vanadium based catalytic system for room temperature oxidation of alcohols to aldehydes and ketones. *Tetrahedron Lett.* **2014**, *55*, 5029–5032.

[16] Alexander, I. K.; Anguelina, P. K.; Kiyotaka, A.; Yoshio, M.; Toshihiro, K.; Takafumi, S.; Yasuhiro, I. Supported Gold Catalysts Prepared from a Gold Phosphine Precursor and As-Precipitated Metal-Hydroxide Precursors: Effect of Preparation Conditions on the Catalytic Performance. *J. Catal.* **2000**, *196*, 56-65.

[17] Flora, B.; Anna, C.; Maela, M.; Ping, L.; Tomoki, A.; Satoshi, I.; Masatake, H. Au/TiO_2 Nanosized Samples: A Catalytic, TEM, and FTIR Study of the Effect of Calcination Temperature on the CO Oxidation. *J. Catal.* **2001**, *202*, 256-267.

[18] Masatake, H.; Masakazu, D. Advances in the catalysis of Au nanoparticles. *Appl. Catal. A: Gen.* **2001**, *222*, 427-437.

[19] Claudia, B.; Francesca, P.; Laura, P.; Michele, R. Selective liquid phase oxidation using gold catalysts. *Top. Catal.* **2000**, *13*, 231-236.

[20] Zhang, Y.; Nathan, W. F.; Robert, J. C.; Hongjie, D. Metal coating on suspended

carbon nanotubes and its implication to metal–tube interaction. *Chem. Phy. Lett.* **2000**, *331*: 35-41.

[21] Carabineiro, S. A. C.; Martins, L. M. D. R. S.; Avalos-Borja, M.; Buijnsters, J. G.; Pombeiro, A. J. L.; Figueiredo, J. L. Metal coating on suspended carbon nanotubes and its implication to metal–tube interaction. *Appl. Catal. A: Gen.* **2013**, *467*, 279–290.

[22] Carabineiro, S. A. C.; Thavorn-Amornsri, T.; Pereira, M. F. R.; José L. F. Adsorption of ciprofloxacin on surface-modified carbon materials. *Water Res.* **2011**, *45*, 4583–4591.

[23] Mahata, N.; Pereira, M. F. R.; Suárez-García, F.; Martínez-Alonso, A.; Tascón, J. M. D.; Figueiredo, J. L. Tuning of texture and surface chemistry of carbon xerogels. *J. Colloid Interface Sci.* **2008**, *324*, 150–155.

[24] Pumakala, V. S.; Filomena, G.; Freitas, M. M. A.; Pereira, M. F. R.; José L. F. Surface activation of a polymer based carbon. *Carbon.* **2004**, *42*, 1321–1325.

[25] Carabineiro, S. A. C.; David, T. T. *Catalytic Applications for Gold Nanotechnology*, In: Nanocatalysis, Eds. U. Heiz and U. Landman, Springer-Verlag, Berlin, Heidelberg, New York, **2007**, 377-489.

[26] Sónia. A. C. C.; David. T. T. *"Gold Catalysis"*, In: Gold: Science and Applications, Eds. C. Corti, R. Holliday, CRC Press, Taylor and Francis Group, Boca Raton, London, New York, **2010**, 89-122.

[27] Soria, M. A.; Pérez, P.; Carabineiro, S. A. C.; Maldonado-Hódar, F. J.; Mendes, A.; Luis, M. M. Effect of the preparation method on the catalytic activity and stability of Au/Fe_2O_3 catalysts in the low-temperature water–gas shift reaction. *Appl. Catal. A: Gen.* **2014**, *470*, 45– 55.

[28] Lev, D. G.; Keith, E. G. Characterization of Porous Glasses: Simulation Models, Adsorption Isotherms, and the Brunauer−Emmett−Teller Analysis Method. *Langmuir.* **1998**, *14*, 2097-2111.

Chapter 4 MWCNT supported copper nanoparticles used for degradation of pigments

1. Introduction

Carbon nanotubes (CNTs) have been reported for their unique properties such as chemical stability, electrical conductivity, mechanical strength, thermal stability, and the high surface area[1]. However, due to CNT's macromolecular structure and natural tendency to agglomerate, they are insoluble in organic solvents. In order to solve this problem, the surface of these materials is functionalized by chemical modification, like non-destructive oxidation. For this purpose, an acid treatment is usually applied, oxidizing CNT side-walls with hydroxyl (-OH), carboxyl (-COOH) and carbonyl (-C=O) functional groups[2]. Additionally, functionalization of CNT also provides the creation of a bonding site for the metal matrix and a highly dispersed system[3].

There's a diversity of methods to prepare Cu-CNT composites, namely molecular-level mixing, chemical reduction methods, thermal reduction, microemulsion technique, polyol method and AC/DC discharge[3]. All this methods are related to the same problem, which is the oxidation of Cu nanoparticles to CuO/Cu_2O. So, in this work, we tried two different techniques to produce the nanocomposite.

Although CNTs are known mostly for their useful properties, there is the issue of poor wetting by metals. Therefore, the properties of their surfaces do not have catalytic effect. In order to solve this problem, copper nanoparticles are added on the surface of CNTs to increase the catalytic effect. On the other hand, adding the CNT to a copper matrix results in the formation of a nanomaterial with enhanced properties[4].

During the last decade, CNTs have become a subject of high interest for some industry fields. Specially, the potential applications for MWCNTs have been studied to a higher extent due to the combination of exceptional physico-chemical properties and a wide range of active sites.

Current industrial applications contain, for instance, electronics, sensors and sporting goods. Mid-term include coatings, catalysts, textiles & fibers, among others.

Finally, the long-term category is focused on microwaves antennas, medical implants and drug delivery[1].

The use of nanomaterials as a possible solution for environmental problems, is one of the most important application of Nanotechnology related materials [1]. Industrial dyes are one of the largest groups of organic compounds causes of pollution and water resource consumption. The removal of these colors and other organic materials is a priority for ensuring a safe and clean environment. Advanced oxidation processes (AOPs) has been used to degrade dyes in aqueous media without the formation of hazardous by-products [2]. AOPs are based on the generation of very reactive species such as hydroxyl radicals (OH^-) that oxidize a broad range of pollutants very quickly. Irradiation sources have a crucial role in enhancing the activity of catalysts.

2. Experimental

2.1 Materials and Equipments

The reagents used, in the present study, for different chemical reactions were hydrogen peroxide (H_2O_2; purity of 30% v/v) and copper(II) sulphate pentahydrate ($CuSO_4 \cdot 5H_2O$; purity of 99%) from Sigma-Aldrich, acetonitrile (ACN; p.a.) and hydrochloric acid (HCl; purity of 37%) purchased from Panreac, deionised water, ethylene glycol ($C_2H_6O_2$; purity of 99,5%) and tetrafluoroboric acid 50% ($HBF_4 \cdot H_2O$) purchased from Riedel-deHaen, multiwalled carbon nanotubes Baytubes 150HP from Bayer Materials. Methylene blue (MB), amaranth, tartrazine, brilliant blue and indigo dyes were purchased from Merck. All the reagents used for this experiment were analytical grade and were used without further purification. Deionized water was used for all the experiments. The structures of dyes chosen as the target compounds are shown in **Table 4- 1**.

Table 4- 1 Structure of the pigments used in catalytic study.[a]

Structure	Name
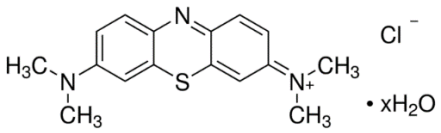	methylene blue[b]
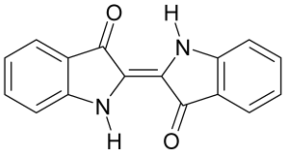	indigo[c]

[a] The other pigments are mentioned in **Table 1- 3** chapter 1. [b] The IUPAC name of methylene blue is 3,7-bis(Dimethylamino)-phenothiazin-5-ium chloride. [c] The IUPAC name of indigo is 2,2'-Bis(2,3-dihydro-3-oxoindolyliden).

SEM was performed on a FEI Quanta 200 apparatus. X-ray diffraction tests were performed at room temperature on a Rigaku MiniFlexTM II system using CuKα radiation (λ= 0.15418 nm). The microwave apparatus is a MonoWave 300, Anton Paar.

2.2 Synthesis of Cu-MWCNT nanocomposite

MWCNT supported copper nanoparticles were synthesized following a microwave-assisted modified polyol procedure[5]. In a typical synthesis, 10 mL of a $CuSO_4 \cdot 5H_2O$, 0.01 M solution in ethylene glycol (EG) was mixed with 74 mg of carbon support in a flask. The suspension was stirred for 30 min and then 10 mL of a solution of $HBF_4 \cdot H_2O$, 0.04 M, in EG, was slowly added under vigorous agitation. After additional stirring for 15 min, the reaction mixture was irradiated for 5 min under 300 W using microwave. Agitation (600 rpm) was continued during irradiation and the reactant mixture reached a temperature of about 150 ℃. After cooling at 55 ℃, the suspension was filtrated and washed with acetone several times before being dried first at 60 ℃ in air over-night.

2.3 Degradation of Dye

Typically 10 mg of dye were added to 1000 mL of double distilled water used as stock solution. About 10 mg of synthesized Cu-MWCNT nanoparticles was added to 100 mL of methylene blue dye solution. A control was also maintained without addition of Cu-MWCNT nanoparticles. Before exposing to irradiation, the reaction suspension was well mixed by being magnetically stirred for 30 min to clearly make the equilibrium of the working solution. Afterwards, the dispersion was put under the sunlight and monitored from morning to evening sunset. At specific time intervals, aliquots of 2-3 mL suspension were filtered and used to evaluate the photocatalytic degradation of the dye. The absorbance spectrum of the supernatant was subsequently measured using UV-Vis spectrophotometer at the different wavelength. Concentration of dye during degradation was calculated by the absorbance value at the maximum absorption peak wavelength. Percentage of dye degradation was estimated by the following formula:

$$\%\text{Decoloration} = \quad 100 \cdot \frac{(C_0 - C)}{C_0} \qquad (3)$$

where C_0 is the initial concentration of dye solution and C is the concentration of dye solution after photocatalytic degradation.

3. Results and discussion

3.1 Synthesis of Cu-MWCNT nanocomposite

Figure 4- 1 shows the XRD pattern of Cu-MWCNT produced by using ethylene glycol that promotes the formation of Cu nanoparticles but also copper oxides. Ethylene glycol is a mild oxidant and hence was used in the current work to produce Cu-MWCNT composite powder. Its mild oxidation prevents contamination or unwanted materials as we can see in the X-ray diffraction results. Copper nanoparticles are present in their pure form.

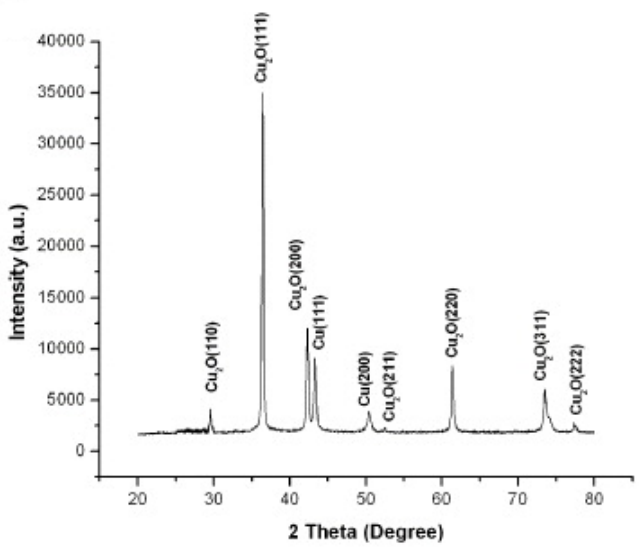

Figure 4- 1 XRD spectra of Cu-MWCNT produced.

Figure 4- 2 represents the SEM images showing the microstructure of Cu-MWCNTs composites fabricated in the present work. MWCNTs can be seen dispersed homogeneously throughout the Cu matrix. A highly dispersed system with minimal agglomeration of MWCNTs is essential for the Cu-MWCNTs composite to have optimal qualities. Better dispersion aids in the formation of an optimal interface between the Cu matrix and MWCNTs, and the interfacial bonding between Cu and MWCNTs is enhanced via good dispersion of MWCNTs.

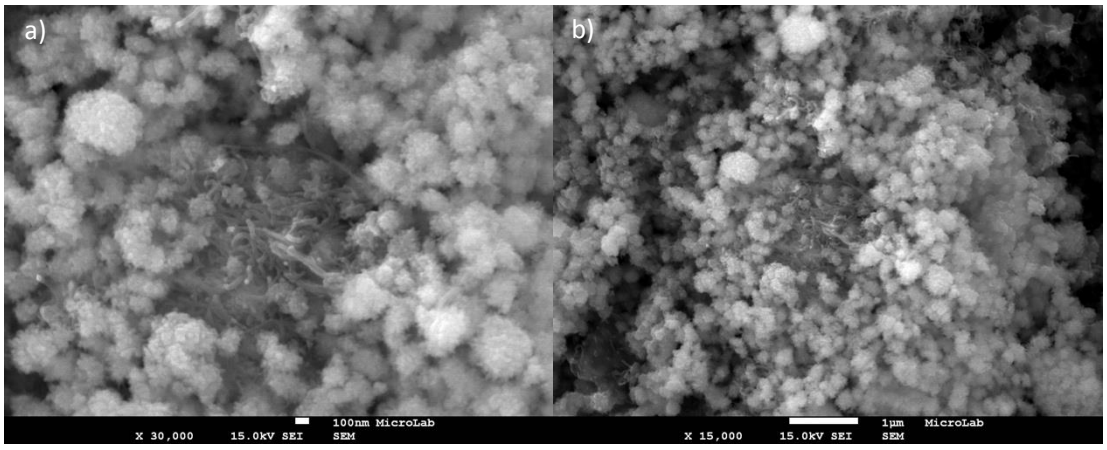

Figure 4- 2 SEM images of Cu-MWCNT nanocomposite powder. a) x30000; b) x15000.

3.2 Degradation of Dye

Regarding the pigment analysis, we used five pigments as models to analyze the catalytic activity of MWCNT coated Cu (Cu-MWCNT) to decolorize the pigments.

We carried out a series of experiments to investigate the catalytic activity of the catalyst in different pigments at different pH values. The shifts of the maximum absorption wavelength are shown in the **Table 4- 2**:

Table 4- 2 Maximum absorbance wavelength of the pigments at studied pH value.

Pigment	λ(pH=2) /nm	λ(pH=7) /nm	λ(pH=12) /nm
Amaranth	521	521	494
Tartrazine	427	426	400
Brilliant blue	627	627	627
Methylene Blue	660	660	660
Indigo	610	610	610

All pigments solutions were studied at 2.0, 3.0, 5.0, 7.0, 10.0, 20.0, 33.0 and 100.0 mg/L of standard series and the absorbency of which were was determined at the highest absorbance wavelength. In **Figure 4- 3** we present the Methylene blue (MB) UV-VIS spectra.

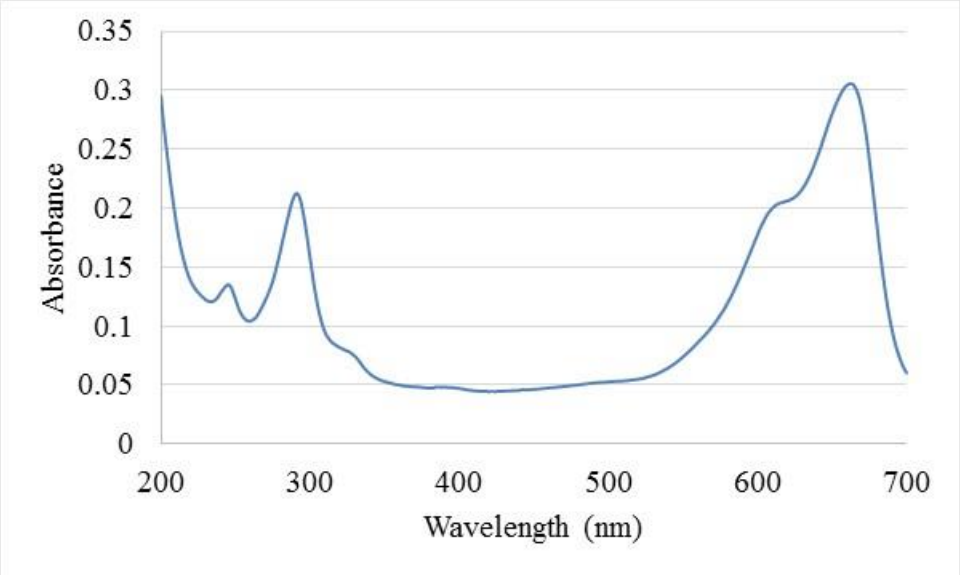

Figure 4- 3 UV spectra of Methylene blue.

Regarding the results, a linear correlation is good at 660 nm in low concentration of absorbency data analysis. The different pigments are determined by UV-Vis at their maximum wavelength. Then the experimental data is used for calculation of the decoloration rate (equation 4).

$$\%\ Decoloration\ rate = \frac{(A_0 - A_t)}{A_0} \times 100 \qquad (4)$$

Where A_0 and A_t are the original dye solution absorbance and the absorbance at various intervals of time (t), respectively. A_0 and A_t are proportional with C_0 and C_t, respectively, where C_0 is the initial concentration of dye and C_t is the concentration of dye at any time, based on Beer–Lambert's law.

Effect of the pH

pH value is one of the most important parameter in the catalytic degradation reactions. It influences both the surface charge of the catalysts and the adsorption behavior of pigments[6]. In this section we studied the decoloration of pigments in acid (pH=2), neutral (pH=7) and base (pH=12) solution. In order to study the effect of pH, adsorption is carried out mixing the Cu nanocomposite with the different pigment solutions, by stirring, for 5 minutes. The pH of the solution studied was obtained (2.0, 7.0 and 12.0) by the addition of either HCl (37%) or NaOH (0.1 mol/L). After 60 minutes all pigments, except Indigo, shown 100% decoloration for all the pH values studied. The relationship observed between absorption of the pigments and varying pH is presented in **Figure 4- 5**. The kinetic study is investigated and shown in **Figure 4- 6**. The decoloration rate (%) is shown in **Table 4- 3**.

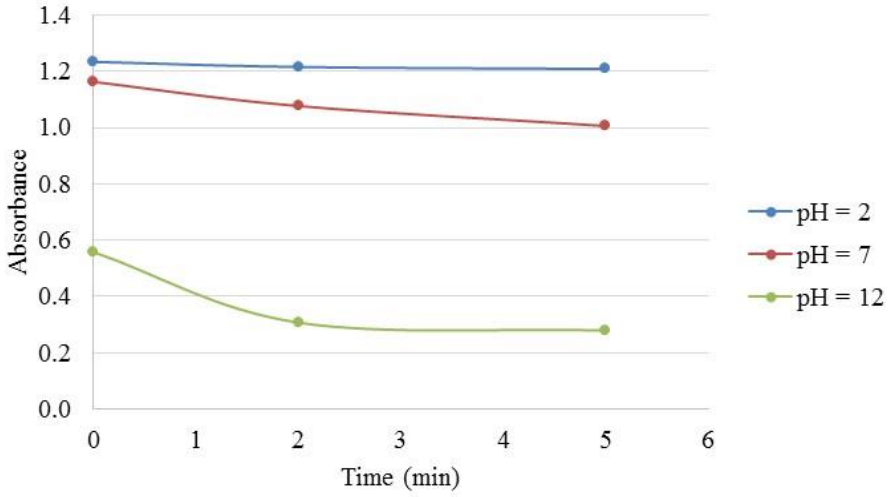

a) Amaranth

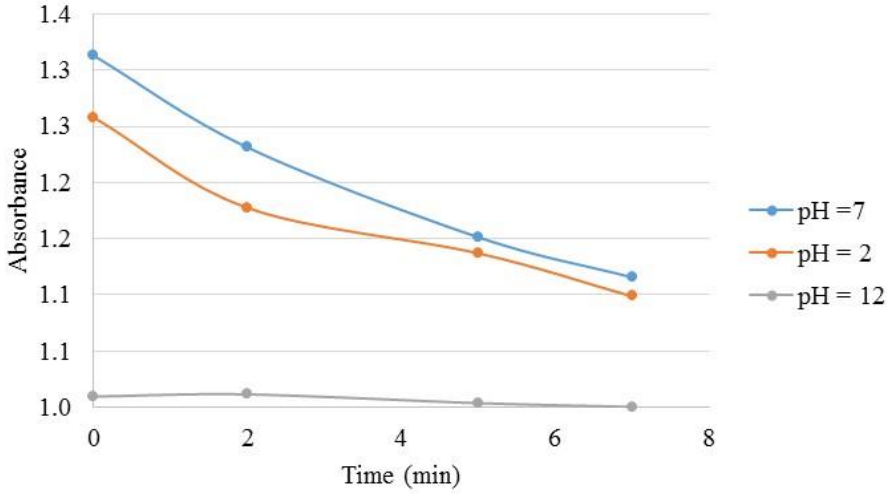

b) Tartrazine

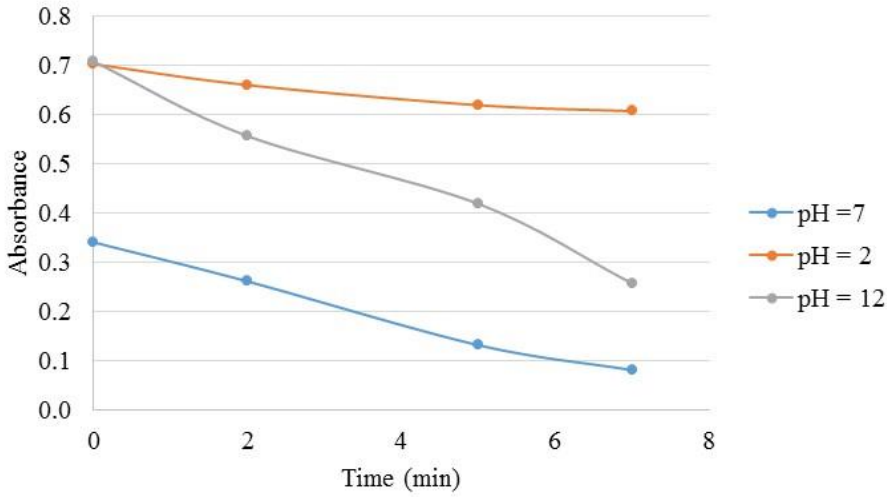

c) Brilliant blue

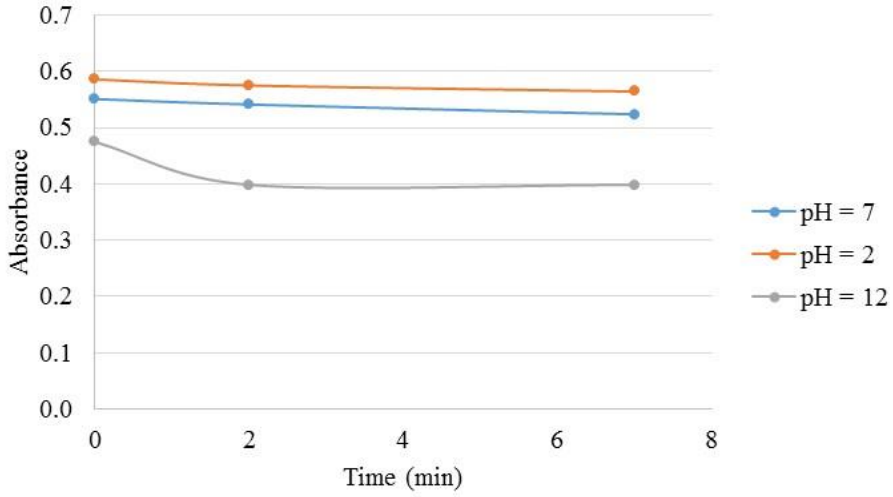

d) Methylene Blue

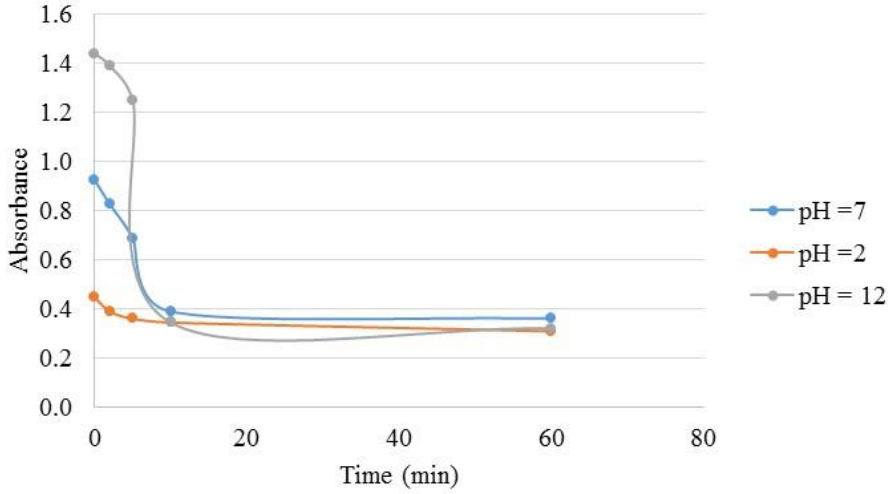

e) Indigo

Figure 4- 4 Plot of absorbance at maximum absorption wavelength of all pigments, as a function of time at pH 2, 7 and 12.

Regarding the decoloration of amaranth pigment (**Figure 4- 4 (a)**), at lower pH the surface of the amaranth pigment is positively charged. The positive charged catalyst surface can adsorb the negatively charged dye anion. Thus the catalyst promotes the reduction of the pigment. With a higher pH, the mechanism of the decoloration of pigment changes from reduction to oxidation. With the presence of H_2O_2 as oxidant, the rate of degradation increases with the increasing of pH. The enhancement effect of H_2O_2 is because the hydrogen peroxide can accept electrons to prevent the recombination of hole-electron pairs, and promote the generation of hydroxyl radicals[7,

[8]. At pH 12, the negatively charged catalyst surface results in a high rate of degradation of amaranth pigment.

Regarding tartrazine pigment, an increase in the pH solution promotes an increase in decoloration rate, but at pH 12, the decoloration rate becomes negligible. Alkaline conditions promoted reactive oxygen species generation and consequent dye degradation. Results from electron spin resonance spin-trap spectroscopy[9] suggested that at high pH, both hydroxyl radical (•OH) and singlet oxygen ($^1O_2$) were responsible for dye decoloration, whereas at acidic conditions, the consumption of $^1O_2$ became dominant. Similar results have been reported previously[10], using photo oxidation with TiO_2.

Brilliant blue presents the best decoloration rate of all the pigments studied, regardless of the pH. The decoloration is mainly attributed to the variation of surface charge properties of the catalyst at different pH values. Contrary to some studies published[11] the decoloration rate increases until neutral pH (76%) and then slightly decreases at higher pH values (63%). This behavior does not show the same trend as reported by Papnai et al[12]. Variation of surface charge properties of the catalyst at different pH values is likely to be the reason of the different behavior.

The removal of methylene blue increases from 3.4 % to 16.11 %, when the pH of the solution is increased from 2.0 to 12.0 (**Figure 4- 4 (d)**). The maximum methylene blue adsorption is observed at higher pH range. This is due to the cationic configuration of methylene blue, where the adsorption can be favoured in alkaline solution. Similar trend was reported[13] for photo oxidation with TiO_2, but the full decoloration occurs over 10h, while in our studies we observe full decoloration after only 1h.

For Indigo, the basic medium has the best decoloration rate. This is due to the formation of different forms as a function of pH[14] and how the different forms of indigo interact with the sodium present in the basic medium.

Table 4- 3 Apparent constant rate and decoloration rate (%) for the different pigments.

Pigment	pH	K*app* min^{-1}	Time min	Decoloration rate (%)
Amaranth	2	0.0286	7	13.52
	7	0.0039	7	2.03
	12	0.1300	7	49.96
Brilliant Blue	2	0.0161	7	13.63
	7	0.2286	7	76.25
	12	0.1553	7	63.70
Indigo	2	0.0680	60	30.92
	7	0.1053	60	61.00
	12	0.0812	60	77.73
Tartrazine	2	0.0137	7	12.66
	7	0.0190	7	15.04
	12	0.0021	7	0.92
Methylene Blue	2	0.0043	7	3.67
	7	0.0145	7	4.93
	12	0.0028	7	16.11

4. Conclusion

In conclusion, the Cu-MWCNT nanoparticles were synthesized by using a microwave assisted polyol process. A highly dispersed system of Cu-MWCNT nanoparticles was observed by SEM images. The catalytic activity of decolorization of pigments was evaluated by a kinetic study of degradation of amaranth, tartrazine, brilliant blue, methylene blue and indigo pigments monitored by UV-Vis. The effect of pH value was also evaluated. An efficient degradation was observed. The excellent catalytic activity of Cu-MWCNT nanoparticles against pigment molecules made it efficient for the treatment of waste water and pigment effluent.

References

[1] Mubarak, N. M.; Sahu, J. N.; Abdullah, E. C.; Jayakumar, N. S. Removal of Heavy Metals from Wastewater Using Carbon Nanotubes. *Sep. Purif. Rev.* **2014**, *43*, 311–338.

[2] Vassilios, T.; Vasillios, G.; Eudokia, O.; Michael, K.; Dimitrios, P. Synthesis and Characterization of Carbon Nanotube/Metal Nanoparticle Composites Well Dispersed in Organic Media. *Carbon*. **2006**, *44*, 848–853.

[3] Sunil, K. S.; Maneet, L.; Lata; Soumya, R. K.; Rakesh, B. M. Synthesis Of Cu/CNTs Nanocomposites for Antimicrobial Activity. *Adv. Nat. Sci.: Nanosci. Nanotechnol.* **2012**, *3*, 045011.

[4] Walid, M. D. Processing and Characterization of CNT/Cu Nanocomposites by Powder Technology *Powder Metall. Met. Ceram.* **2008**, *47*, 531-537.

[5] Marinaro, M.; Mancini, M.; Nobili, F.; Tossici, R.; Damen, L.; Marassi, R. A newly designed Cu/Super-P composite for the improvement of low-temperature performances of graphite anodes for lithium-ion batteries. *J. Power Sources.* **2013**, *222*, 66-71.

[6] Vinod, K. G.; Rajeev, J.; Alok, M.; Tawfik, A. S.; Arunima, N.; Shilpi, A.; Shalini, S. Photo-catalytic degradation of toxic dye amaranth on TiO_2/UV in aqueous suspensions. *Mater. Sci. Eng. C.* **2012**, *32*, 12–17.

[7] Idil, A. A.; Isil, A. B.; Detlef, W. B. Advanced oxidation of a reactive dyebath effluent: comparison of O_3, H_2O_2/UV-C and TiO_2/UV-A processes. *Water Res.* **2002**, *36*, 1143–1154.

[8] Mallika, P. K.; Saha, S. K. Oxidation of direct dyes with hydrogen peroxide using ferrous ion as catalyst. *Sep. Purif. Technol.* **2003**, *31*, 241-250.

[9] Meng, L.; Weiwei, H.; Yi, L.; Haohao, W.; Wayne, G. W.; Y. Martin, L.; Jun-Jie, Y. FD&C Yellow No. 5 (Tartrazine) Degradation via Reactive Oxygen Species Triggered by TiO_2 and Au/TiO_2 Nanoparticles Exposed to Simulated Sunlight. *J. Agric. Food Chem.* **2014**, *62*, 12052–12060.

[10] Xinsheng, Peng.; Izumi, I. Manganese Oxyhydroxide And Oxide Nanofibers For

High Efficiency Degradation of Organic Pollutants. *Nanotechnol.* **2011**, *22*, 015701.

[11] Neema, P.; Ameta, K. L. Cerium-Iron Oxide Catalyzed Photodegradation of Brilliant Blue G. *Chem. Sci. Trans.* **2014**, *3*, 1001-1006.

[12] Noritaka, M. *Modern Heterogeneous Oxidation Catalysis: Design, Reactions and Characterization*, Ch. 8, John Wiley & Sons, **2009**, 356.

[13] Kamila, B.; Julia, C.; Diana, D.; Antoni, W. M. Methylene Blue and Phenol Photocatalytic Degradation on Nanoparticles of Anatase TiO_2. *Polish J. of Environ. Stud.* **2010**, *19*, 685-691.

[14] Baig, G. A. Dyeing Nylon With Indigo In Various Ph Regions *Autex Res. J.* **2010**, *10*, 21-25.